Instituto Tecnológico y de Estudios Superiores de Monterrey

Campus Monterrey

School of Engineering and Sciences

TECNOLÓGICO DE MONTERREY®

Implementation of a Fuzzy Logic Based System for the Generation of a Risk Indicator in a DC Electric Arc Furnace

A dissertation presented by

Omar Erives Sánchez

Submitted to the

School of Engineering and Sciences

in partial fulfillment of the requirements for the degree of

Doctor of Philosophy

in

Engineering Science

Major in Electrical Engineering

Monterrey Nuevo León, May 15th, 2019

Declaration of Authorship

I, Omar Erives Sánchez, declare that this thesis titled, 'Implementation of a Fuzzy Logic Based System for the Generation of Risk Indicator in a DC Electric Arc Furnace' and the work presented in it are my own. I confirm that:

- This work was done wholly or mainly while in candidature for a research degree at this University.
- Where any part of this thesis has previously been submitted for a degree or any other qualification at this University or any other institution, this has been clearly stated.
- Where I have consulted the published work of others, this is always clearly attributed.
- Where I have quoted from the work of others, the source is always given. With the exception of such quotations, this thesis is entirely my own work.
- I have acknowledged all main sources of help.
- Where the thesis is based on work done by myself jointly with others, I have made clear exactly what was done by others and what I have contributed myself.

Omar Erives Sánchez

Monterrey Nuevo León, May 15th, 2019

Acknowledgements

In my journey towards this PhD, I received help and guidance of some respected persons, who deserve my deepest gratitude.

I am especially thankful to Dr. Osvaldo Micheloud, who, as my teacher and mentor, has taught me more than I could ever give him credit for, not only about scientific research, but life in general. He has shown me what a good scientist and person should be. I sincerely appreciate all the help that he provided for this project, not only for his active work, but also for his support since I came to Monterrey six years ago.

I would like to express my deepest gratitude to all of those with whom I have had the pleasure to work during this project. Each one of the members of my Dissertation Committee have provided me personal and professional guidance; as well as my friends in the "Consorcio Empresarial". In addition, I am grateful to Tomás Galván, Ricardo Ramírez, Nelson Matarazzo, Marco Ruiz and Rafael González, who helped me during my stay in Ternium.

My acknowledgement would be incomplete without thanking my family; whose love and guidance were there for me in whatever dream I pursue. I cannot express enough thanks for them, because this achievement would not have been possible without their unselfish love and support throughout the years.

I would also like to expand my gratitude to all those who have directly and indirectly guided me in writing this thesis.

This thesis would not have been possible without the financial support of CONACYT and Ternium, who granted me the scholarship to pursue this doctorate in Tecnológico de Monterrey and a maintenance grant for living.

I dedicate this thesis to:

My Mother María de Lourdes

My Father Javier

My Brother Aldo

Implementation of a Fuzzy Logic Based System for the Generation of a Risk Indicator in a DC Electric Furnace

by

Omar Erives Sánchez

Abstract

The main objective of this research was to find a very robust EAF arc coverage indicator that may alert the furnace operator in advance of reaching any risky operating condition and build a reliable prototype that will prove its accuracy under real field conditions. The steps to accomplish this objective were:

-Develop a mathematical tool, using fuzzy logic to design algorithms that could at least give outputs that were in line with the predictions of arc coverage done by the best furnace operator. This point is covered in chapter 3 of the dissertation.

-Study the correlation between vibration and arc coverage, then research for an adequate technique to measure vibration under very hard environment conditions. Develop mathematical tools to process vibration signals and correlate them with measured water panel temperature. In chapter 4 is detailed the information regarding this point.

-Study how to anticipate any risky operation situation and alert the furnace operator to take immediate actions, like graphite and oxygen injection or power control to avoid furnace damage. Combine different variables that today are measured at any EAF, like water panels temperature and its rate of change in time with vibration and sound, to have a more robust EAF "risk indicator". Chapter 5 covers this point with detail.

-Build a system that can run all these algorithms in real time under a steel shop environment condition. Make the final tuning of the entire system under real working conditions in a steel shop with a DC EAF and probe its reliability and accuracy along several weeks of field work. This point is described in chapter 6.

In light of all the above-mentioned activities and the field experimental results obtained, it is clear that the objectives of the research proposal were fully accomplished and the developed "EAF risk indicator" is a novel contribution to improve safety in the steel industry and at the same time increase productivity and reduce maintenance costs.

List of Figures

Fig. 2.1 Main electrical components of the EAF 4
Fig. 2.2 Different types of bottom electrode: Nippon and Danieli designs 6
Fig. 2.3 Representation of the striking stage: beginning and after boring period concludes 8
Fig. 2.4 Representation of the fusion stage: scrap falling from the walls, foamy slag 9
Fig. 2.5 Control loops of the DC EAF 10
Fig. 3.1 Representation of temperature using a crisp set and a fuzzy set 15
Fig. 3.2 Fuzzification procedure 16
Fig. 3.3 Triangular membership function 17
Fig. 3.4 Trapezoidal membership function 17
Fig. 3.5 Gaussian membership function 18
Fig. 3.6 Sigmoidal membership function 18
Fig. 3.7 Singleton membership function 19
Fig. 3.8 Two arbitrary fuzzy sets 20
Fig. 3.9 Triangular membership functions for an arbitrary input 23
Fig. 3.10 Discrete fuzzy distribution 26
Fig. 3.11 Automation of a DC EAF using a fuzzy system 28
Fig. 3.12 Membership functions for vibration level, power level and risk level 29
Fig. 3.13 Fuzzy matching procedure for certain vibration and power levels 29
Fig. 3.14 Clipped MFs after inference procedure 31
Fig. 3.15 Fuzzy output of the Mamdani model 31
Fig. 3.16 Crisp output after defuzzification 32
Fig. 3.17 Behavior of a TSK model 33
Fig. 4.1 Damping of vibrations in the furnace shell: uncovered and covered arc 35
Fig. 4.2 Laser vibrometer at the steel shop 36
Fig. 4.3 Representation of the signal path of the laser vibrometer 37
Fig. 4.4 Vibrometer placement inside the steel shop 37
Fig. 4.5 Processing of the acquired signal 38
Fig. 4.6 Reflective materials: micro spheres fabric and prismatic vinyl 38
Fig. 4.7 Reflective materials glued to the magnets 39
Fig. 4.8 Reflective magnets mounted in the EAF 39
Fig. 4.9 Reflective magnets mounted in the EAF after 24 hours of operation 40
Fig. 4.10 Surface of the reflective magnet covered by metallic particles 40
Fig. 4.11 Raw vibration signal and RMS value during boring period 41
Fig. 4.12 Raw vibration signal and RMS value after boring period 42
Fig. 4.13 Reflective plate 43
Fig. 4.14 Vibrometer over unstable floor and Reflective plate mounted at the EAF 43
Fig. 4.15 Laser vibrometer inside the security cage 44
Fig. 4.16 Vibration signal under poor reflection conditions 44

Fig. 4.17 Partial obstruction of the laser 45
Fig. 4.18 Reflective material affected by high temperature 45
Fig. 4.19 Intact reflective surface after several days mounted at the EAF 46
Fig. 4.20 Best configuration encountered to carry out the vibration measurement 46
Fig. 4.21 Screenshot of the vibration measurement 47
Fig. 4.22 Electric power and panel temperatures 48
Fig. 4.23 Relevant signals plotted simultaneously for analysis 49
Fig. 4.24 Electric power and panel temperatures 50
Fig. 4.25 Relevant signals plotted simultaneously for analysis 51
Fig. 4.26 Electric power and panel temperatures 52
Fig. 4.27 Relevant signals plotted simultaneously for analysis 53
Fig. 5.1 Generation of an arc coverage signal for control purposes 55
Fig. 5.2 Membership functions for vibration, temperature slope and electric power levels 56
Fig. 5.3 Membership functions of risk level for Mamdani and TSK models 56
Fig. 5.4 Polynomial adjust over panel temperature data 58
Fig. 5.5 Secant line crossing a function 58
Fig. 5.6 Temperature slope obtained after polynomial adjust 59
Fig. 5.7 Two temperature slopes plotted simultaneously 60
Fig. 5.8 Maximum slope value after comparison 60
Fig. 5.9 Electric power, temperature and slope, RMS vibration, Mamdani and TSK outputs 62
Fig. 5.10-5.13 Electric power, temperature and slope, raw and RMS vibration, TSK output 64
Fig. 5.14 RSV-150 laser vibrometer at Tecnológico de Monterrey campus 69
Fig. 5.15 RSV-150 aiming to the new measurement point 70
Fig. 5.16 Membership functions for inputs of the RSV-150 measurement campaign 70
Fig. 5.17 Comparison of the output of the TSK model using triangular and trapezoidal MFs 71
Fig. 5.18-5.24 Electric power, temperature and slope, raw and RMS vibration, TSK output 72
Fig. 6.1 Diagram of the arc coverage application 81
Fig. 6.2 Generators connected to the data acquisition system 82
Fig. 6.3-6.5 Arc coverage application running in real time 83
Fig. 6.6 Comparison between arc coverage indicator and its proportional analog signal 86
Fig. 6.7 processing unit of the vibrometer installed inside a steel box 86
Fig. 6.8 Laser emitter installed in the steel shop 87
Fig. 6.9 Data acquisition system installed in the computer room of the EAF 87
Fig. 6.10 Three-input fuzzy model 89
Fig. 6.11 New MFs for the real time application 89
Fig. 6.12-6.14 Electric power, panel temperatures and risk indicator three-input fuzzy system 90
Fig. 6.15 Four-input fuzzy model 93
Fig 6.16 Membership functions for the sound input 93
Fig, 6.17 Membership functions for the auxiliary input of the main fuzzy system 94
Fig. 6.18-6.20 Electric power, panel temperatures and risk indicator four-input fuzzy system 95
Fig 6.21 Five-input fuzzy system 98

Fig 6.22 Membership functions for the temperature input 98
Fig 6.23 Membership functions for the auxiliary input of the main fuzzy system 99
Fig. 6.24-6.28 Electric power, panel temperatures and risk indicator five-input fuzzy system 100
Fig 6.29 Screen that shows the risk indicator to the operator of the EAF 105

Contents

Abstract vii

List of Figures ix

Chapter 1. Introduction 2

1.1 Objective 2

1.2 Hypothesis 2

1.3 Justification 3

Chapter 2. The DC Electric Arc Furnace 4

2.1 Main electrical components of the DC EAF 5

2.2 Basic operation of the DC EAF 7

2.2.1 Steelmaking process in the EAF 8

2.2.2 The control system 11

2.3 Foaming slag 12

2.3.1 Foaming Slag Control 13

2.4 Electric arc coverage in the DC EAF 14

Chapter 3. Fuzzy Logic 16

3.1 Membership functions 17

3.2 Basic operations in fuzzy sets 20

3.2.1 T-norms and S-norms 21

3.2.2 Fuzzy set properties 22

3.3 Fuzzy rules 23

3.3.1 Antecedent and consequent of fuzzy rules 23

3.4 Recommendation for the design of MFs 23

3.5 Fuzzy Rule based system 24

3.5.1 Mamdani Model 25

3.5.2 Application example using Mamdani model 28

3.5.3 Larsen Model 33

3.5.4 Takagi-Sugeno-Kang (TSK) Model 33

Chapter 4. Vibration measurements 36

4.1 Vibration measurement equipment Polytec CLV-2534-2 36

4.1.1 CLV-2534-2 tests 37

4.1.2 Examples of uncovered arcs 48

4.1.3 Examples of covered arc 53

Chapter 5. Off-line implementation of the multivariable fuzzy system 56

5.1 Membership functions and rules 56

5.2 Conditioning of input data for the fuzzy model 58

5.3 Results using the CLV-2534-2 vibrometer 62

5.4 Vibration measurement equipment RSV-150 70

5.4.1 Membership functions and rules using the RSV-150 71

5.4.2 Results using the RSV-150 vibrometer 73

Chapter 6. On line Implementation of the multivariable fuzzy system 82

6.1 Real time operation of the risk indicator in the DC EAF 87

6.1.1 Three-Input Fuzzy Model 89

6.1.2 Four-Input Fuzzy Model 95

6.1.3 Five-Input Fuzzy Model 100

Chapter 7. Conclusions **108**

Bibliography **110**

Chapter 1. Introduction

The electric arc furnace (EAF) is one of the most used technologies worldwide. Electric Arc Furnaces contribute to one-third of the total world's steel production. This volume of production implies that small improvements in its energy consumption could represent significant economic savings [1]. Currently, there are several areas of opportunity that can be exploited in order to make the use of energy in the process more efficient and reduce losses. The electric arc produces a huge amount of radiation, this allows the melting of metallic scrap inside the furnace. The amount of radiation emitted by the arc is intrinsically related to arc's length, an increase in length leads to increase the radiation emitted [2, 3]. A common operative practice consists in to operate the EAF with long electric arcs when a good arc coverage can be ensured, for example, when foamy slag surrounds the arc, forming a submerged arc which decreases radiation losses, energy losses, and refractory wear [4].

The radiation emitted by the arc is so intense that if there is no scrap or foamy slag to contain it, the refractory walls and the water-cooled panels can be damaged. To avoid this, and to increase energy efficiency the arc length should be controlled, considering, that there is a compromise between arc length and arc stability [1]. The most important factor holding back the dynamic automation of important process parameters, like the arc length considering the arc coverage, is the lack of information about the process conditions inside the EAF [5]. The correct detection of bad coverage of the electric arc, has been limited by the impossibility to install sensors inside the furnace due to the high temperature, because of this the analysis of variables measured outside the EAF such as shell furnace's vibrations, has become an important source of information about the state of the electric arc. It is clear that the implementation of a good arc coverage indicator will help to homogenize the operator's practices like the injection of foaming agents or adaptation of the electrical set point due to a bad coverage of the arc, those practices typically rely on the expertise of each operator and this inevitably leads to human error.

1.1 Objective

Develop a multivariable fuzzy logic-based system able to quantify the level of coverage of the electric arc during the operation of a DC furnace, this in order to achieve the optimum equilibrium between safety, energy savings and productivity along the process.

1.2 Hypothesis

With traditional mathematical tools is difficult to obtain the mathematical model of a complex process like is the melting in the EAF. In contrast, heuristics tools like fuzzy logic can provide a low-cost solution for modeling and control complex industrial processes. A fuzzy logic application depends on a set of rules in order to work; the rules can be established with the help of expert

operators who has a deep knowledge and experience about the process. In the present work, a MISO (multiple input-single output) fuzzy system is proposed in order to determine the arc coverage level along the melting process of a DC EAF. The inputs for the fuzzy system are the vibrations of the EAF, the electric power level and the temperature slope of the water-cooled panels. The fuzzy system is intended to emulate the expertise of the best operators in such a way that all the operators have a common tool for the improvement of operational practices.

1.3 Justification

A reliable arc coverage detection will allow a more efficient use of the electric energy during the melting process; this implies a reduction in the operative costs of the furnace for the concept of energy. In addition, a good coverage of the arc ensures an increment in the lifespan of refractory and water-cooled panels; this also reduces the operative costs of the EAF. Another important factor is related to the safety along the process, an uncovered electric arc is a potential danger because it can produce serious damage to the EAF and compromise the health of the workers around the equipment, and this is a strong motivation to maintain a good coverage of the electric arc during specific stages of the melting process.

Chapter 2. The DC Electric Arc Furnace

The EAF is a nonlinear load that consumes a lot of energy in order to convert solid materials, like metallic scrap or Direct Reduced Iron (DRI), into liquid state [6]. The use of EAFs to produce steel has expanded during the last decades, the AC EAF was the first development regarding the use of electric energy to produce steel, the power and size of these equipment began to increase, and its operation became more and more popular. Due to the necessity to optimize the operation and reduce production costs the EAF, like many other technologies, had to evolve along the time. This evolution led AC EAF process to step into the Ultra High Power (UHP) operation, in which the use of transformers with the capacity to work with higher voltages, allow to use even three times more power in EAFs of conventional size. The UHP scheme carry on advantages regarding the operation but inevitably other disadvantages like considerable flicker, increment in the refractory wear and higher electrode consumption [4, 7].

The mentioned disadvantages of the UHP operation gave birth to the idea of a Direct Current (DC) arc as heat source, working in a concentric position respect the furnace vessel [8]. It was at the end of 1970, with the progress in the field of power electronics, when was possible to convert, economically, three-phase alternating current into direct current using controlled rectifiers. Many studies were conducted at that time, leading in 1982 to the implementation of the first operative DC EAF for steelmaking [8, 9]. Some of the advantages achieved with the DC EAF are:

- Reduction in electrode consumption: This due to the cathodic polarization of the graphite electrode [10].

- Reduction in the acoustic noise level: In direct current operation there is not zero crossing, this implies that the electric arc does not have to reignite like in every cycle of AC operation.

- Reduction in network flicker: Due to the response speed of the rectifier current control, the voltage variations (flicker) are lower in comparison with the AC operation. The electric current control also contributes to less mechanical stress in the components of the EAF when short circuits occurs [10].

- More uniform thermal load inside the furnace: This due to the concentric heat source coming from a single electric arc [9].

Despite the advantages of the DC EAF, there are still improvement areas for its operation. The melting process is very complex, this along the stochastic nature of the electric arc, can limit the experimental work in the EAF to the measure of temperature and heat transfer rate [11]. It is important to mention that other variables that are not usually measured along the process, like vibrations of the furnace shell, can give good information regarding the electric arc state. To

optimize the operation of the EAF the goal is to reduce the power on time and energy consumption, in other words is necessary to improve the power delivery from the electric arc to the metallic charge [6, 12]. To achieve this, it is necessary to avoid that the radiation of the electric arc "escape" to the furnace walls and water-cooled panels. In other words, it is important to maintain the electric arc covered with solid material or foaming slag along the melting process. Mathematical models can be implemented in order to estimate the arc coverage levels of the arc, however develop an effective mathematical model for an EAF is a challenging task due to the nature of the process. Typically simplifications are made in order to find an approximated model, however this models may not capture some important characteristics of the process [7].

2.1 Main electrical components of the DC EAF

The EAF is a complex equipment with many sub systems working together. Mechanical, hydraulic, and electric components are required for the operation of the EAF. In this section are explained the main electrical components that makes the operation and control of the EAF possible. In Fig. 2.1 the principal components are shown.

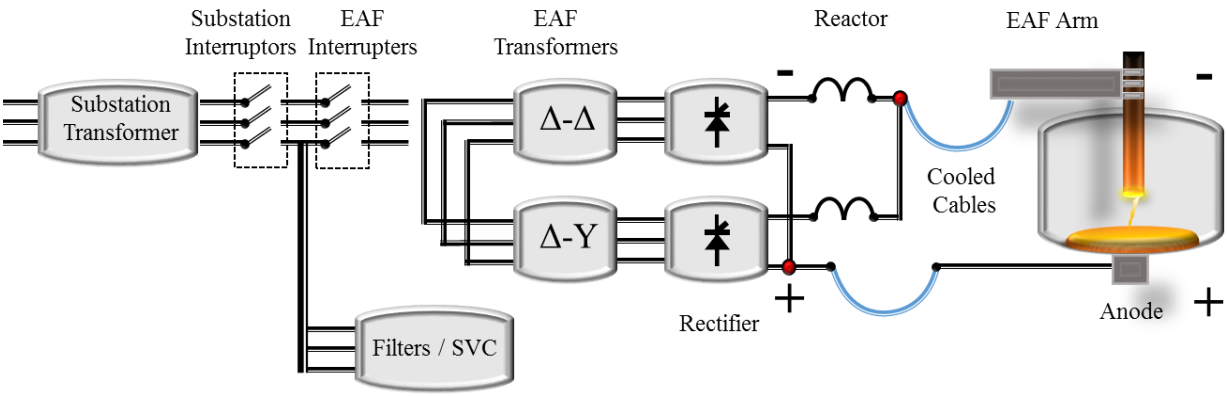

Fig. 2.1 Main electrical components of the EAF

Substation transformer

Its function is to reduce the supply voltage (400 kV, 230 kV or 115 kV) to a medium voltage level (13.8 kV or 34.5 kV) and simplify the management of electrical conductors inside the plant.

Interrupters

They allow the connection and disconnection of the different circuit components.

EAF transformer

Unlike the AC EAF, the DC EAF can have more than one transformer connected to a rectifier. Besides to allow a voltage reduction, the secondary of these elements is matched with the type of rectifier circuit (6 pulse, 12 pulse etc.) The DC EAF transformers can operate without a tap changer, this because the rectifiers allow to modify the power delivery. However, some EAF builders install a tap changer on the high-voltage end of the rectifier transformers for power factor optimization purposes [9].

AC-DC Rectifier

The main function of the rectifier is to convert de AC current into DC current, the control of the firing angle of the thyristors allow to control the electric current of the EAF, in fact during normal operation it is intended to maintain the DC electric current as constant as possible.

Reactor

This element limits short circuit current slope (only for 10 to 100 ms) when the electrode makes contact with the solid metallic charge, this gives the rectifier time to respond and control the current protecting the thyristors.

Cooled cables

They function as an interface between the fixed rectifier and the mast, which is a moving part that raises and lower the graphite electrode.

Furnace Arm

The arm holds the electrode, this moving part is connected to the mast with a hydraulic system. They are of two types of arms:

- Tubular bus: In this configuration the arm holds a tubular bus that conducts the current to the electrode

- Conductor arm: This type of arm conducts the electric current for it outside part to the electrode. A conductor arm is usually cooled with water. Its construction allow a minimum reactance in the secondary system of the EAF (only in the case of DC EAFs) [13].

Graphite electrode

This is one of the most expensive supplies of the steel mill, it is a consumable element of the EAF in whose tip the electric arc is ignited towards the metallic charge. In Ternium EAFs the typically diameters for the electrodes range from 24 to 28 inches [13].

Bottom electrode

It is the anode or positive pole, which is immersed in refractory material. In Fig. 2.2 different types of bottom electrodes are shown. In the case of Ternium, both, the technology of Clecim/Nippon Steel, which consist in billet of steel cooled by an external jacket, and the technology of Danieli (internal cooling) are used in the different EAFs of the plant.

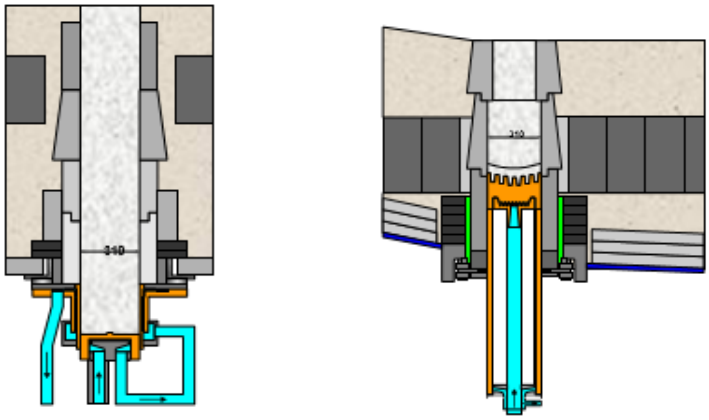

a) **b)**

Fig. 2.2 Different types of bottom electrode a) Nippon design, b) Danieli design

The temperatures of the anodes must be monitored continuously when the EAF is operating, this in order to avoid damage and accidents. The bottom electrode is the most critical component in the DC EAF. Its lifetime is limited and it requires a very narrow online monitoring of its critical variables, for example, cooling water temperature and refractory temperature [10].

2.2 Basic operation of the DC EAF

In order to convert solid material into liquid steel the electric arc is ignited after a short circuit between the cathode and the metallic charge, the radiation of the arc considerably contributes to melt the solid charge, this radiation is intense enough to even damage the EAF. The DC EAF usually works with one or two graphite columns as cathodes. The electric current come back

through an arrangement of conductors (anode) installed at the bottom of the furnace, the anode is in physical contact with meltdown material. This configuration requires an essential operative practice known as hot heel. To ensure that in the case of maximum current any of the bottom conductors is not at risk of melting due to overloading. The liquid hot heel stablish a uniform electrical contact between the solid charge and the anode [9, 13]. Another important consideration along the melting process is the arc length, which can be selected depending on three methods of operation, which are:

- Slag free
- Partly covered with slag
- Fully covered

These methods of operation impact directly in the electric power level selected, for example, a slag free operation, used at the beginning of the melting process, requires a low power short arc in order to protect the EAF components, however, when the arc is covered by scrap the power can be increased [8]. The melting process consist in different stages which present different requirements regarding the arc length and power selection, the different melting stages are detailed in the section below.

2.2.1 Steelmaking process in the EAF

The multiples stages for the production of steel using an EAF can be resumed as:

- Preparation and charge
- Striking and fusion
- Refining
- Tapping
- Secondary metallurgy

Preparation and charge

The preparation refers to the repairs made on the refractory, this is achieved projecting Magnesium Oxide (MgO) in the worn outs points. This stage takes place immediately after the emptied of the liquid steel of the previous tapping. Once the repairs are completed the EAF is charged with one or more scrap basket [13]. In certain plants, the charge process can be carry on in two phases, this depends on the availability of DRI and a continuous feeding system. If it is the case, in the first charge phase, the EAF is pre charged with DRI along the scrap using the basket. In the second phase the rest of DRI is loaded through the roof by the continuous feeding system [14].

Striking

In the striking stage, the electrode is lowered until it makes it contact with the metallic charge, leading to the electric arc ignition. As said before in this stage is important to work with a short electric arc, to avoid damage in the furnace walls and roof. The short arc bores through the solid charge forming a cavity, then the arc is enlarged increasing the radiation and allowing the fusion stage to begin. Fig. 2.3 a) schematizes the beginning of the striking stage and Fig. 2.3 b) the boring of the solid scrap [9, 15].

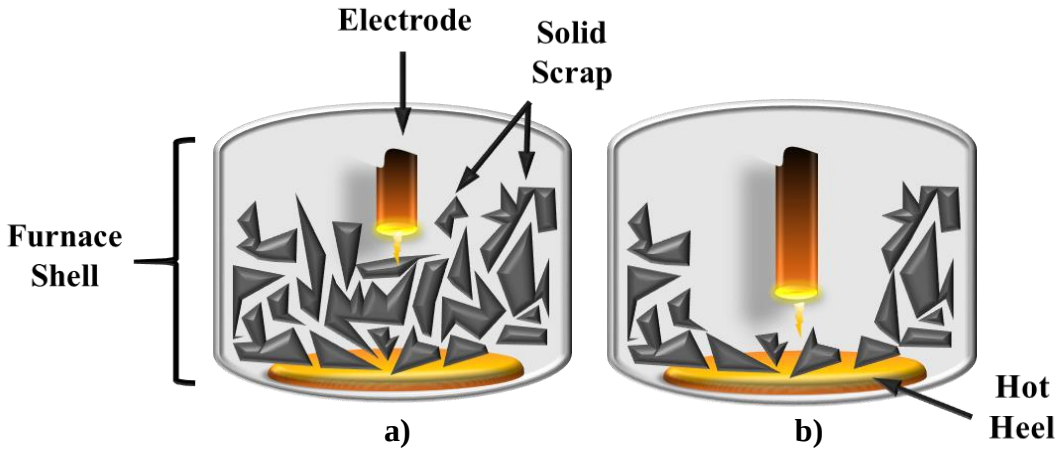

Fig. 2.3 Representation of the striking stage a) at the beginning, b) after boring period concludes

During the striking stage, the vibration of the EAF is very intense, once the boring period concludes a significant reduction in the furnace vibration typically occurs.

Fusion

In the fusion stage the transformation of solid metallic charge into a liquid metal bath occurs, this process requires a great heat source, which comes from the electric arc, which radiation is about 30 % of the arc power. In order to accelerate the heating and melting process, gas burners are aimed at the cold points far away from the electrode [14]. In this stage short circuits between the charge and the electrode occurs, mainly for the falling of the scrap inside the cavity formed during the striking period [6]. In Fig. 2.4 a) is schematized the enlargement of the electric arc with falling scrap, while in Fig. 2.4 b) is shown the end of the fusion stage when a complete liquid bath with foamy slag is achieved.

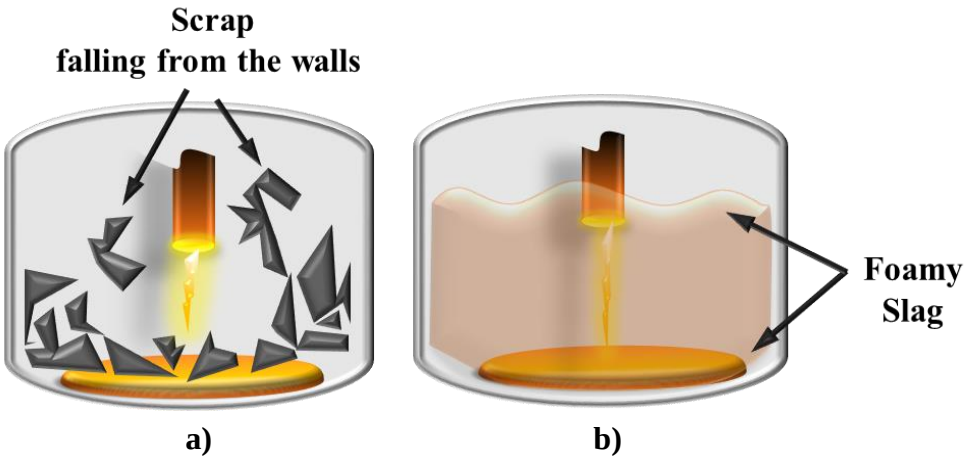

Fig. 2.4 Representation of the fusion stage a) scrap falling from the walls, b) foamy slag

Once the solid material falls from the walls uncovering the arc, foaming agents must be injected to the EAF, this order to produce foamy slag, which shields the arc radiation protecting the furnace. A good foamy slag can ensure work with a high-power long arc safely. If the foamy slag quality is not good enough to fully covering the arc, the power must be reduced in order to protect the EAF.

Refining

This stage follows the fusion stage; here oxygen is injected for metallurgical reasons. During the refining multiple reactions occurs due to the interaction between oxygen and the different chemical elements dissolved in the bath [14]. The main reactions are:

- Reduction of carbon content, this is known as decarburization
- Reduction of the phosphorus content, this is known as dephosphorization
- Oxidation of other elements such as manganese, silicon and chromium

In this stage, the metallic charge is in the liquid state and the electric arc lengths can be maintained constant [6].

Tapping

The emptying consists in the transfer of the liquid steel from the EAF in order to recharge the equipment with solid material. The emptying process last approximately two to three minutes, then the liquid steel goes to the secondary metallurgy stage.

Secondary metallurgy

In this stage, additional elements are added to the metallic bath, this in order to modify its chemical composition and to produce a specific type of steel. The type of steel depends of the final application [16], for example, the steel specification regarding its chemical composition, is not the same for a steel intended to produce tubes for oil extraction in deep water and steel intended for the automotive industry.

2.2.2 The control system

Two control loops constitute the whole control system of the DC EAF, the voltage loop and the current loop, these loops can be adjusted independently from each other. An analogy with the speed control of DC motors can be made. In the inner and fast control loop the current is regulated by the rectifiers, the firing angle is changed in order to maintain the arc current as constant as possible, this is supported by the smoothing reactor in the system. The outer and slower superimposed control loop regulates the voltage, this by the mechanical actuator that shortens or lengthens the electric arc [8, 9]. In Fig. 2.5 the control loops of the DC EAF are schematized.

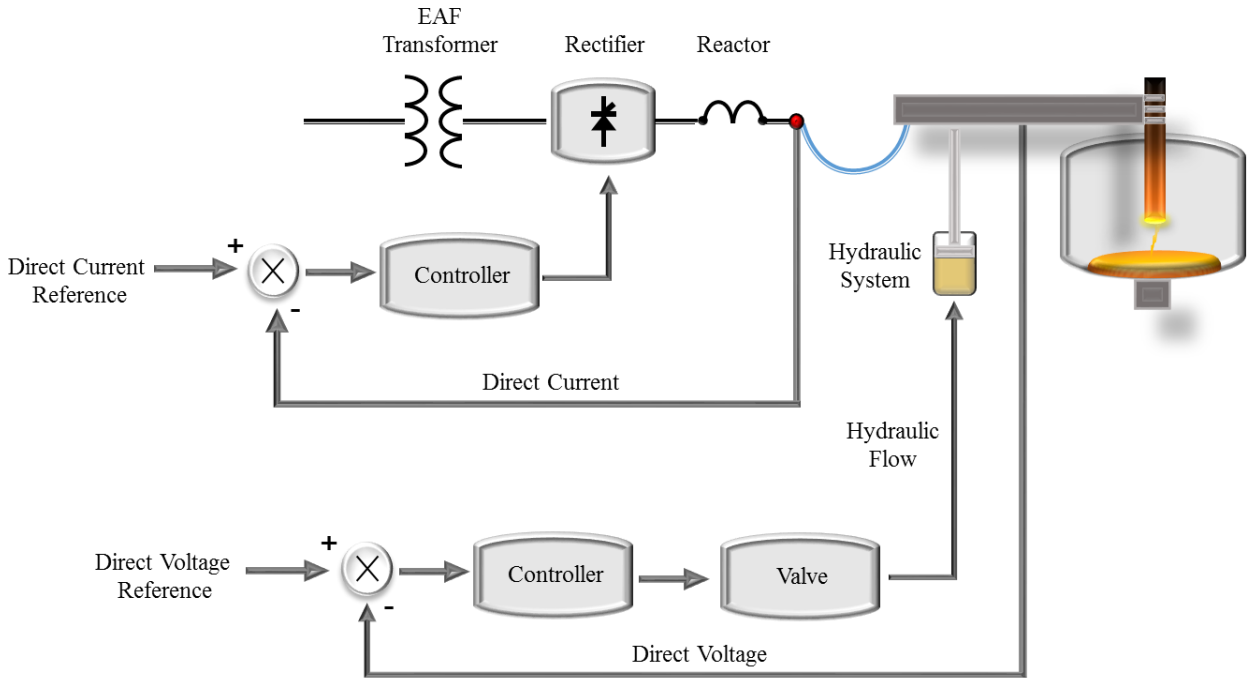

Fig. 2.5 Control loops of the DC EAF

Regarding the voltage control is important to mention that during arcing considerable voltage fluctuations can occur, this because the electrode position system cannot compensate fast enough,

due to its inertia, the changes in the arc length. These voltage fluctuations can introduce perturbations in the power supply network due to fluctuations in the active and reactive power [8].

2.2.2.1 Power selection

For setting the power operating point in the EAF, it is important to consider that the arc should melt the charge without causing excessive damage to the refractory or cooled panels. The electric current should be minimized as long as the condition in the EAF allows it, this in order to reduce losses in the electrical components and the consumption of electrode; this mainly applies in the furnace melting stage. Finally, the combination of voltage and current must guarantee the stability of the arc to avoid its extinction as possible.

The following considerations should be made for a good electrical practice:

- In the striking stage short arcs and low powers should be used to avoid damage the roof of the EAF and breakage of electrodes. However, the selected power must ensure rapid penetration of the electrodes into the solid charge.
- In the fusion stage, the use of long arcs with high power is preferred. Here must be ensured that the walls and the roof of the EAF are always protected first with solid charge and then with foamed slag.

- In the stage of refining or adjustment of coal, lower power and short arcs are used because there is no slag protection.

2.3 Foaming slag

The slag is one of the most important tools regarding the processing of the liquid bath in order to produce high quality liquid steel. One of the biggest innovations in the operation of EAFs, is the foamy slag, this practice appeared at the end of the seventies. The foaming occurs due to the remaining gas generated by the combustion of carbon and the reduction of FeO. The foamy slag is constituted in approximately 90 to 95 percent of gas, the volume of the flat slag increment 10 to 20 times at end of the foaming process [14, 17]. The principal interdependent parameters that influence the foaming capability of the slag are:

- Slag chemical composition (basicity)
- Slag temperature
- Slag viscosity
- Carbon content of the steel bath
- Amount of lime in the slag

The quality of foamy slag is an important parameter that is typically evaluated by an expert. The prediction of the slag quality is difficult due its non-linearity and fast changes. The quality depends on many factors such as DRI to scrap ratio and additives [18]. The quality of the slag affects the following operating conditions of the EAF:

- Thermal and chemical insulation of the liquid bath: The foaming slag protects the liquid bath from oxidation and prevents the heat of liquid steel from escaping into the environment [16]. In other words, the thermal performance is improved and in consequent there is a reduction in the energy cost because the increase in heat retention [18].

- Reduction of arc noise: When the foamy slag covers the electric arc, the acoustic noise is significantly reduced. Although the control of slag efficiency (arc coverage) can be carried out with other methods, the intensity of this noise can be a very useful tool. Besides the reduction in acoustic sound mechanical vibrations are reduced during the melting process [18].

- Coverage of the electric arc: As said before the slag can be manipulated in order to increase its volume and shield the electric arc. If there is no good coverage of the arc by the slag, damage to the cooled panels occurs, causing water to leak into the furnace with a high risk of explosion. Leakage of water into the refractory humidifies and degrade the refractory causing steel and slag drilling in the shell. A good arc coverage, which is related to a good foamy slag, makes it possible to work with long arcs at high powers achieving a good energy transfer and acceptable refractory wear [14, 17].

2.3.1 Foaming Slag Control

In order to produce a homogeneous foamy slag, carbon monoxide bubbles must be generated, to achieve this the amount of coal and oxygen fed to the EAF must be controlled. These elements are typically injected to the EAF by means of lances and injectors. The amount of material injected can be controlled by two methods:

- Using an operating diagram
- Manually under the criterion of the operator

When an operating diagram is used, the material amount feed depends on the melting progress measured through energy consumption, however in many cases, the operating diagrams are rigid, and they do not adapt to varying operating conditions. In the other hand in manual operation the operator decides the amount of material injected depending on the furnace behavior, in fact the control of the overall melting process has traditionally been in the hands of the operator. The manual approach requires high attention from the operator which can lead to human errors. The

drawbacks of both modes of operation explains why research is still being done in order to automated process parameters in the EAF like the foaming of the slag, which impact directly in the arc coverage [5, 17].

2.4 Electric arc coverage in the DC EAF

The most effective mechanism, to transfer heat from the electric arc to the metallic scrap is the arc radiation. However, if the electric arc is not well covered with slag, the high radiation can compromise the furnace integrity. As said before, the amount of radiation emitted by the depends on arc's length, an increase in arc length leads to increase the radiation emitted [2, 3]. To avoid damage in the EAF, and increase energy efficiency, the arc length should be controlled, considering, that there is a compromise between arc length and arc stability, and ensuring that a good coverage of the arc is achieved [1].

Typically, in the DC EAF there is just one electric arc in contrast with the AC EAF where three arcs melt the charge. This implies that in DC operation the radiation of the single arc is very high. Consider a DC EAF working at 80 MW, with a direct current of 115 kA and a voltage of 696 V. For a DC electric arc 1 V DC correspond to approximately 0.6 to 1.2 mm in arc length, resulting in a total theoretical arc length of 400 to 830 mm. In the other hand in an AC EAF working at 80 MW power the electric arc length would be approximately in the range of 210 mm to 350 mm. For the same power the DC arc is longer that the AC arcs, here the importance to guarantee a good arc coverage. As said before at the beginning of the melting process the EAF works at low power, until the solid charge shields the arc radiation, then the power is increased. When the liquid bath phase is reached, a good level of foamy slag must be produced in order to cover and shield the electric arc and avoid damage in the walls and roof elements. In conclusion along the different stages of the melting process is important to ensure that radiation is not hitting towards the cooled panels and the roof of the EAF [9] .

A first approach to determine whether radiation is reaching the EAF walls is the monitoring of panel temperatures. However, the temperature increase usually present a delay up to 30 s due to the slag coating over the panels, because of this temperatures are not suitable for being used as input for an arc coverage or slag level control [3]. On the other hand, the temperature slope gives more relevant information regarding the arc coverage; this because a high change of rate can be used to predict a temperature peak. In the last decade several research have been carried out in other to estimate certain characteristics of the foamy slag or the arc coverage level, for example, in [19] the vibrations of the shell of an AC EAF were used to characterize the foamy slag height. However, there are just a few studies in this topic regarding the operation of DC EAFs.

In [20] a fuzzy method using vibration and power as inputs was implemented, in order to measure the changes in the level of the foamy slag, in an AC EAF. In this study three accelerometer were

placed around the furnace shell dividing it in three sections. However, the mounting of sensors in the furnace shell involves dealing with high operation temperatures that may damage the electronic components; also, the movements of the furnace may damage the cable of the sensors. In other studies, like [21-23], the prediction of the slag height or coverage level of the arc is based on the acoustic noise produced along the process. However, in an industrial environment like a steel shop, other high noise sources can affect the accuracy of the method, especially if there is another EAF working in the same steel shop [18]. Obtain a reliable arc coverage signal along the melting process can lead to some benefits, for example, a better power regulation of the EAF, this mean to carry out a control action (power reduction for example) when the arc is not well covered, this will lead to a reduction of refractory wear and thermal losses. Furthermore, an arc coverage signal can be used to regulate the feeding of foaming agents in order to optimize the foaming slag production [17].

Chapter 3. Fuzzy Logic

Traditional tools for computing and modeling typically works with crisp data, for example, in set theory an element belong or not to a specific set, in other words an element cannot belong simultaneously to two or more sets**.** This dichotomous way to process data discards the fact that, in real world, most process and phenomena are not crisp. The limitation of crisp models to represent some complex high nonlinear process, where linguistic uncertainties play some role, gave birth to fuzzy logic [24, 25]. In different engineering areas, fuzzy logic has found successful applications, like data mining, process control, patter recognition, system identification etc. [26].

A fuzzy logic application employs fuzzy sets that can be defined as sets of data with not well-defined boundaries, for example, the human perception of "hot and cold" does not have straight values that define a solid boundary between the set hot and the set cold. Fuzzy logic allows partial belonging of an element to the different sets that conforms the universe of discourse. The natural notion of fuzzy sets allows gradual transitions and overlaps between them. In Fig. 3.1 a) the concept of "hot and cold" is represented using classical sets, while in Fig. 3.1 b) is represented using fuzzy sets. The vertical axis represents the level of belonging or membership degree that a numeric variable over the horizontal axis takes respect each set, each set is identified with a linguistic variable and represented with a membership function (MF) [25, 27].

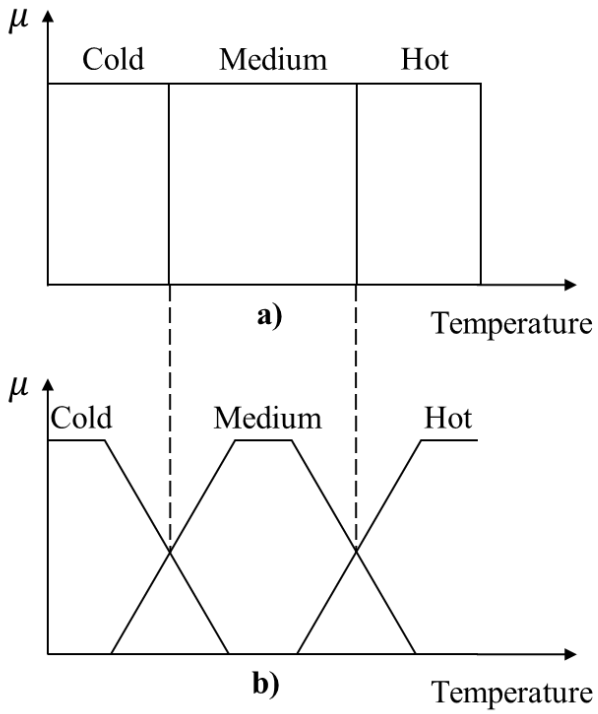

Fig. 3.1 Representation of temperature using a) crisp set, b) fuzzy set

Suppose a measure from an arbitrary sensor, the rigid value can be fuzzified using the membership functions showed in Fig. 3.1 b), to do this the measured is placed over the horizontal axis then is projected towards the vertical axis, the intersection with the membership functions gives the membership degree (μ) of the measure respect one or more sets. The fuzzification of an arbitrary rigid value is shown in Fig. 3.2

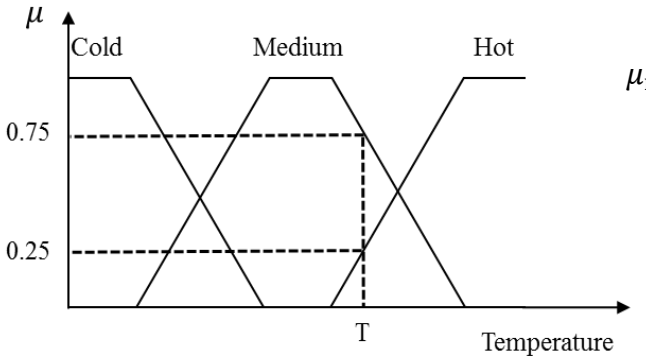

$$\mu_{\text{medium}}(T) = 0.75 \quad (3.1)$$

$$\mu_{\text{hot}}(T) = 0.25 \quad (3.2)$$

Fig. 3.2 Fuzzification procedure

As can be inferred the selection of the parameters that define a membership function is crucial for the development of fuzzy applications, this task can be carry out in various ways including: trial and error processes, statistical techniques, genetic algorithms and neural networks [27]. Being the last method, which gives rise to neuro fuzzy systems.

Another important motivation for the use of fuzzy logic involves the economic factor. The precise modeling and analysis of a complex process can be too expensive, thus an equilibrium between precision and significance must be reached [24]. Fuzzy applications are intended to find a balance between simplicity and exactness [28]. In this context fuzzy logic allows to develop approximate solutions that are economically viable and accurate enough to satisfy certain operative criteria, because of this fuzzy logic has found so many successful applications in industry [27].

3.1 Membership functions

A membership function (MF) is a curve that allows the mapping of a fuzzy set with a membership value between 0 and 1 [29]. In theory, a MF can be constructed with arbitrary shape, however a good practice is to define fuzzy sets using MFs defined by few parameters. The principal consideration for its design is that a MF must provide a smooth transition between fuzzy sets, this from regions that belongs completely to a set to regions completely outside the set [27]. The MFs used in the present work are listed below.

- Triangular
- Trapezoidal

- Gaussian
- Sigmoidal
- Singleton

Triangular Membership Function

Is one of the simplest and most used MFs, is defined by three parameters $\{a, b, c\}$ and can present a symmetric or asymmetric shape. The mathematical formulation for a triangular MF is shown below.

$$\text{triangle}(x) = \begin{cases} 0 & x \leq a \\ \frac{(x-a)}{(b-a)} & a \leq x \leq b \\ \frac{(c-x)}{(c-b)} & b \leq x \leq c \\ 0 & x \geq c \end{cases} \quad (3.3)$$

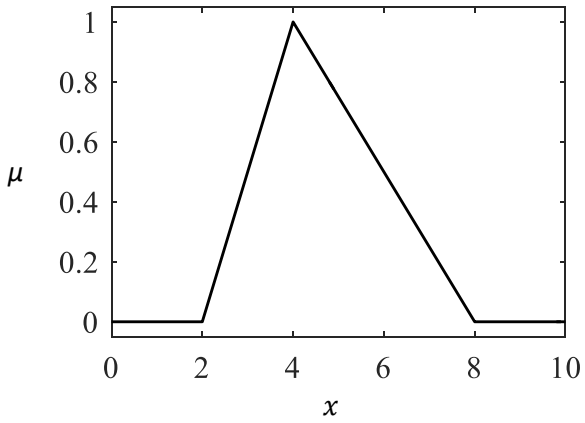

Fig. 3.3 Triangular membership function

Where a, b and c are the vertices of the triangle. In Fig. 3.3 a triangular MF defined by the parameters $a = 2$, $b = 4$ and $c = 8$ is shown.

Trapezoidal Membership Function

A trapezoidal membership is similar to a truncate triangular MF, it can present a symmetric or asymmetric shape and is define by four parameters $\{a, b, c, d\}$. The mathematical formulation for a trapezoid MF is shown below.

$$\text{trapezoid}(x) = \begin{cases} 0 & x < a \\ \frac{(x-a)}{(b-a)} & a \leq x \leq b \\ 1 & b \leq x \leq c \\ \frac{(d-x)}{(d-c)} & b \leq x \leq c \\ 0 & x \geq d \end{cases} \quad (3.4)$$

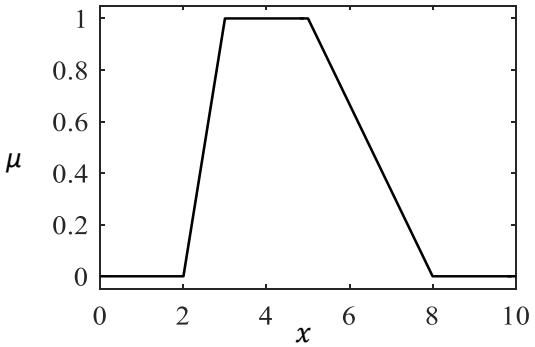

Fig. 3.4 Trapezoidal membership function

Where a, b, c and d are the vertices of the trapezoid. In Fig. 3.4 a trapezoid MF defined by the parameters $a = 2$, $b = 3$, $c = 5$ and $d = 8$ is shown

Gaussian Membership Function

Gaussian membership function presents a symmetric shape, is defined by two parameters $\{m, \sigma\}$, the mathematical formulation for a Gaussian MF is shown below.

$$\text{gaussian}(x) = \exp\left(-\frac{(x-m)^2}{2\sigma^2}\right) \quad (3.5)$$

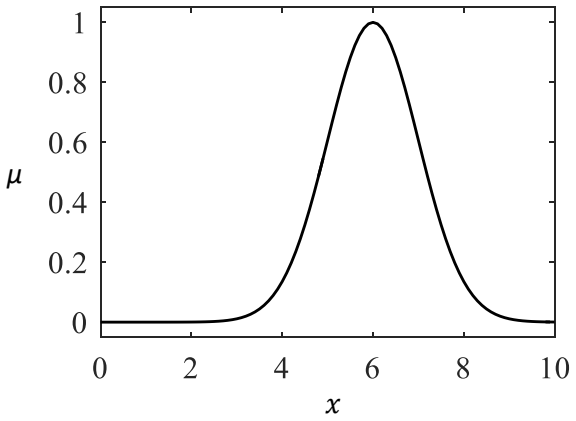

Fig. 3.5 Gaussian membership function

Where m is the center and σ is the width of the function. In Fig. 3.5 a Gaussian MF defined by the parameter $m = 6$ and $\sigma = 1$ is shown.

Sigmoidal Membership Function

The sigmoidal MF can be symmetrical or asymmetrical and can be open to the right or left [29]. Sigmoidal function is defined by two parameters $\{a, b\}$. The mathematical formulation for a sigmoidal MF is shown next.

$$\text{sigm}(x) = \frac{1}{1 + \text{e}^{-a(x-b)}} \quad (3.6)$$

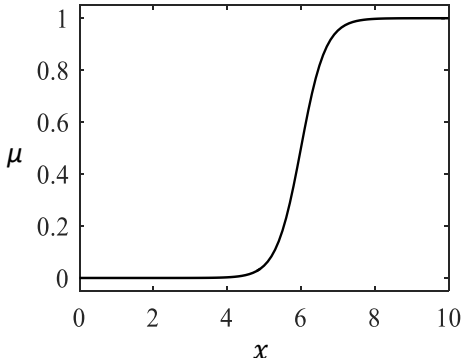

Fig. 3.6 Sigmoidal membership function

For all the different types of sigmoid MFs at the membership value $\mu = 0.5$ the inflection point occurs. In Fig. 3.6 a sigmoid MF defined by the parameters $a = 3$ and $b = 6$ is shown.

Singleton Membership Function

This MF has is defined by just one parameter $\{a\}$, the membership value of the singleton is 1 at a and 0 elsewhere. The mathematical formulation for a singleton MF is shown below.

$$\text{singleton}(x) = \begin{Bmatrix} 1 & x = a \\ 0 & x \neq a \end{Bmatrix} \quad (3.7)$$

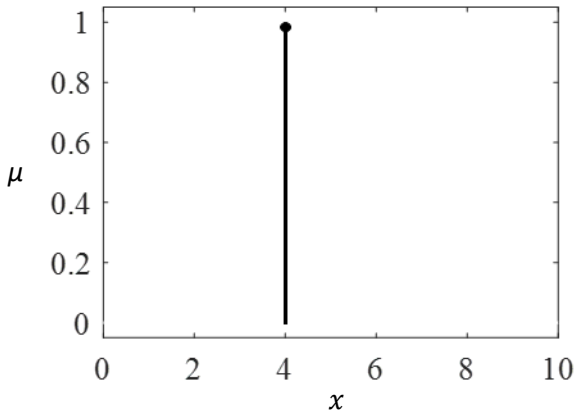

Fig. 3.7 Singleton membership function

The singleton is the simplest MF usually used in the consequent part of fuzzy rules in Sugeno systems; this will be explained in later sections. In Fig. 3.7 a singleton defined by the parameter $a = 4$ is shown. Despite all the types of MFs presented in this section, is recommended, in order to solve practical problems, to limit the use of these MFs to one or two types per application, this consideration is enough to solve most problems [29].

3.2 Basic operations in fuzzy sets

Fuzzy sets can be viewed as a generalization of classical sets; in similar way, the operations applied to classical sets can be generalized to be applied to fuzzy sets. The basic classical sets operations are intersection, union and complement, this operations correspond to the logical operators AND, OR, NOT [24]. In the same line, the fuzzy intersection, union and complement correspond mathematically to the fuzzy operators AND, OR, NOT. Consider the universe of discourse x and two fuzzy sets *A* and *B* each defined by Gaussian MFs as shown in eq. 3.8 and 3.9, the sets are shown in Fig. 3.8

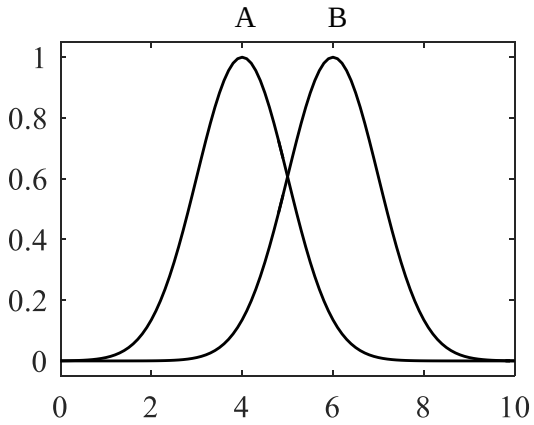

Fig. 3.8 Two arbitrary fuzzy sets

$$\mu_{\mathrm{A}}(x) = \exp\left(-\frac{(x-m)^2}{2\sigma^2}\right)\Big|_{m=4,\sigma=1} \quad (3.8)$$

$$\mu_{\mathrm{B}}(x) = \exp\left(-\frac{(x-m)^2}{2\sigma^2}\right)\Big|_{m=6,\sigma=1} \quad (3.9)$$

The union of the sets gives as result the elements that belong to either A or B. the operation is denoted by A ∪ B, in this case the max operator was used to compute the union as can be seen in eq. 3.10.

$$\mu_{\mathrm{A}\cup\mathrm{B}}(x) = \mu_{\mathrm{A}}(x) \vee \mu_{\mathrm{B}}(x) = \max\big(\mu_{\mathrm{A}}(x), \mu_{\mathrm{B}}(x)\big) \quad (3.10)$$

The intersection of the sets gives as result the elements shared by both sets. The operation is denoted by A ∩ B. To compute the intersection the min operator was used as shown in eq. 3.11.

$$\mu_{\mathrm{A}\cap\mathrm{B}}(x) = \mu_{\mathrm{A}}(x) \wedge \mu_{\mathrm{B}}(x) = \min(\mu_{\mathrm{A}}(x), \mu_{\mathrm{B}}(x)) \quad (3.11)$$

The complement or negation operation of one set correspond to difference between 1 and the MF of the set as shown in eq. 3.12.

$$\mu_{\overline{\mathrm{B}}}(x) = 1 - \mu_{\mathrm{B}}(x) \quad (3.12)$$

3.2.1 T-norms and S-norms

In the previous section the union and intersection operations were performed using the min and max operators, however there are not the only pairs of operators that can be used to perform conjunction and disjunction in fuzzy sets [24]. The triangular norms (T-norms) are the collection of operators intended to compute conjunction, while triangular conorms (S-norms) are the operators intended to perform disjunction. Once a conjunction operator is selected the selection of the disjunction operator must ensure logical duality between both [27]. To ensure logical duality between T-norms and S-norms the following condition must be satisfied.

$$1 - t\big(\mu_{\mathrm{A}}(x), \mu_{\mathrm{B}}(x)\big) = s\left(\big(1 - \mu_{\mathrm{A}}(x)\big), \big(1 - \mu_{\mathrm{B}}(x)\big)\right) \quad (3.13)$$

In fact, an S-norm can be computed from a T-norm and vice versa using eq. 3.13.

3.2.2 Fuzzy set properties

Like in classical sets theory, fuzzy sets present some properties important to mention. Considering three fuzzy sets A, B and C the following properties can be established [24].

Double negation	Idempotency	Commutativity
$\overline{(\bar{A})} = A$	$A \cup A = A$ $A \cap A = A$	$A \cap B = B \cap A$ $A \cup B = B \cup A$
Associative laws	**Distributive laws**	**Absorption**
$(A \cup B) \cup C = A \cup (B \cup C)$ $(A \cap B) \cap C = A \cap (B \cap C)$	$A \cup (B \cap C) = (A \cup B) \cap (A \cup C)$ $A \cap (B \cup C) = (A \cap B) \cup (A \cap C)$	$A \cap (A \cup B) = A$ $A \cup (A \cap B) = A$

De Morgan's Laws

$$\overline{(A \cup B)} = \bar{A} \cap \bar{B}$$
$$\overline{(A \cap B)} = \bar{A} \cup \bar{B}$$

All these properties can be expressed using the MFs of the sets A, B, C [29].For example, the associative laws can be rewritten as follows:

$$\big(\mu_{\mathrm{A}}(x) \vee \mu_{\mathrm{B}}(x)\big) \vee \mu_{\mathrm{C}}(x) = \mu_{\mathrm{A}}(x) \vee \big(\mu_{\mathrm{B}}(x) \vee \mu_{\mathrm{C}}(x)\big) \quad (3.14)$$

$$\big(\mu_{\mathrm{A}}(x) \wedge \mu_{\mathrm{B}}(x)\big) \wedge \mu_{\mathrm{C}}(x) = \mu_{\mathrm{A}}(x) \wedge \big(\mu_{\mathrm{B}}(x) \wedge \mu_{\mathrm{C}}(x)\big) \quad (3.15)$$

In addition, the expressions above can be computed using any pair con T-norm and S-norm for the AND and OR operators. In eq. 3.16 and 3.17 the min and max operators were used for the associative laws.

$$\max\left(\max\big(\mu_{\mathrm{A}}(x), \mu_{\mathrm{B}}(x)\big), \mu_{\mathrm{C}}(x)\right) = \max\left(\mu_{\mathrm{A}}(x), \max\big(\mu_{\mathrm{B}}(x), \mu_{\mathrm{C}}(x)\big)\right) \quad (3.16)$$

$$\min\left(\min\big(\mu_{\mathrm{A}}(x), \mu_{\mathrm{B}}(x)\big), \mu_{\mathrm{C}}(x)\right) = \min\left(\mu_{\mathrm{A}}(x), \min\big(\mu_{\mathrm{B}}(x), \mu_{\mathrm{C}}(x)\big)\right) \quad (3.17)$$

3.3 Fuzzy rules

Fuzzy rules are a powerful tool that allow fuzzy systems to capture human knowledge that present some implicit vagueness [24], usually this "imprecise" knowledge involves the behavior of complex processes. Two types of fuzzy rules can be mentioned, fuzzy implication rules and fuzzy mapping rules, being the last one the most interesting for the present work. A set of fuzzy mapping rules allow to approximate an unknown mathematical function that express an nonlinear input-output relation [7, 27]. Each rule of the set work in some region of the global response of the approximate function, in other words, every single rule gives a partial conclusion (local model) regarding the input data. The combination of the partial conclusions gives the global output of the fuzzy system.

3.3.1 Antecedent and consequent of fuzzy rules

A fuzzy rule is expressed in the form *IF {antecedent} THEN {consequent}*. The antecedent also known as "if part" defines a condition that can be satisfied to certain degree, while the consequent, also known as "then part", represented a conclusion derived from the compliance of the condition of the rule. Considerer the next example rule intended to represent certain operative condition in an EAF:

IF Shell Vibration is *High* THEN Arc Coverage Level is *Low*

Where the linguistic variables *High* and *Low* can be modeled using MFs such triangular, Gaussians or any type of the described at the beginning of this chapter. The antecedent of a rule can be constructed combining multiple simple conditions using the logic operators AND, OR, NOT [27], for example:

IF Shell Vibration is *High* AND Power Level is *Low* THEN Arc Coverage Level is *Medium*

To compute the logic operator in the antecedent of a fuzzy rule any pair of T-norm and S-norm can be selected. However, some pairs of T-norms and S-norms can work better for certain problem.

3.4 Recommendation for the design of MFs

Consider the fuzzy sets $\mathrm{B}_i, \mathrm{B}_j, \mathrm{B}_k$ for the input variable x as shown in Fig. 3.9, some recommendations regarding the design of antecedent MFs are:

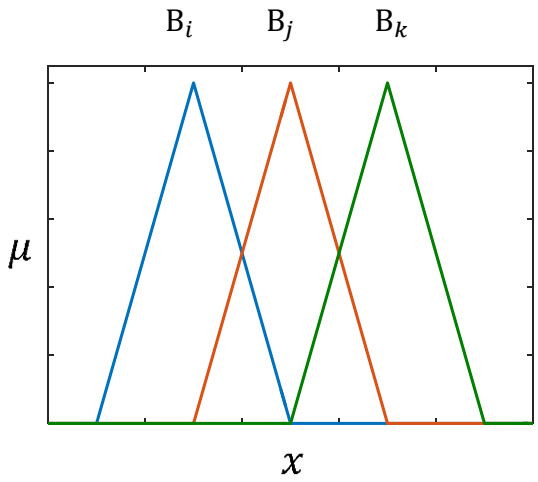

Fig. 3.9 Triangular membership functions for an arbitrary input

- The overlaps must occur only between the closest MFs, with this in mind the intersection between B_i and B_k is formally expressed as:

$$B_i \cap B_k = \emptyset \quad (3.18)$$

- An input x triggers more than one MF, therefore for any input there are relevant MFs whose values must sum nearly one [27], this is formally expressed as follows:

$$\mu_{B_i}(x) + \mu_{B_j}(x) + \mu_{B_k}(x) \cong 1 \quad (3.19)$$

- A good practice to develop an application is using symmetrical MFs unless there is a good reason to choose asymmetric MFs

Respect the consequent of fuzzy rules, three principal types can be mentioned [27], these are:

- Fuzzy consequent: IF…THEN y is B_i, where B_i is a fuzzy set
- Crisp consequent: IF…THEN $y = a$, where a is a numeric value
- Functional consequent: IF x_1 is B_i AND x_2 is B_j THEN $y = a_0 + a_1 \times x_1 + a_2 \times x_2$, where a_0 to a_2 are constants

Fuzzy consequents are used in Mamdani models, while functional and crisp consequents are used in Takagi-Sugeno-Kang systems, these models will be described in next sections.

3.5 Fuzzy Rule based system

A fuzzy rule base system (FRB) allows the mapping of input and output spaces using a set of fuzzy rules. The set of rules contain knowledge about a process and can be seen as a processing unit. To

obtain a conclusion from inputs through the set of rules an inference algorithm must be performed. The most used algorithm in fuzzy logic applications is known as fuzzy rule-based inference which consists of four steps [24, 27] which are detailed below.

1. Fuzzy Matching or fuzzification: In this step, a numeric input is transformed into a fuzzy statement**.** Here is calculated the degree to which the input data match the antecedent of the fuzzy rules (membership degree), then the firing strength of each rule is obtained computing the rule's logic operators.

2. Inference: Here is calculated the conclusion of each rule, to do this the consequent MF of the rules is affected by the firing strength previously obtained.

3. Combination: In this step a general conclusion (global output of the system) is obtained from the combination of the partial conclusions of each rule.

4. Defuzzification: here a non-fuzzy output is obtained for control purposes or additional processing.

As can be expected there are multiple mathematical tools and operators to perform the different steps of the algorithm. We will refer to a specific set of tools as fuzzy model. There are three basic fuzzy models: Mamdani, Larsen and Takagi-Sugeno-Kang (TSK), they are discussed in the next section.

3.5.1 Mamdani Model

Mamdani model was the first fuzzy rule-based system developed, the model can accept crisp inputs which are subjected to fuzzification [28], or accept fuzzy inputs directly. In Mamdani model the rules present fuzzy consequents, the inference is computed through clipping method and the logic operator used are min and max. The structure of the rules in a Mamdani is described as follows:

R_i: IF x_1 is A_{i1} AND x_2 is A_{i2} AND… x_n is A_{in} THEN y is C_i

Where the subscript i denote the rule number, the variables x_1 to x_n are crisp inputs to the model, A_{i1} to A_{in} are the relevant fuzzy sets of the antecedent part, C_i is the fuzzy consequent of the rule. Once a set of inputs enters to the model, fuzzy matching is computed evaluating the inputs in the relevant MFs. The firing strength α_i of the rule is obtained applying the min operator over the membership values computed after fuzzy matching procedure.

$$\phi_i = \min\left(\mu_{A_{i1}}(x_1), \mu_{A_{i2}}(x_2), \dots, \mu_{A_{in}}(x_n)\right) \quad (3.20)$$

The inference of the rule is the computed by clipping method as follows:

$$\mu_{C_i^*}(y) = \min\left(\phi_i, \mu_{C_i}(y)\right) \quad (3.21)$$

Where $\mu_{C_i^*}(y)$ denote the clipped MF of the consequent part of the rule. The min operator perform the clipping procedure. The global output of the model is the combination of each rule inference using max operator as follows:

$$\mu_{\text{global}}(y) = \max\left(\mu_{C_1^*}(y), \mu_{C_2^*}(y), \dots, \mu_{C_n^*}(y)\right) \quad (3.22)$$

Finally, Mamdani model is flexible regarding the defuzzification method employed if needed. The most common defuzzification methods are listed below.

3.5.1.1 Defuzzification methods

Centroid

In this method is calculated the weighted average of the fuzzy distribution obtained after the combination procedure. If the output of the fuzzy system is defined by a discrete universe, a numeric example is shown in the next page; the centroid is calculated using eq. 3.23.

$$DO = \frac{\sum_i \mu_{global}(y_i) * y_i}{\sum_i \mu_{global}(y_i)} \quad (3.23)$$

Where DO denotes the defuzzified ouput.

In other hand if the output of the fuzzy system is defined by a continuous universe the centroid is calculated using eq. 3.24.

$$DO = \frac{\int \mu_{global}(y) * x \, dx}{\int \mu_{global}(y) \, dx} \quad (3.24)$$

Height method

This is a simplification of centroid method, first the heights at the midpoint of each MF that contribute to the output of the system are obtained, then centroid method is applied to this crisp height using the eq. 3.25.

$$DO = \frac{\sum_i h_i * y_i}{\sum_i h_i} \quad (3.25)$$

This method is often considered an approximation to the centroid defuzzification [27].

Mean of Maximum

In this method is calculated the average of the highest values of the fuzzy distribution obtained after the combination process, the defuzzied output is calculated with eq. 3.26.

$$DO = \frac{\sum_i^M y_{i_{max}}}{M} \quad (3.26)$$

Where $x_{i_{max}}$ denote the crisp values with highest membership of the output distribution, and M is the number of highest values.

3.5.1.2 Defuzzification examples

In order to illustrate the application of the different defuzzification formulas described previously, consider the arbitrary discrete fuzzy output shown in Fig. 3.10 whose crisp output is obtained using discrete centroid, height and mean of maximum method

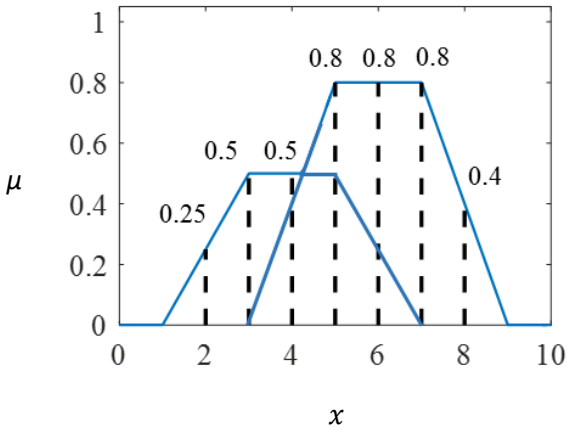

Fig. 3.10 Discrete fuzzy distribution

The values were chosen just for demonstrative purposes.

Discrete centroid

$$DO = \frac{2 * 0.25 + 3 * 0.5 + 4 * 0.5 + 5 * 0.8 + 6 * 0.8 + 7 * 0.8 + 8 * 0.4}{0.25 + 0.5 + 0.5 + 0.8 + 0.8 + 0.8 + 0.4} = 5.33 \quad (3.27)$$

Height method

$$DO = \frac{4 * 0.5 + 6 * 0.8}{0.5 + 0.8} = 5.23 \quad (3.28)$$

Mean of maximum

$$DO = \frac{5 + 6 + 7}{3} = 6 \quad (3.29)$$

As can be seen the three formulas compute similar results. When a fuzzy system is designed, the selection of the defuzzification method depends on the application.

3.5.2 Application example using Mamdani model

To show the workflow in a Mamdani model an application example is described. The goal of this example consists in represent how to estimate the risk level (*RL*) due to arc coverage during the operation of DC EAF. The *RL* is estimated measuring the vibrations (*VL*) in the furnace shell and the power levels (PL) during the melting process, this is schematized in Fig. 3.11.

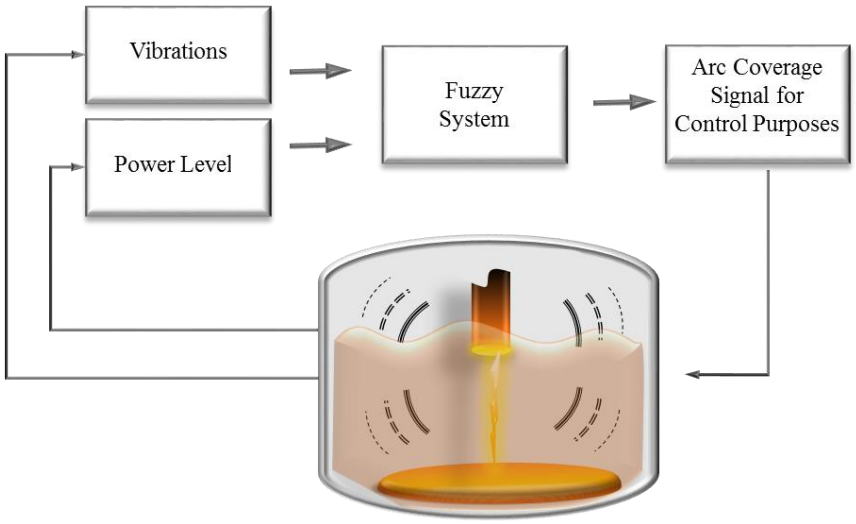

Fig. 3.11 Automation of a DC EAF using a fuzzy system

The rules to obtain the risk level based on vibrations and power level are shown next, these rules are just for demonstrative purposes.

R_1: IF *VL* is Low AND *PL* Low THEN *RL* is Safe

R_2: IF *VL* is Medium AND *PL* is Low THEN Arc *RL* is Normal

R_3: IF *VL* is High AND *PL* is Low THEN Arc *RL* is Normal

R_4: IF *VL* is Low AND *PL* is Medium THEN Arc *RL* is Safe

R_5: IF *VL* is Medium AND *PL* is Medium THEN *RL* is Normal

R_6: IF *VL* is High AND *PL* is Medium THEN *RL* is Caution

R_7: IF *VL* is Low AND *PL* is High THEN *RL* is Safe

R_8: IF *VL* is Medium AND *PL* is High THEN *RL* is Caution

R_9: IF *VL* is High AND *PL* is High THEN Arc *RL* is Caution

R_{10}: IF *VL* is Low AND *PL* is Ultra-High THEN *RL* is Safe

R_{11}: IF *VL* is Medium AND *PL* is Ultra-High THEN *RL* is Caution

R_{12}: IF *VL* is High AND *PL* is Ultra-High THEN *RL* is Danger

The membership functions for the input variables are shown in Fig. 3.12. a) and b), while the membership functions for the output is shown in Fig. 3.12 c).

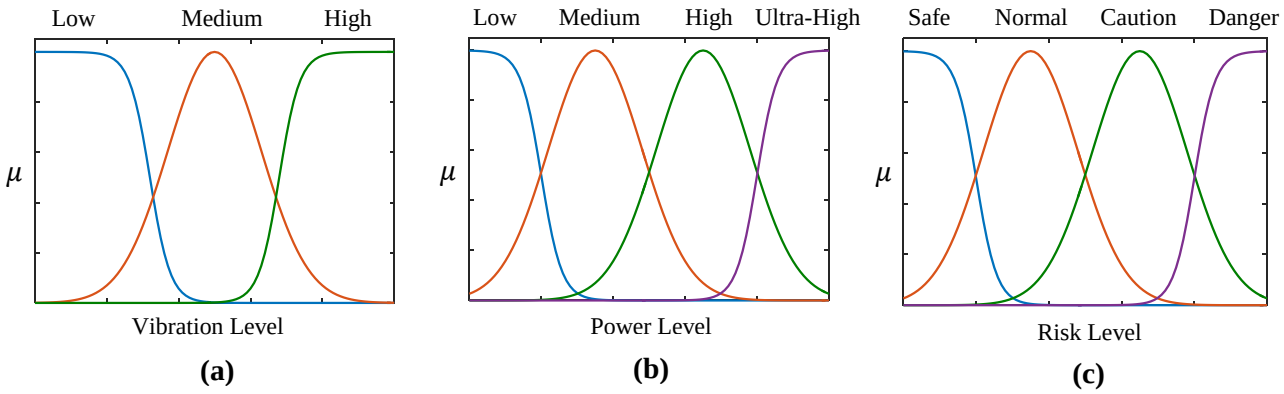

Fig. 3.12 Membership functions for a) vibration level, b) power level and c) risk level

Is important to mention that in this example the membership functions were arbitrary selected as Gaussian and Sigmoidal just for demonstrative purposes.

Fuzzy Matching

Suppose that at certain moment of the melting process measures of vibration and power are carried out. In the fuzzy matching stage, the inputs are fuzzified using the corresponding membership functions as is shown in the Fig. 3.13.

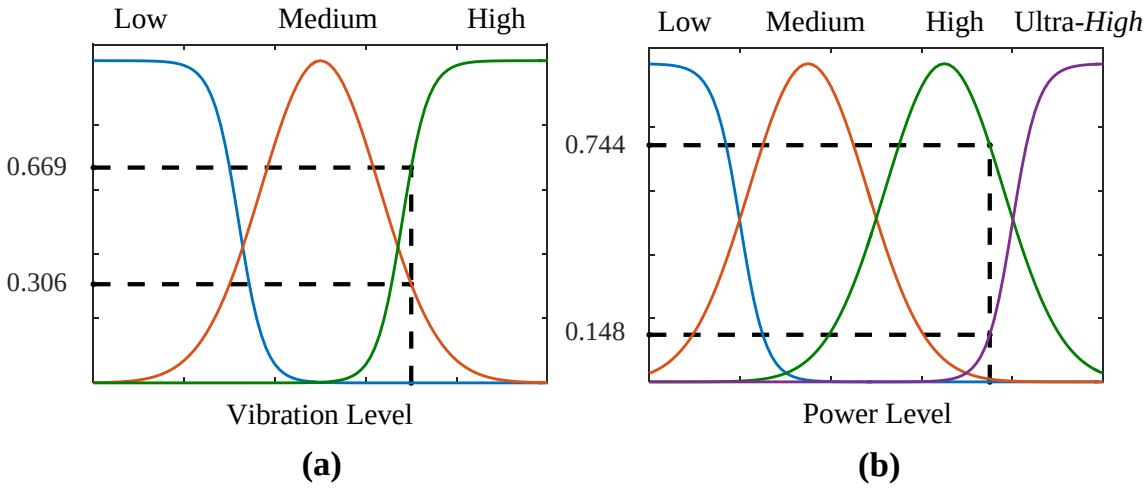

Fig. 3.13 Fuzzy matching procedure for certain a) vibration level and certain b) power level

Note how in this case the membership values do not sum up to 1 but sum up to values near 1 as explained in the recommendations of section 3.4, specifically in eq. 3.19. For the given inputs, the MFs intersected are relevant for the rules 8,9,11 and 12.

R_8: IF *VL* is Medium AND *PL* is High THEN *RL* is Caution

R_9: IF *VL* is High AND *PL* is High THEN Arc *RL* is Caution

R_{11}: IF *VL* is Medium AND *PL* is Ultra-High THEN *RL* is Caution

R_{12}: IF *VL* is High AND *PL* is Ultra-High THEN *RL* is Danger

The next step consists in compute the conjunction AND of the relevant rules, this in order to obtain the degree to which the input data match the antecedents (firing strength). To perform the conjunction AND the min operator is applied over the fuzzified input data, the result gives the firing strengths of the relevant rules as follows:

$$\phi_8 = \min\left(\mu_{\text{Medium}}(VL), \mu_{\text{High}}(PL)\right) = \min(0.306, 0.744) = 0.306 \quad (3.30)$$

$$\phi_9 = \min\left(\mu_{\text{High}}(VL), \mu_{\text{High}}(PL)\right) = \min(0.669, 0.744) = 0.669 \quad (3.31)$$

$$\phi_{11} = \min\left(\mu_{\text{Medium}}(VL), \mu_{\text{ultra-High}}(PL)\right) = \min(0.306, 0.148) = 0.148 \quad (3.32)$$

$$\phi_{12} = \min\left(\mu_{\text{high}}(VL), \mu_{\text{ultra-High}}(PL)\right) = \min(0.669, 0.148) = 0.148 \quad (3.33)$$

These firing strengths are used in the next step to compute the partial conclusions of the relevant rules.

Inference

In the inference step are obtained the partial conclusions of the rules 8, 9 11 and 12. The consequent MFs of each rule is clipped according to its previously calculated firing strength. To perform the clipping procedure the min operator is used as shown in eq. 3.34 to eq. 3.37, the Fig. 3.14 shows the clipped MFs.

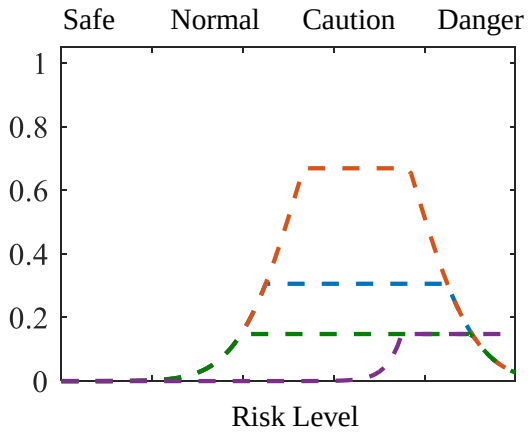

Fig. 3.14 Clipped MFs after inference procedure

$$\mu_{\text{Caution}_8^*}(CL) = \min\left(\phi_8, \mu_{\text{Caution}}(CL)\right) \quad (3.34)$$

$$\mu_{\text{Caution}_9^*}(CL) = \min\left(\phi_9, \mu_{\text{Caution}}(CL)\right) \quad (3.35)$$

$$\mu_{\text{Caution}_{11}^*}(CL) = \min\left(\phi_{11}, \mu_{\text{Caution}}(CL)\right) \quad (3.36)$$

$$\mu_{\text{Danger}_{12}^*}(CL) = \min\left(\phi_{12}, \mu_{\text{Danger}}(CL)\right) \quad (3.37)$$

Combination

In Mamdani model the combination of the partial conclusion is performed using the max operator over the clipped MFs, the procedure is carried out applying eq. 3.38. In Fig. 3.15 the global output of the Mamdani model is shown.

$$\mu_{\text{global}}(RL) = \max\left(\mu_{\text{caution}_8^*}(RL), \mu_{\text{caution}_9^*}(RL), \mu_{\text{caution}_{11}^*}(RL), \mu_{\text{Danger}_{12}^*}(RL)\right) \quad (3.38)$$

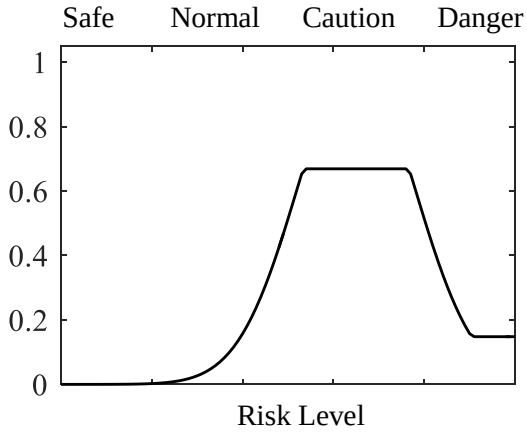

Fig. 3.15 Fuzzy output of the Mamdani model

In some applications, this fuzzy global output is enough to satisfice some working criteria, however an extra step can be performed if a crisp output is required.

Defuzzification

In this case, the discrete centroid was applied to the global fuzzy output shown in Fig. 3.16, which gives as result the crisp value shown in in the red line of Fig. 3.16.

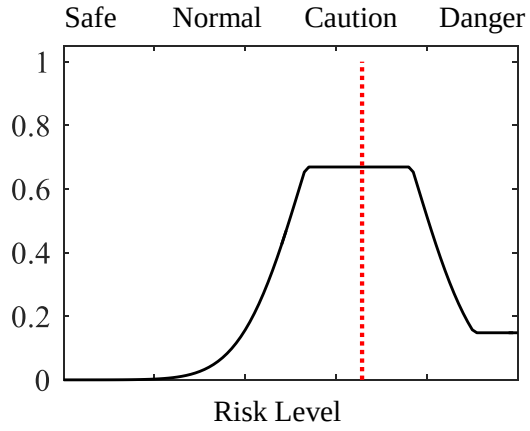

Fig. 3.16 Crisp output after defuzzification

3.5.3 Larsen Model

This model is similar to Mamdani model; it only differs in the way that the inference step is performed. The structure of the rules, the pairs of T-norms and S-norms and the defuzzification methods are the same as in Mamdani model. In this method, the MFs of the consequents are scaled down in proportion to firing strength of the rules, instead of being clipped as in Mamdani model [27, 29]. The inference of a rule is computed by scaling method as follows:

$$\mu_{C_i^*}(y) = \phi_i * \mu_{C_i}(y) \quad (3.39)$$

Where $\mu_{C_i}(y)$ and ϕ_i are the consequent MF and the the firing strength of the rule respectively. The scaled MF is represented by $\mu_{C_i^*}(y)$.

3.5.4 Takagi-Sugeno-Kang (TSK) Model

This model was introduced one decade after the Mamdani model, the inputs to this model are crisp and the rules present functional consequents, this allow to reduce the number of rules needed, in comparison with Mamdani model. Typically, the rule consequent is a linear equation, which parameters are the input variables of the fuzzy model. Each rule is a local linear model that approximate a nonlinear function in some interval, this is similar to piecewise linear approximation, with the difference that in fuzzy models the transition between local models is gradual [27]. The structure of the rules in TSK model id described as follows

R_i: IF x_1 is A_{i1} AND x_2 is A_{i2} AND x_n is A_{in} THEN $y = f_i(x_1, x_2, \dots, x_n)$ (3.40)

Where the subscript i denote the rule number, the variables x_1 to x_n are crisp inputs to the model, A_{i1} to A_{in} are the relevant fuzzy sets respect each input, f_i is the functional consequent of the rule. Typically, the linear function adopts the form:

$$f_i(x_1, x_2, \dots, x_n) = c_{i0} + c_{i1}x_1 + \dots + c_{in}x_n \quad (3.41)$$

where $c_{i0}\ to\ c_{in}$ are constants.

The firing strength of the relevant rules can be obtained in the same way as Mamdani model, this is applying the min operator over the membership values computed after fuzzy matching step.

$$\phi_i = \min\left(\mu_{A_{i1}}(x_1), \mu_{A_{i2}}(x_2), \dots, \mu_{A_{in}}(x_n)\right) \quad (3.42)$$

The firing strength can be also computed using the product operator as follows:

$$\phi_i = \mu_{A_{i1}}(x_1) \times \mu_{A_{i2}}(x_2) \times \dots \times \mu_{A_{in}}(x_3) \quad (3.43)$$

In TSK model the firing strengths of the rules becomes weights to perform an interpolative process that gives the global output of the model. Let L be the number of local linear models, the global output of the TSK model is defined as follows:

$$y = \frac{\sum_{i=1}^{L} \phi_i \left(c_{i0} + c_{i1}x_1 + \dots + c_{in}x_n\right)}{\sum_{i=1}^{L} \phi_i} \quad (3.44)$$

For demonstrative purposes suppose that the parameters of the MFs and the linear equations are established, the behavior of a TSK model is shown in Fig. 3.17.

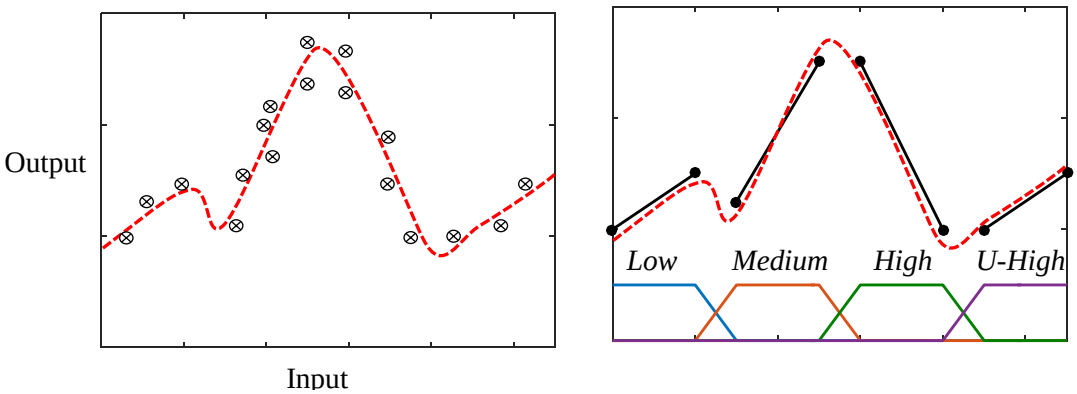

Fig. 3.17 Behavior of a TSK model

The use of linear models in the consequent part of the rules allow reducing the number of rules needed to capture the behavior of a complex nonlinear process. To implement an order one TSK model for mapping purposes, some input-output measures of the process are needed. The input-output data allow constructing the local linear models that fits better the data along the different working regions. When a direct measure of the process output is not available an order zero TSK model can be implemented. Here the consequent of the rules are constant values, this is $f_i = c_{i0}$. Finally, the crisp output of the system is computed as follows:

$$y = \frac{\sum_{i=1}^{L} \phi_i c_{i0}}{\sum_{i=1}^{L} \phi_i} \quad (3.45)$$

As can be noted in eq. 3.45 an order zero TSK the defuzzification procedure is carried out using height method shown before in eq. 3.25. For the TSK model is recommended to identify its parameters using learning algorithms.

Chapter 4. Vibration measurements

Vibration is an indirect variable of the melting process that gives relevant information regarding the arc coverage level. A first approach indicates that when the electric arc inside the furnace is well covered by metallic scrap or foamy slag, the vibrations in the equipment are less intense in comparison with the operation of the furnace with fully uncovered or poorly covered electric arcs. [3, 20, 23]. This occurs because the scrap and the slag attenuated the acoustic pressure before it can reach the furnace walls. In Fig. 4.1 is schematized the attenuation in different scenarios.

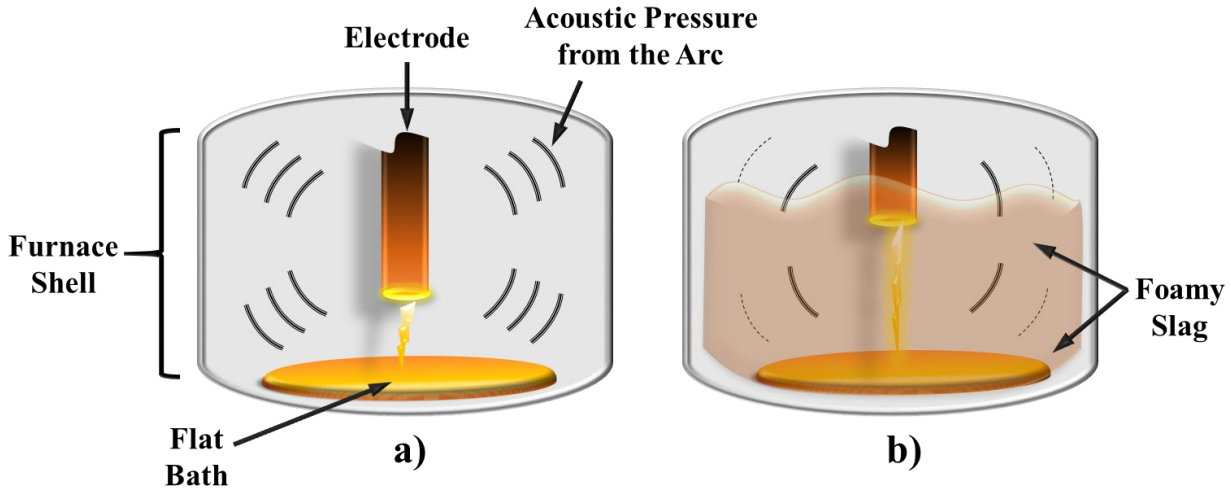

Fig. 4.1 Damping of vibrations in the furnace shell a) uncovered arc, b) covered arc with foamy slag

Nevertheless, as said before vibrations are an indirect variable. In order to have sufficient information to determine whether the electric arc has emitted radiation to the walls or not monitoring of electrical variables is necessary too [20], this will be detailed in further sections of the present work. Vibration has been studied more extensively in AC EAFs, however, few studies can be found in literature regarding vibration measurements in DC EAFs. To validate that vibrations indeed gives good information in DC operation, a measurement campaign was planned in Ternium Guerrero plant, specifically in the Fuchs EAF.

4.1 Vibration measurement equipment Polytec CLV-2534-2

To perform first measurement campaign the CLV-2534-2 vibrometer from Polytec was used. The equipment features a low power helium-neon laser, which must strike a reflective surface solid mounted on the vibrating object, the measurement is made by a heterodyne interferometer.

Depending on the speed of the vibrating object and the amplitude of its movement, a frequency modulation is generated over the laser due to Doppler Effect. The modulated signal enters to a demodulator whose output is feed to a filter, the filter provides a voltage output proportional to the instantaneous velocity of the vibrating object. The voltage output is positive when the object moves towards the sensor head and negative when it moves in the opposite direction [30]. In Fig. 4.2 the laser vibrometer is shown inside the steel shop.

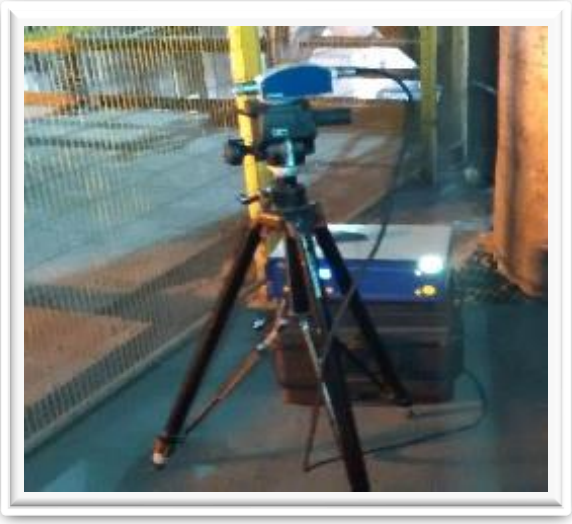

Fig. 4.2 Laser vibrometer at the steel shop

4.1.1 CLV-2534-2 tests

Remember that the fuzzy model proposed in this work consist of three inputs that are vibration, electric power and temperature slope. Of all of them, the most difficult variable to measure is vibration. For the first measuring campaign the CLV-2534-2 vibrometer was used, the equipment allow measure without direct contact of the sensor with the EAF, allowing to work at a safe distance, far away from the heat of the molten steel. The same equipment was use in [31] in order to measure the vibrations in an AC EAF. In Fig. 4.3 a representation of the signal path of the laser vibrometer is shown.

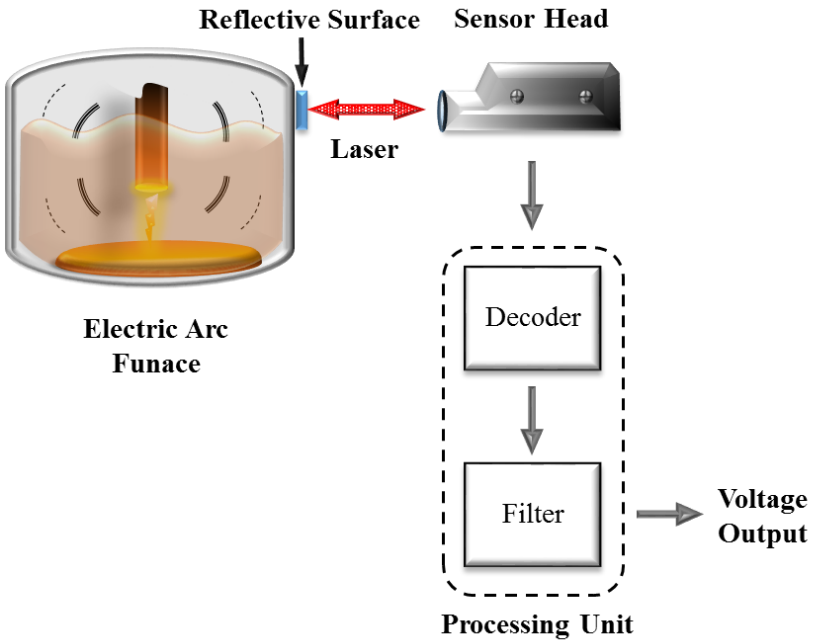

Fig. 4.3 Representation of the signal path of the laser vibrometer

There are two types of filter available in the equipment, the first one is a low pass filter that have got third order Bessel characteristics, the second one is a 4th order Butterworth high pass filter. The output signal takes values from 10 V to -10 V. The broadband velocity decoder is universally suitable for applications in the frequency range from 0.5 Hz to 3.2 MHz The three measurement ranges 10 mm/s/V, 100 mm/s/V and 1000 mm/s/V cover most technical applications, being the first one the used to perform the measurement in the EAF. The vibrometer was placed inside a security cage from where the laser can be aimed to the furnace. A cable must be installed from the security cage to the operator's cabin, where the acquisition system was placed. In Fig. 4.4 the placement of the laser vibrometer is shown.

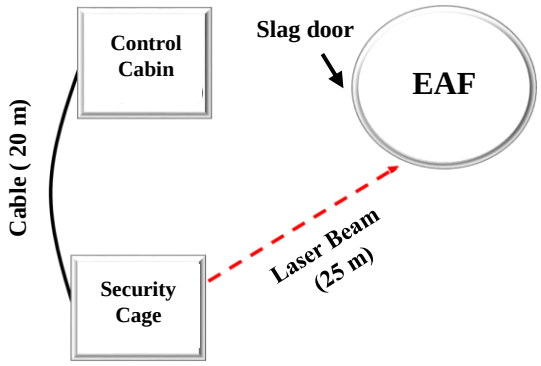

Fig. 4.4 Vibrometer placement inside the steel shop

It was important to check that the cable did not suffer any damage during the installation; to do this a signal generator was placed at the security cage. A Triangular signal of 100 Hz was generated and acquired at the operator's cabin, the spectrum of the signal was also obtained. The acquisition test was successful, there was not attenuation in the signal as can be seen in Fig. 4.5. In addition, there was not significant noise in the signal even with the EAF working.

.

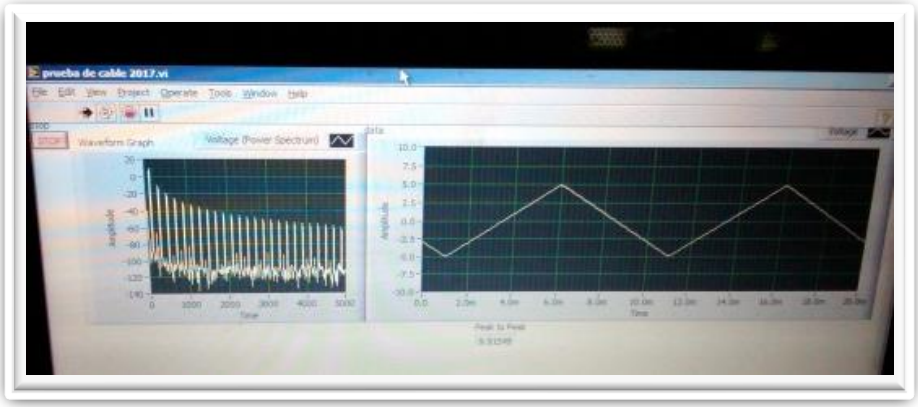

Fig. 4.5 Processing of the acquired signal

As said before for the operation of the CLV vibrometer, a reflective surface must be mounted on the furnace shell. In order to ensure a successful measure. Two materials were chosen to perform the test, reflective fabric with micro spheres and high intensity prismatic vinyl. Fig. 4.6 a) shows the reflective fabric, while Fig. 4.6 b) shows the prismatic vinyl.

a) **b)**

Fig. 4.6 Reflective materials a) micro spheres fabric, b) prismatic vinyl

These materials were glued to powerful magnets as shown in Fig. 4.7, this in order to be mounted at the EAF shell in a quick and efficient way.

Fig. 4.7 Reflective materials glued to the magnets

Multiple reflective points were placed in the EAF, this in order to determine the zone where the longer life span of the reflective surface occurs. The last is not a trivial activity because the heat, even outside the furnace, could destroy the reflective material. In addition, the measurement point must be visible from the security cage where the vibrometer is placed, the last limits the potential places to test the life span of the reflective material. The magnets were placed at the sell as it can be seen in Fig. 4.8, the picture was taken intentionally with flash, in order to show the reflective properties of the materials.

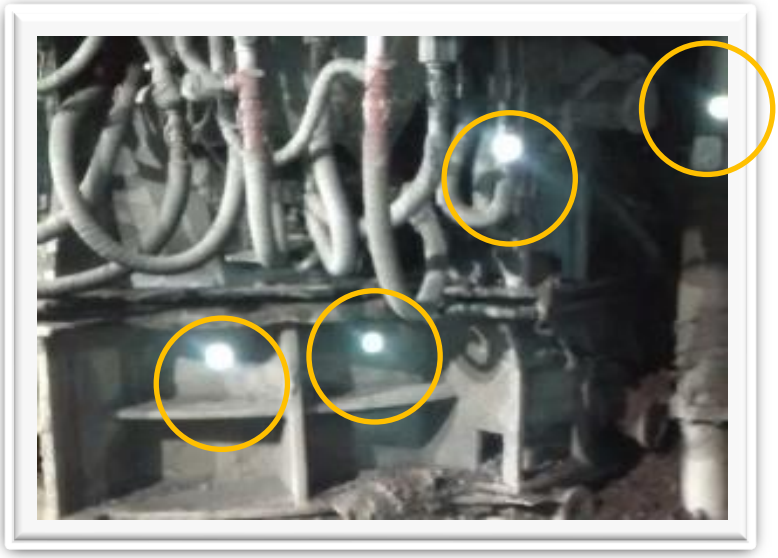

Fig. 4.8 Reflective magnets mounted in the EAF

After 24 hours, the reflective magnets were checked to validate that they maintained their properties. In Fig. 4.9 can be seen that the reflector mounted near the slag gate lost its reflective properties.

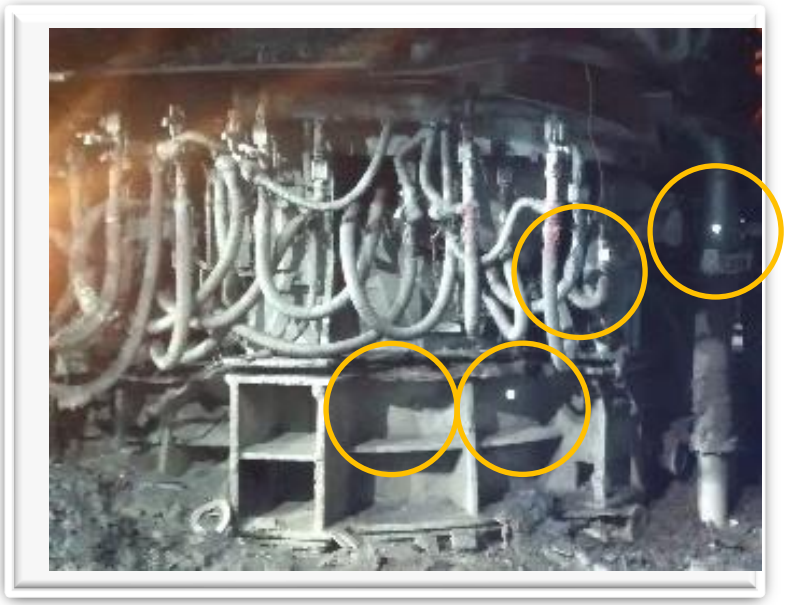

Fig. 4.9 Reflective magnets mounted in the EAF after 24 hours of operation

Three days later the laser vibrometer was taken to the steel shop, the acquisition system was installed in the operator's cabin. To test the proper operation of the vibrometer a speaker playing a sine signal of 500 Hz signal was measured with the laser. Once the proper operation of the vibrometer and the acquisition system was validated, the laser was focused to one of the reflective magnets previously installed at the EAF. Unfortunately, as days go by oxides and metallic particles were attracted to the magnets, covering a big part of the reflective surface as seen in Fig. 4.10.

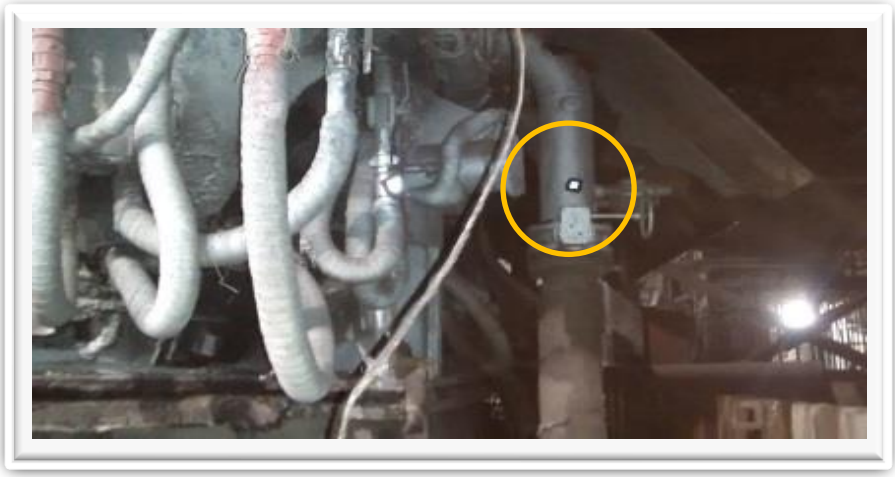

Fig. 4.10 Surface of the reflective magnet covered by metallic particles

Because of this the amount of light reflected to the sensor was really low, making it impossible to perform the measure. A new magnet with clean reflective material was prepared and mounted in the EAF shell, its location was over the pipe showed in Fig. 4.10. The reflected signal increases its quality significantly. However, the measurement cannot be performed uninterrupted because a scrap basket was placed in front of the security cage, blocking the laser. Despite the inconvenience of the scrap basket measurement proceeded at the moments when the basket was moved to charge the EAF. The intensity of the vibration signal was quantified with its RMS value, which was calculated at regular intervals. The sampling frequency of the vibration raw signal was 10 kHz hence every 0.1 ms a raw vibration sample was acquired, to perform the RMS calculation a LabVIEW block was used, the calculation is carry out using eq. 4.1.

$$x_{RMS} = \sqrt{\frac{1}{n}\sum_{i=0}^{n-1} \boldsymbol{x}_i^2} \qquad (4.1)$$

Where $\boldsymbol{x}$ is a vector that contains n number of samples. In this case, 1000 samples per RMS value obtained were used, in other words, each 0.1 s a value of RMS vibration is obtained. Fig. 4.11 shows a screenshot of the vibration signal an its RMS value during the boring period.

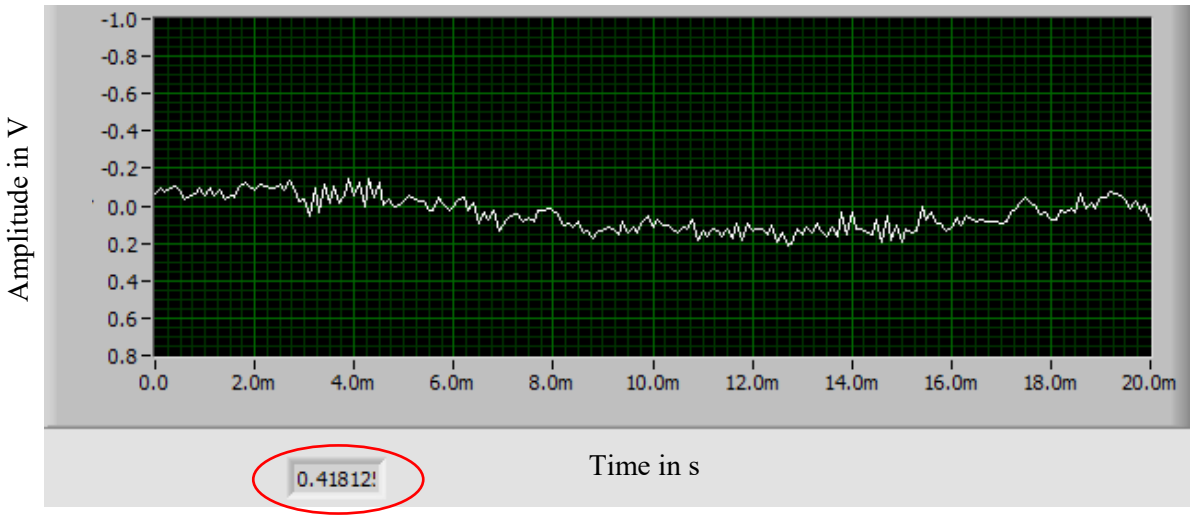

Fig. 4.11 Raw vibration signal and RMS value during boring period

Fig. 4.12 shows the same parameters once the boring period concludes, note how the vertical axis of both figures is different, this happened due to an auto scale mode activated in the acquisition platform when the measurement was done.

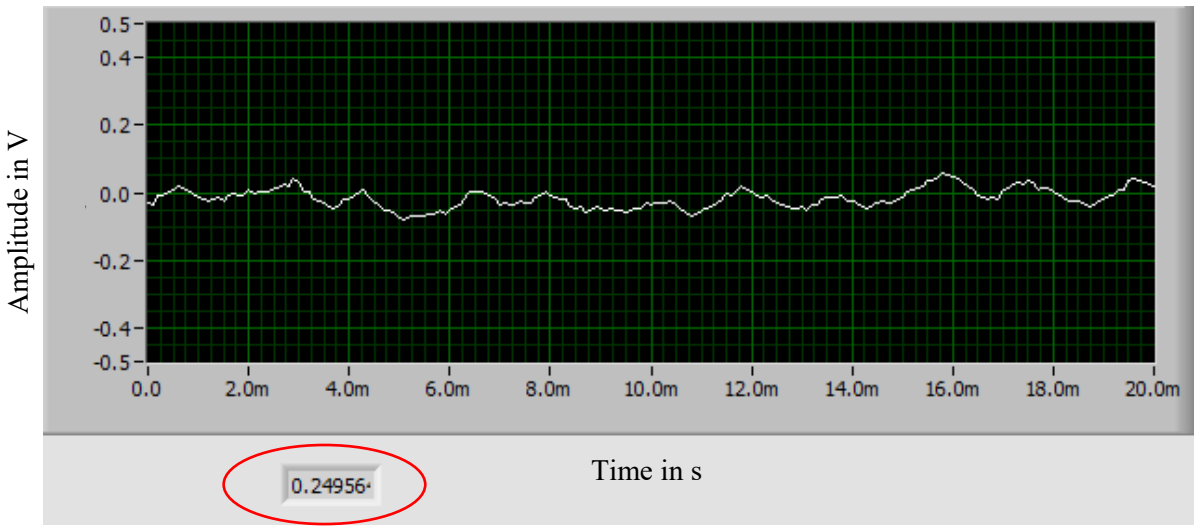

Fig. 4.12 Raw vibration signal and RMS value after boring period

As expected, vibration is less intense after the boring period, this basic test allows to prove that vibration in the EAF can be measure with the laser vibrometer, giving a good starting point for the subsequent experimental tests. In order to improve the following measurements, the high pass filter included in the vibrometer was added to the signal processing. The cut frequency was 100 Hz. The filter allows eliminating from the measurement, low frequency components (movements of the floor and steel shop structure) that do not give any useful information regarding the arc coverage level. The next step consisted in improve the reflective points to avoid excessive buildup of metallic particles over its surface, it also was important to talk with the crane operators to improve the scrap basket positioning issue previously mentioned. To improve the measurement a metallic plate was conditioned with the reflective materials (fabric and vinyl), then a pair of magnets was mounted at the rear of the plate, the arrangement is shown in Fig. 4.13. The green squares represent the magnets at the back of the plate. With this arrangement the majority of metallic particles are attracted to the top and bottom parts of the plate, where the magnets are placed, leaving the central region clean, this is possible because the plate is not strong magnetized in the central region.

Fig. 4.13 Reflective plate

To test the reflective plate, it was placed at approximately 20 meters away from the vibrometer, in a hall of the Tecnológico de Monterrey campus. The objective of this test was to validate that the reflection, at the working distance in the steel shop, is good enough to perform the experiments. The reflection when aiming to the plate was satisfactory. The laser equipment and the acquisition system were taken again to the steel shop to repeat the experiment, but in this case, using the reflective plate instead of the magnets alone. In order to avoid obstruction by the scrap basket, the laser vibrometer was placed in a new location outside the security cage as can be seen in Fig. 4.14 a), the metallic plate was placed in a visible spot from the new vibrometer location, this shown in Fig. 4.14 b).

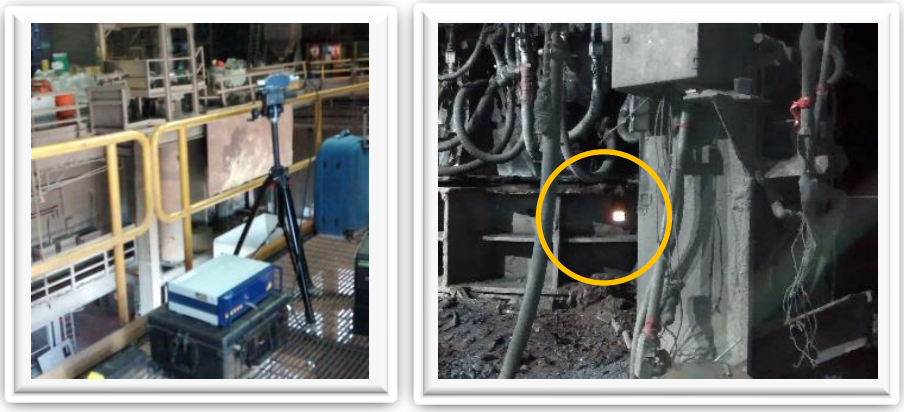

a) **b)**

Fig. 4.14 a) Vibrometer over unstable flor, b) Reflective plate mounted at the EAF

The new location for the vibrometer wasn't optimal due to the unstable floor under the laser emitter. Vibrations were induced when employees walk near the equipment affecting the measure. The laser vibrometer was taken to the security cage again, near its lateral border in order to avoid, as possible, obstructions due to the scrap basket. The laser emitter is shown in Fig. 4.15.

Fig. 4.15 Laser vibrometer inside the security cage

Despite the efforts to ensure that the level of reflection would be satisfactory during the test, this was not the case the reflection level was low. A screenshot of the vibration measurement during the test is shown in Fig. 4.16 and, as can be seen, a lot of noise and anomalous peaks are present in the signal

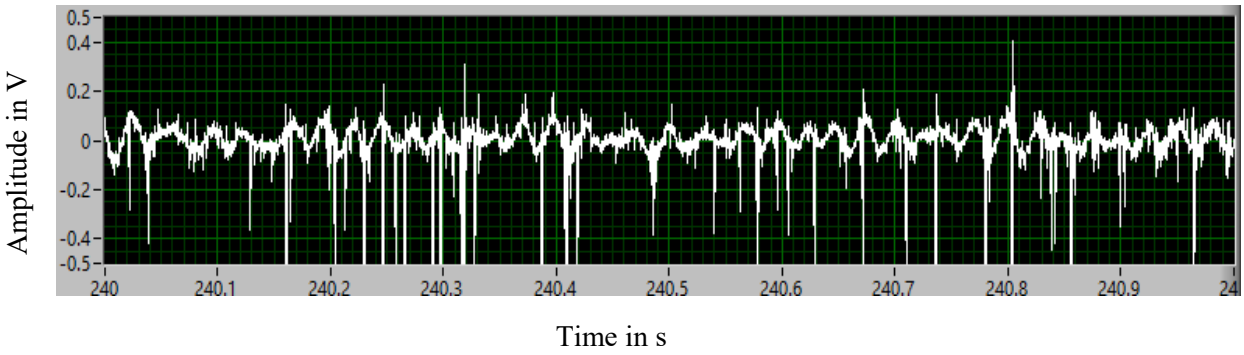

Fig. 4.16 Vibration signal under poor reflection conditions

The bad quality of the reflection, and therefore the noisy vibration signal, is attributed to two reasons. The first one is a partial obstruction of the laser originated by the cage bars, this occurs due to the close angle between the bars and the laser, this phenomenon can be seen in Fig. 4.17.

Fig. 4.17 Partial obstruction of the laser

Another factor that affects the measurement was the premature degradation of the prismatic vinyl due to high temperature, in Fig. 4.18 can be seen the plate after two days of being mounted in the EAF.

Fig. 4.18 Reflective material affected by high temperature

Despite the issues mentioned regarding the bad reflection, important information was obtained during the test. Even with noise in the signal, it was observed that, at the position where the plate was mounted, the vibration tended to be less intense in comparison with the measurement previously done, in which the magnet was placed at the cooled pipe. In fact, the plate was mounted under the slag level, while the magnet at the cooled pipe was placed over the slag level. This is an important observation, the following tests were performed measuring at positions over the slag level, where the vibration is better transmitted. Another important observation was that the reflective material of the magnet, placed at the cooled pipe, did not suffer damage, this despite being mounted at the EAF for several days. In Fig. 4.19 can be seen the reflective magnet after a quick cleaning of the surface.

Fig. 4.19 Intact reflective surface after several days mounted at the EAF

In order to performing a successful measurement, the reflective plate was placed at the cooled pipe, allowing to measure above the slag level, without exposing the prismatic vinyl to excessive heat.

In addition, the laser emitter was moved, and the operators shifted the scrap basket a few meters, in order to solve the issue regarding the security cage bars previously discussed. The laser focused to the plate at the refrigerated pipe is shown in Fig. 4.20.

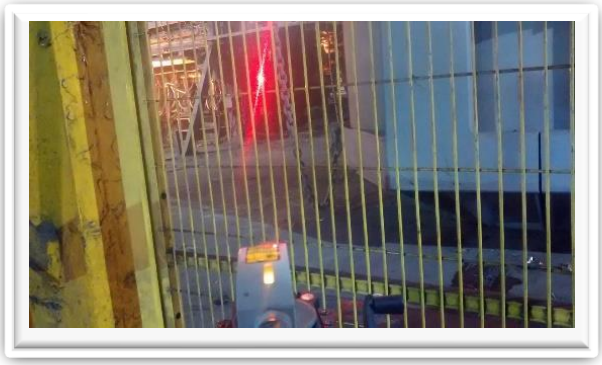

Fig. 4.20 Best configuration encountered to carry out the vibration measurement

The led indicator of the vibrometer indicates a good reflection level (70%), this due to the good condition of the reflective material. With a good and constant reflection, the vibration signal was observed in real time at the operator's cabin. Screenshots of the signal during low and high vibration are shown in Fig. 4.21 a) and b) respectively.

a)

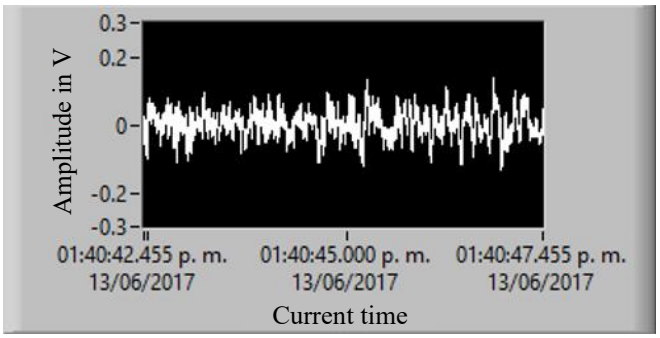

b)

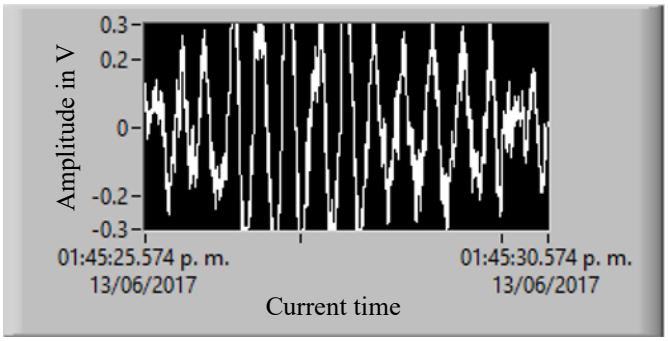

Fig. 4.21 Screenshot of the vibration measurement during a) stable operation and b) unstable operation

4.1.2 Examples of uncovered arcs

During the heat number 16882 considerable panel temperature increase was registered, as shown in the inferior part of Fig. 4.22, the electrical power during the process is also shown in Fig. 4.22. This is visualized in Ternium's platform.

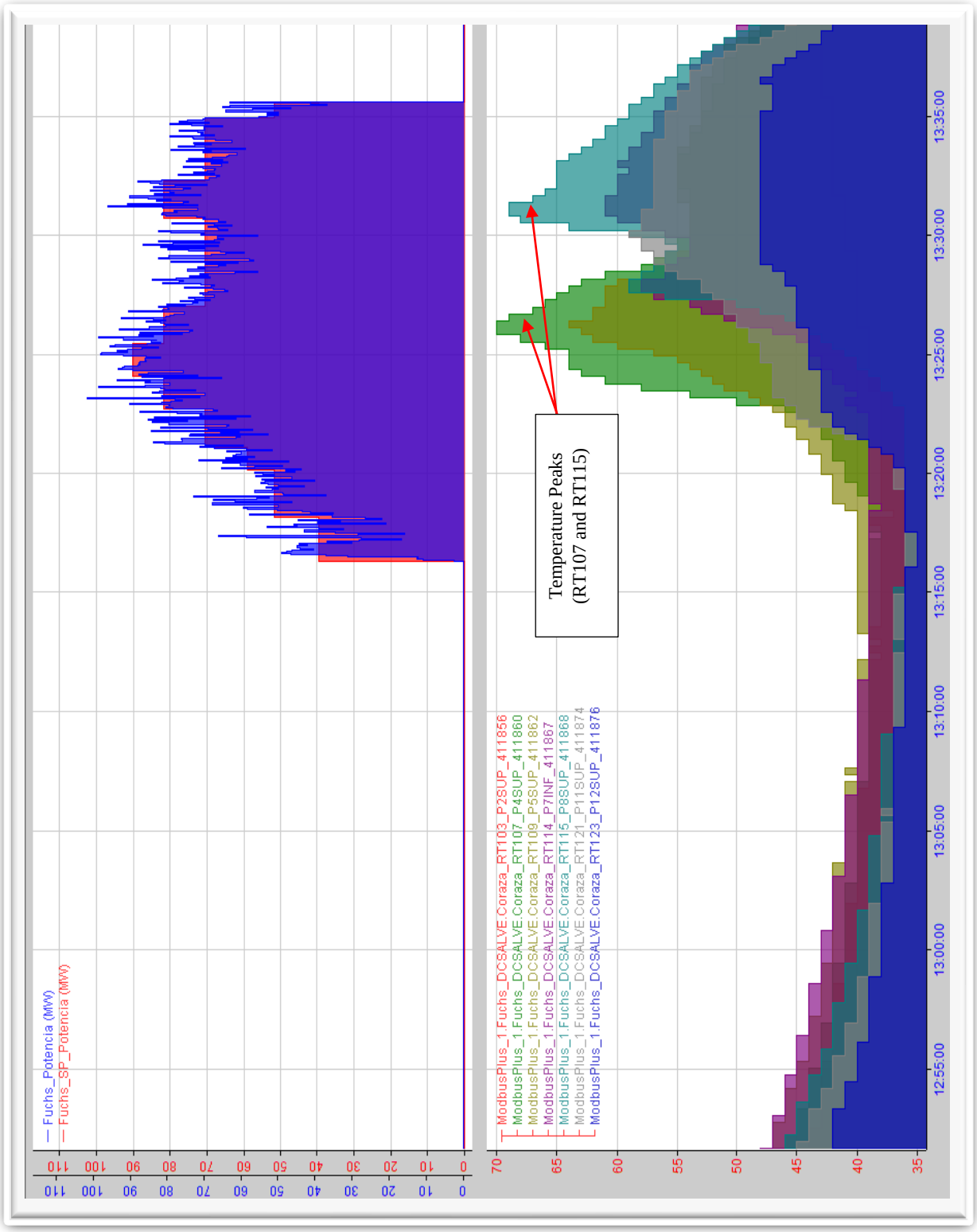

Fig. 4.22 Electric power and panel temperatures

The data was exported from Ternium's database and plotted in the same platform where vibrations are analyzed, it is important to mention, that in order to facilitate the data handling, a new archive of raw signal was created every 5 minutes during the data acquisition, this to avoid the creation of excessively large files. Fig. 4.23 a) shows the electrical power in blue and the power set point in red, b) the vibration raw signal and c) temperature of panels identified as RT103, RT107, RT109, RT114, RT115, RT121, RT123 plotted simultaneously,

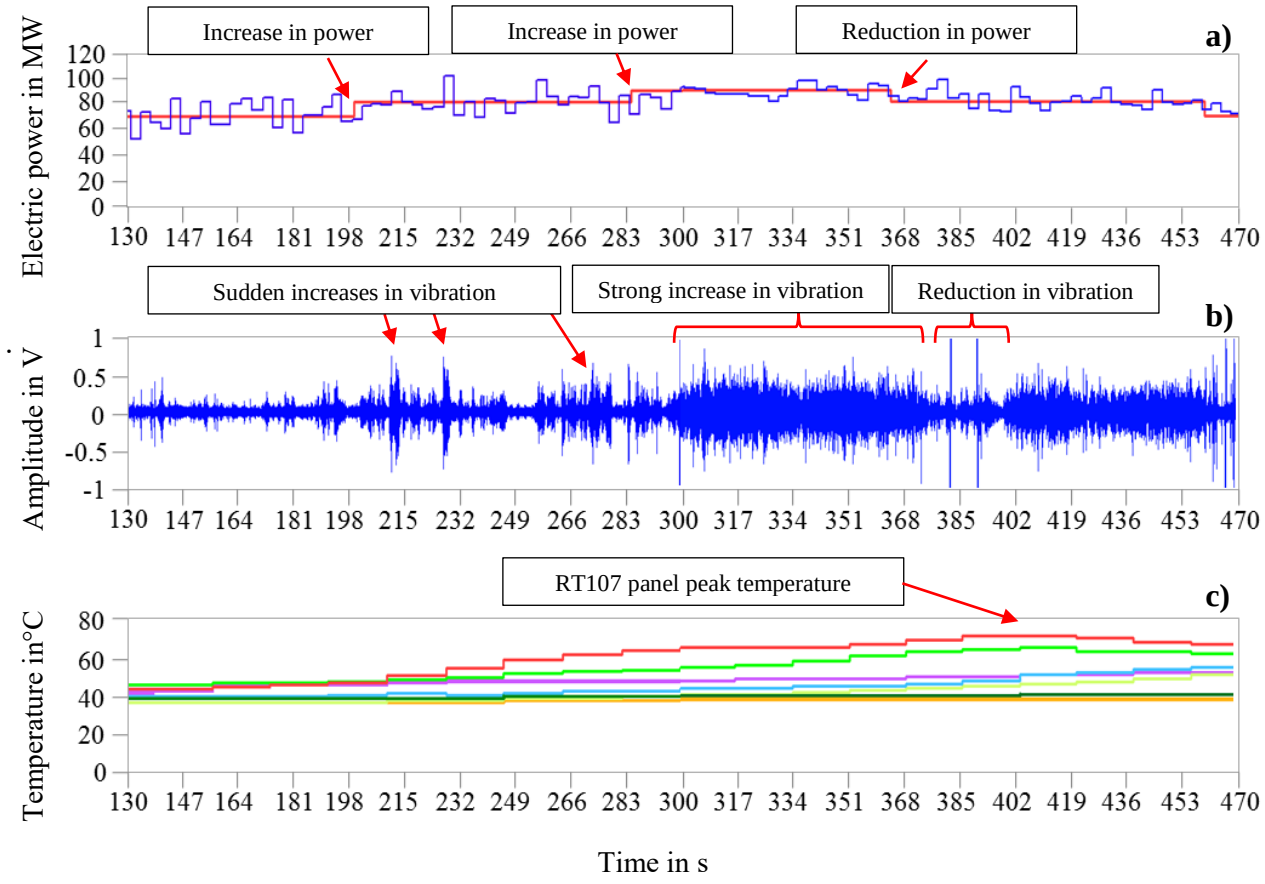

Fig. 4.23 Relevant signals plotted simultaneously for analysis

At 200 s of the first interval shown, the power set point was increased to 80 MW, then sudden peaks appeared in the vibration signal, these peaks can be attributed to a partial uncovered electric arc. Next, at 285 s approximately, the power set point was increased to 90 MW, after this, at 300 s of the second interval, the vibration signal shows a strong increase. From the moment where the strong vibration increase occurs, to the moment when the power set point was reduced due to the increased temperature (360 s of the interval), approximately 60 seconds passed. With the reduction of the electrical power the vibration signal was also reduced, however, 20 seconds later the vibration signal shows a strong increase again; in this case, the electric arc was uncovered again despite the power reduction. This uncovered arc causes the temperature increment of the panel

RT115 shown in Fig. 4.23. During heat number 16883 sharp increases in temperature were also registered, one of which is shown in Fig. 4.24 and corresponds to panel RT121.

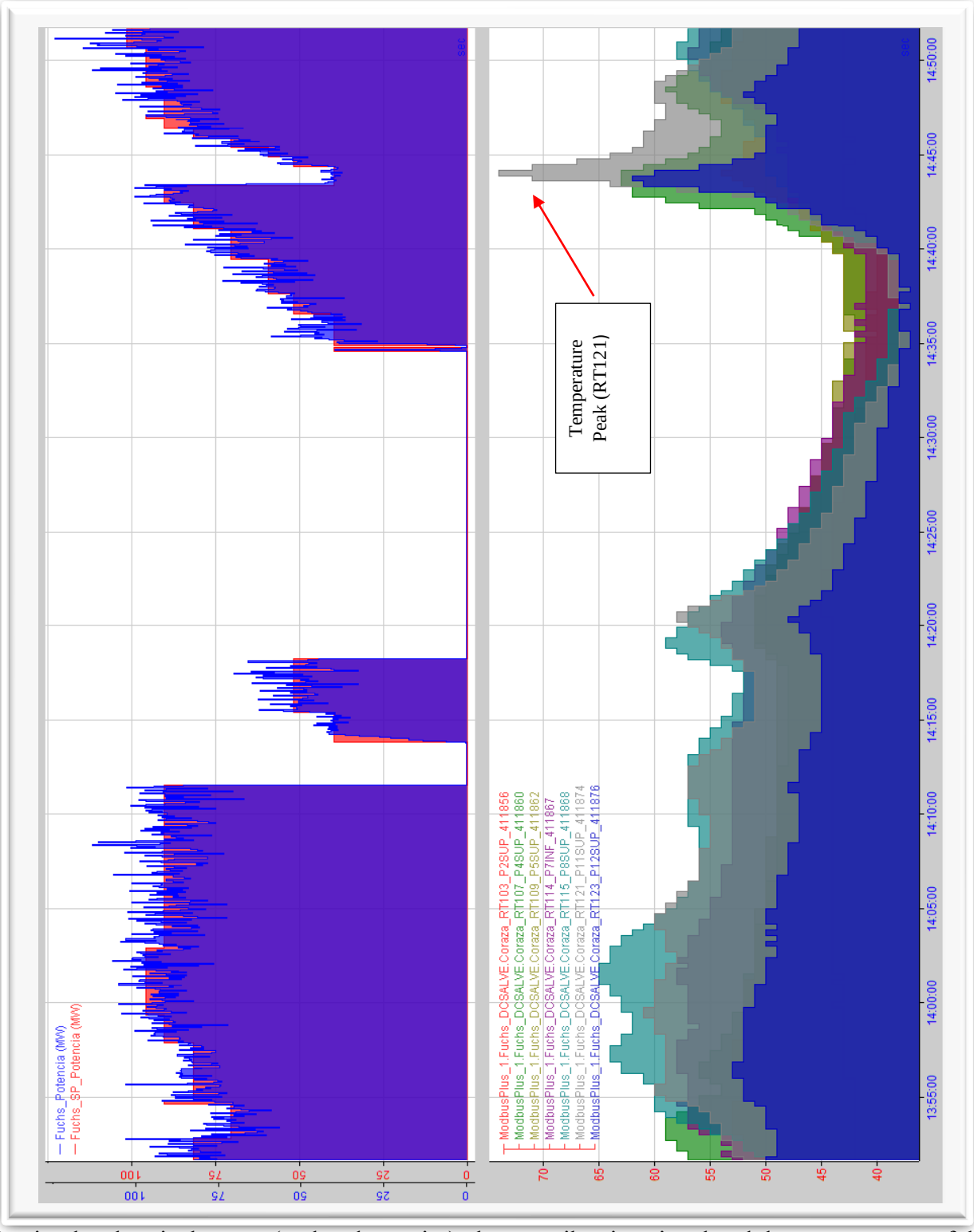

Fig. 4.24 Electric power and panel temperatures

Again, the electrical power (real and setpoint), the raw vibration signal and the temperatures of the panels identified as RT103, RT107, RT109, RT114, RT115, RT121, RT123, were plotted simultaneously as shown in Fig. 4.25.

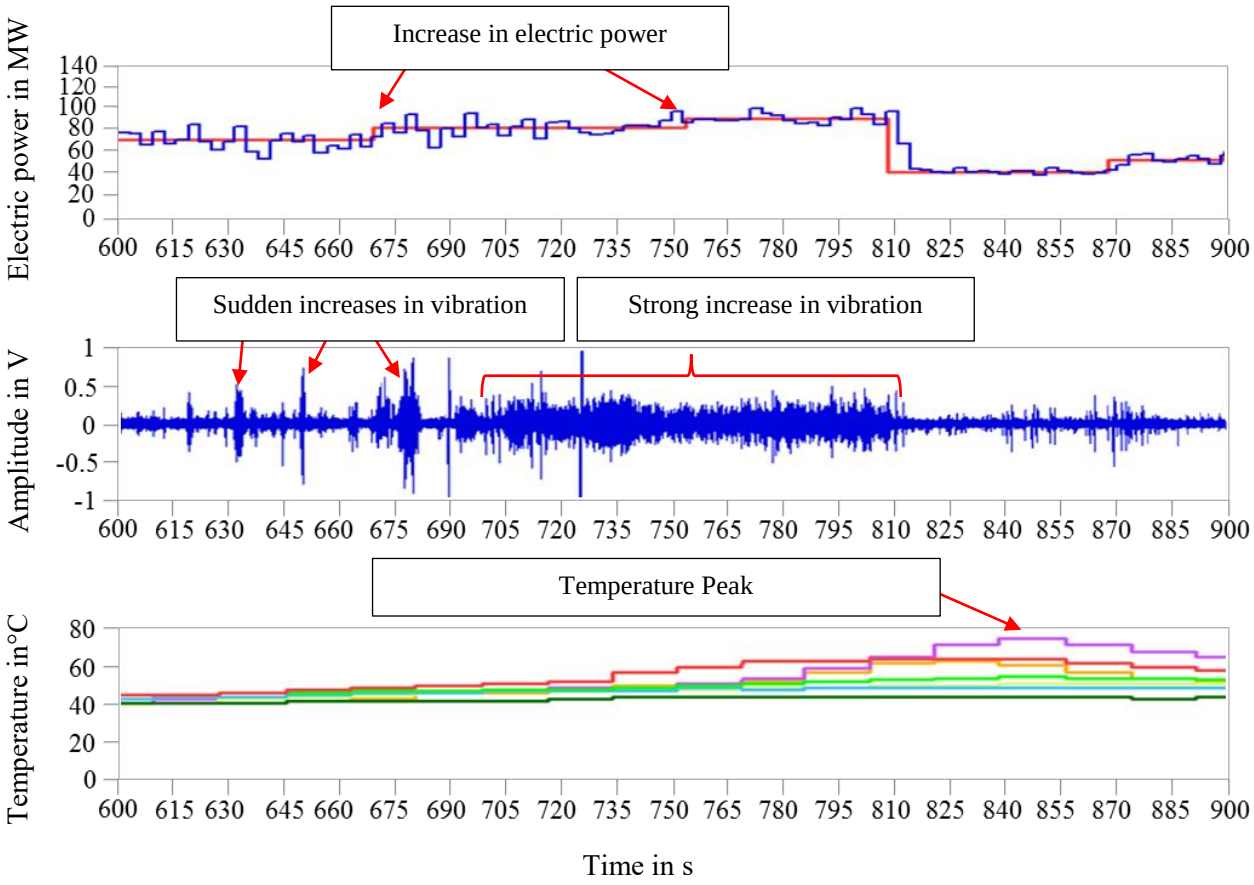

Fig. 4.25 Relevant signals plotted simultaneously for analysis

For the temperature increase of panel RT121, a similar behavior in the vibration signal was observed as in heat 16882. Momentary increases in vibration were registered, after the power increase at 60 s, then seconds later the intensity of the vibration present a strong increment, this being an indication of an uncovered electric arc that caused the panel RT121 heating.

4.1.3 Examples of covered arc

In contrast to the measurements shown in the previous section, the EAF operation with a good coverage of the electric arc is shown now. In the heat 17006 the operation reaches a high-power level of 110 MW as shown in Fig. 4.26 with the label “high power region”. During this interval the temperature of the panels did not show considerable increases.

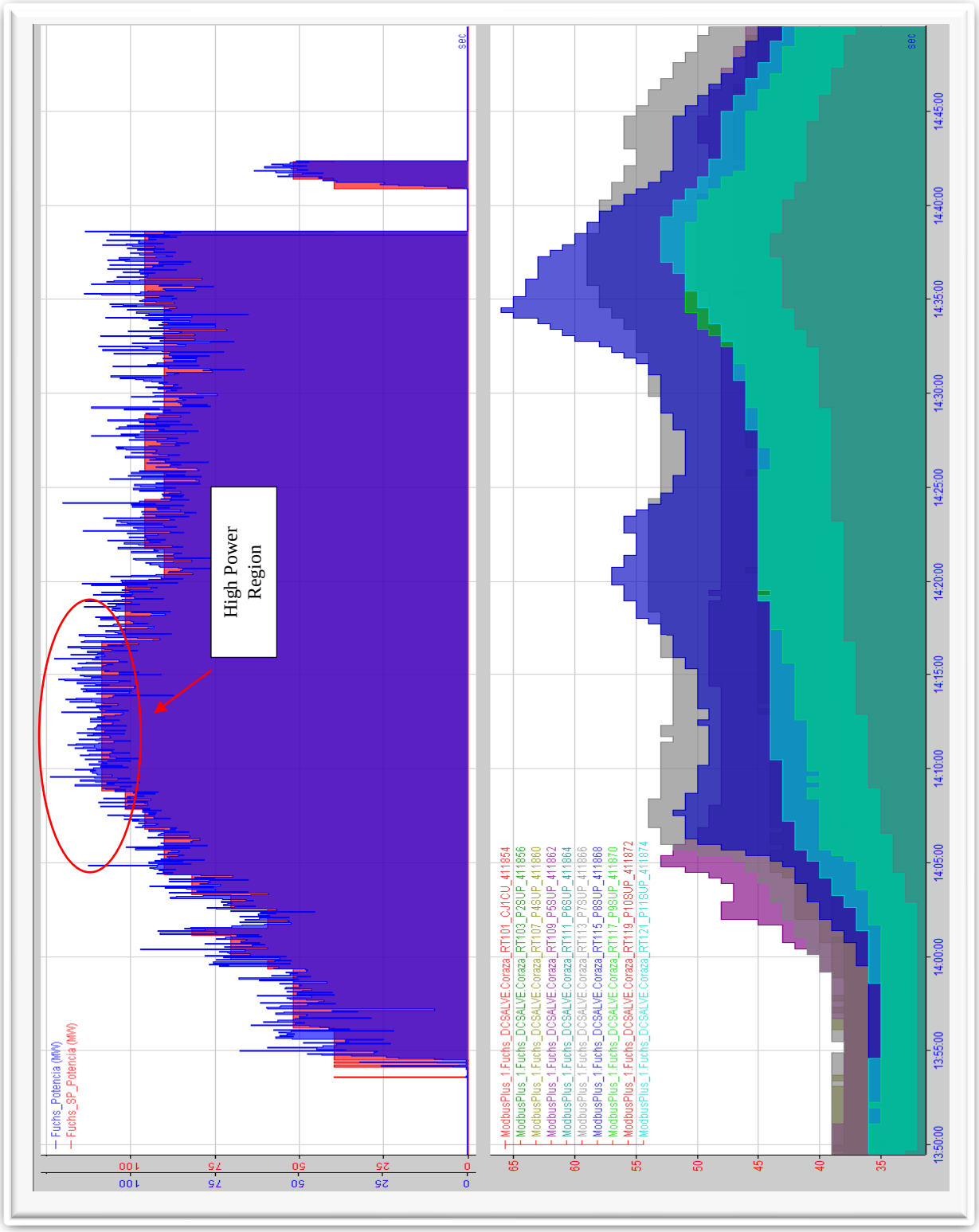

Fig. 4.26 Electric power and panel temperatures

The electrical power (real and setpoint), the raw vibration signal and the temperatures of the panels identified as RT101, RT103, RT107, RT109, RT11, RT113, RT115, RT117, RT119, RT121 were plotted simultaneously as shown in Fig. 4.27.

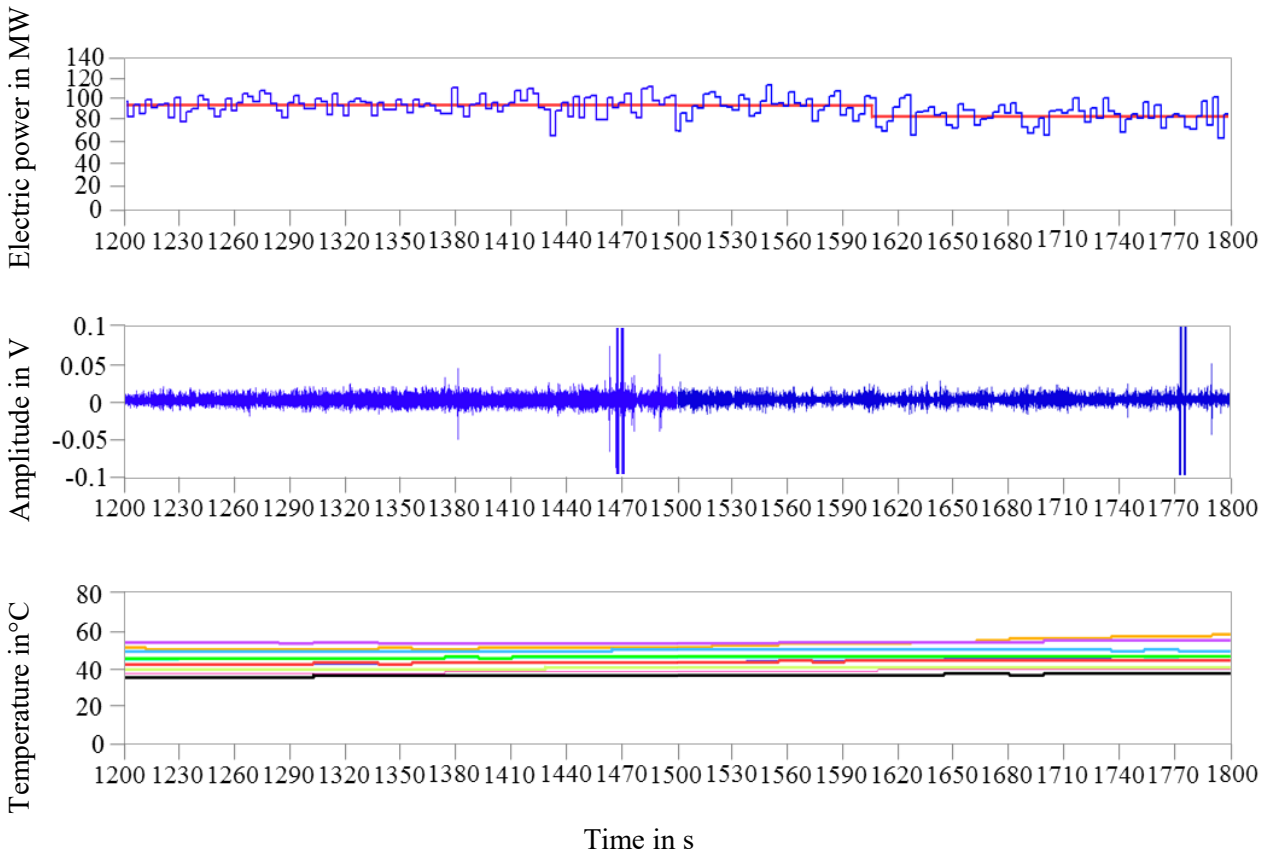

Fig. 4.27 Relevant signals plotted simultaneously for analysis

As can be seen in Fig. 4.27, despite the high-power levels, the operation of the EAF was very smooth, which can be clearly seen in the vibration raw signal. The stable operation is also confirmed observing the panel temperatures, which did not present any substantial increase during the interval.

Chapter 5. Off-line implementation of the multivariable fuzzy system

Once the vibration measurement was accomplished, the implementation of the multi input fuzzy system began. It is important to mention that the fuzzy system was implemented off-line, this means that the inputs were fed to the fuzzy system after saving the data from the melting process and apply some processing like filtering to the signals. As a first approximation two traditional fuzzy models were implemented, a TSK and a Mamdani. The inputs for the systems are the slope of panel cooling water temperature, the RMS value of furnace's shell vibration, and the electric power level. The output of each model is the risk level due to arc coverage, which is limited to values between one and three, where one denotes a good arc coverage or safe operation, two a medium arc coverage or caution operation and 3 a bad arc coverage or danger operation. In Fig. 5.1 is schematized a possible control loop using the arc coverage signal.

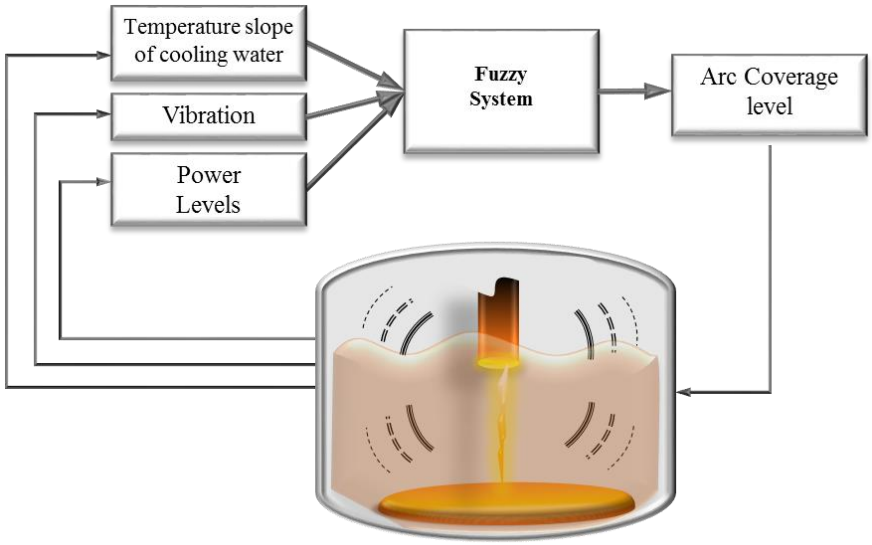

Fig. 5.1 Generation of an arc coverage signal for control purposes

5.1 Membership functions and rules

As said in previous sections, the MFs for the inputs and output of the fuzzy system must be parametrized, this task was performed in an empirical way using data taken directly form the process and interviewing experts with solid knowledge about the EAF. The MFs for the inputs are shown in Fig. 5.2.

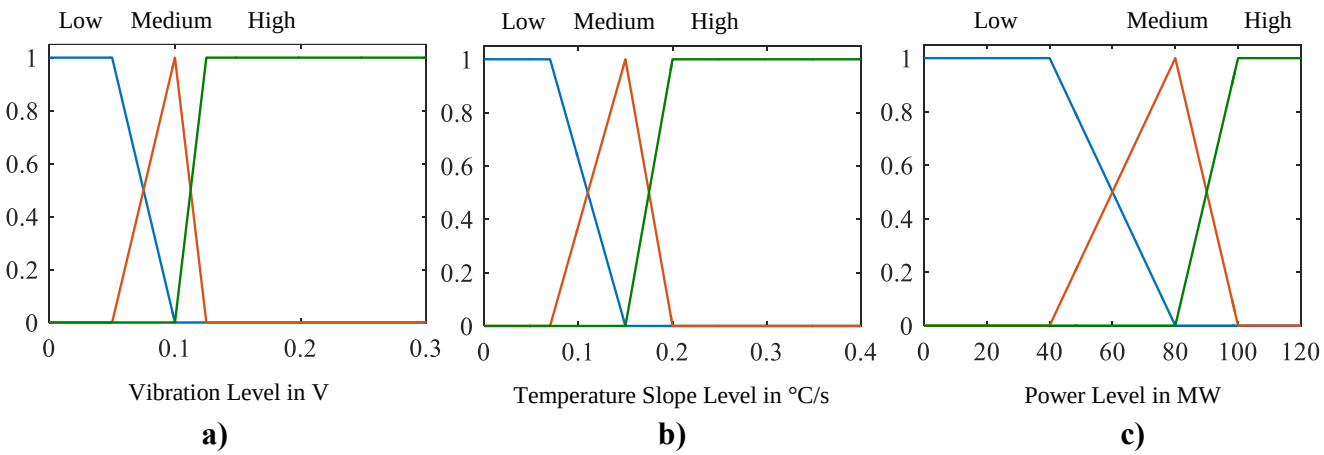

Fig. 5.2 Membership functions for a) vibration level, b) temperature slope level and c) electric power level

The MF's for the output of the Mamdani model are shown in Fig. 5.3 a) while the outputs for the TSK models are shown in Fig. 5.3 b). Remember that in a Mamdani model the rules works with a fuzzy consequent, while a TSK model with a functional consequent.

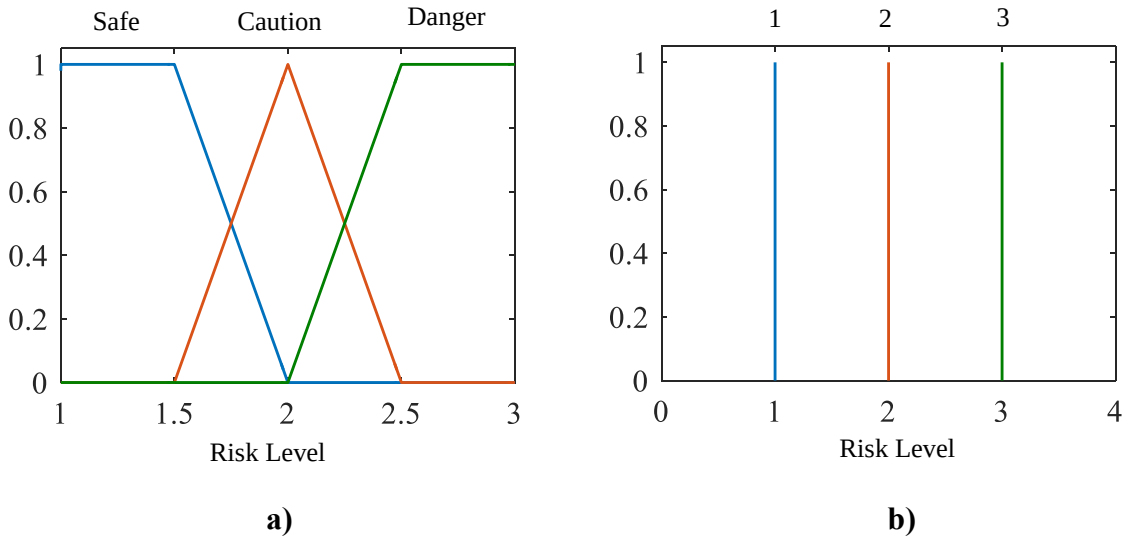

Fig. 5.3 Membership functions of risk level for a) Mamdani model and b) TSK model

For each fuzzy model a set of 27 rules was constructed, these rules are intended to satisfice all the possible operative condition during the melting process. The main objective is to obtain a coherent arc coverage indication at all times of the melting. The sets of rules for the models are shown below in matrix format

TL Low

VL \ PL	Low	Medium	High
Low	Safe	Safe	Safe
Medium	Safe	Caution	Danger
High	Safe	Danger	Danger

TL Medium

VL \ PL	Low	Medium	High
Low	Caution	Caution	Safe
Medium	Caution	Caution	Danger
High	Caution	Danger	Danger

TL High

VL \ PL	Low	Medium	High
Low	Danger	Danger	Danger
Medium	Danger	Danger	Danger
High	Danger	Danger	Danger

It is important to mention that the only difference between the set of rules of the two models is the type of consequent MF, where a fuzzy linguistic variable is used in the Mamdani model and a crisp numeric variable is used for the TSK, in this case 1,2 and 3 represent safe, caution and danger respectively. Despite this difference, it is expected that both models give similar outputs for the same inputs.

5.2 Conditioning of input data for the fuzzy model

As said before one of the inputs of for the fuzzy models is the temperature slope of the cooling water. During normal operation of the EAF the temperatures of the cooling water are measured and registered in Ternium's database, however, the acquisition time of the measure is too slow, giving a discrete representation of the temperatures as shown in the blue line of Fig. 5.4. This discrete temperature behavior is a drawback in order to calculate it slope, which in this case, will be zero when the temperature stay constant and tends to infinity when a drastic change occurs, this depending on the Δt used for the differential quotient.

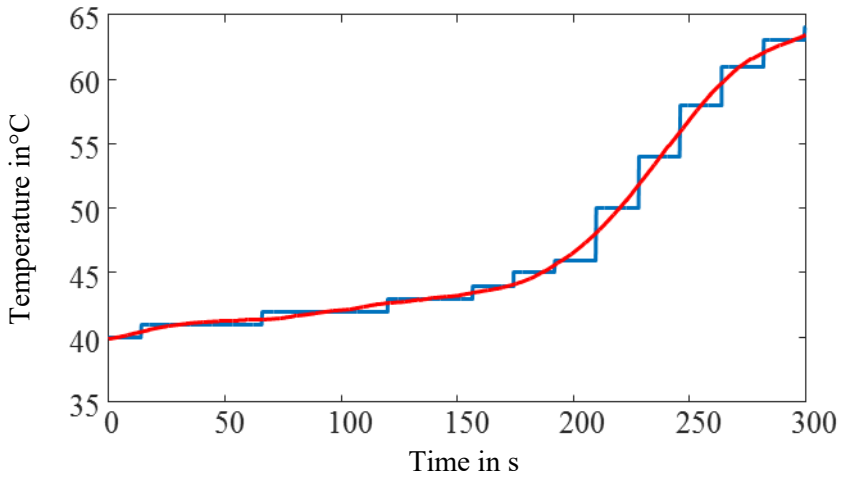

Fig. 5.4 Polynomial adjust over panel temperature data

In order to calculate the slope of the temperature, the database information was used to adjust the coefficients of a polynomic equation, this using the *polyfit* function of MATLAB, which finds the coefficients of a polynomial $P(x)$ of degree n that fits the data y best, in a least-squares sense. P is a row vector of length $n+1$ containing the polynomial coefficients in descending powers as shown in eq. 5.1.

$$P = P(1) * x^n + P(2) * x^{n-1} + \cdots + P(n) * x + P(n+1) \quad (5.1)$$

The degree n is selected by the user. Once the adjust procedure concludes the polynomial was evaluated and new values of temperature were obtained. As can be seen in the red line of Fig. 5.4, the new temperature presents a continuous behavior, which allows performing a numeric slope calculation. To obtain the slope a numerical approximation of the derivative definition was used, which formally expressed in eq. 5.2 using Fig. 5.5 as reference.

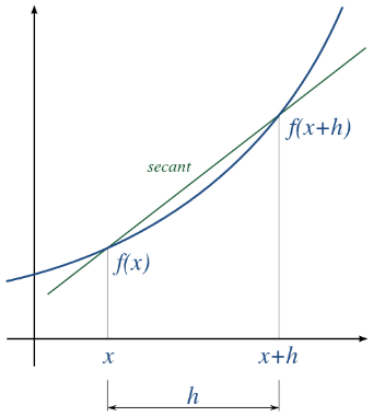

Fig. 5.5 Secant line crossing a function

$$f'(x) = \lim_{h \to 0} \frac{f(x+h) - f(x)}{h} \quad (5.2)$$

In our case the secant between two points with h equal to 1 second was calculated, the units are $°C/s$. Next, to obtain a new slope value the secant travels to the next available points of the polynomial that are 0.1 seconds apart. Here and important clarification must be done, as said in section 4.1.1, the sample frequency of the vibration signal was 10 kHz, which allows to obtain an RMS value of the signal every 0.1 seconds, using 1000 raw samples per calculation. This implies that the slope value must be fed to the fuzzy system every 0.1 seconds too, as well as the electric power. In order to achieve this, the data used to find and evaluate the polynomial, was exported from Ternium´s database using a time base of 0.1 seconds. Doing this the separation between the data points, obtained after the polynomial adjust, remains at 0.1 seconds. Resuming, we have a differential quotient with a constant separation of 1 seconds between points, that travels over the polynomial at steps of 0.1 seconds. Making the calculation over the polynomial points of Fig. 5.4 the graph of Fig. 5.6 is obtained. This is just an approximation of the slope, but it gives a good indication of the rate of change of the adjusted temperature.

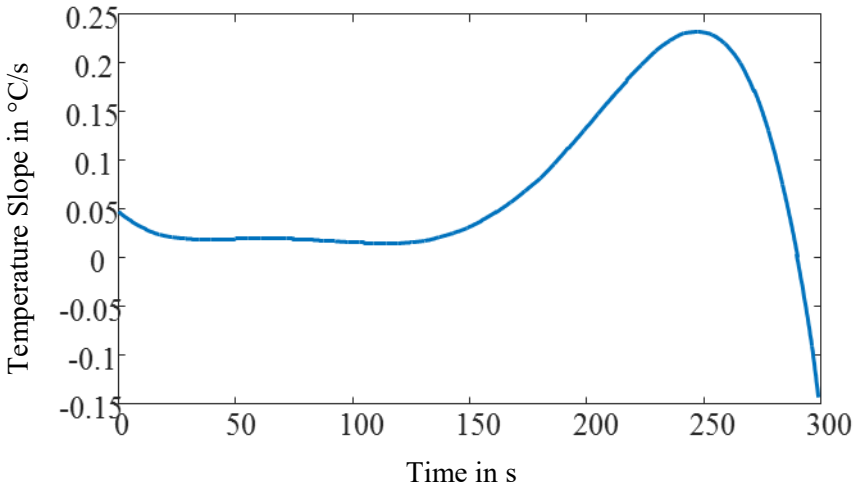

Fig. 5.6 Temperature slope obtained after polynomial adjust

In real time application, the signals will be display in a continuous and smooth fashion due to the use of a time base of 0.1 seconds per calculation. Another important consideration regarding the inputs of the fuzzy model is that there are several cooling panels in the EAF, but only one vibration measurement point, because of this a previous step regarding the slope of the relevant panels was performed. In Fig. 5.7 the temperature slope of two panels is shown.

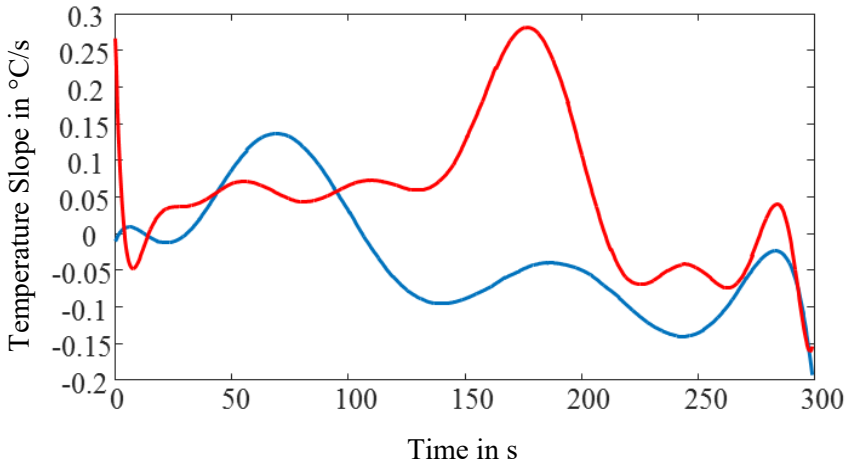

Fig. 5.7 Two temperature slopes plotted simultaneously

The slopes were compared, and the maximum slope value was obtained for the 300 seconds interval of each data archive. The Fig. 5.8 shows the maximum slope, which is indeed one of the inputs of the fuzzy system.

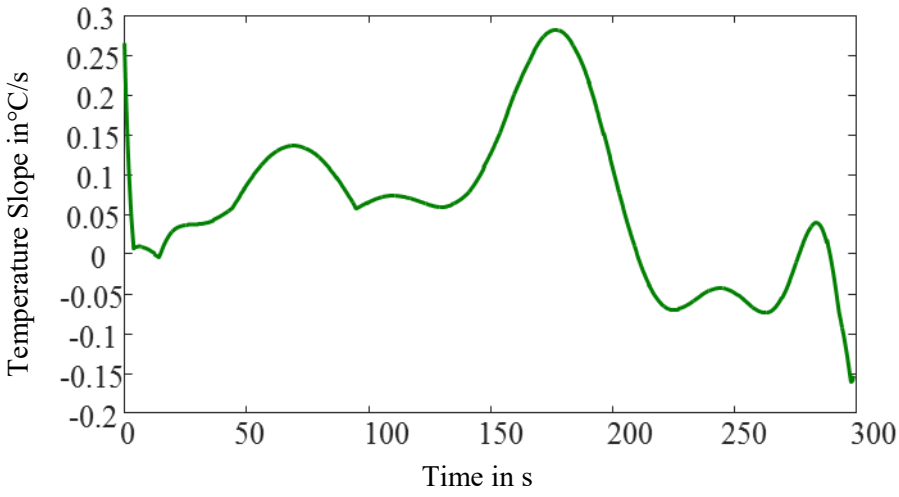

Fig. 5.8 Maximum slope value after comparison

In the case of the raw vibration, its RMS value was obtained using the methodology explained in section 4.1.1 applying eq. 4.1. In addition, after the RMS calculation, the signal enters to a third order Butterworth low pass filter with cut frequency of 0.3 Hz, this in order to reduce rapid oscillations and improve the behavior at the output of the fuzzy system. Finally, the electric power was not subjected to any treatment, this because the membership functions described in next sections allows making an inference despite electric power oscillations, which are not as abrupt as

in the case of vibration. The only consideration was to export the data using the same time base of the other inputs. Summarizing, the inputs to the off-line fuzzy system are:

- The maximum slope value of the water-cooling temperature, after polynomial adjust
- The RMS vibration after a filtering procedure
- The electric power levels during the operation (no conditioning was applied)

5.3 Results using the CLV-2534-2 vibrometer

In order to validate the set of rules and MFs shown in the previous section, real data from the furnace was fed to the fuzzy system. It is important to mention that the results shown in this section were obtained in off-line mode, this because at the moment of the vibration measurement there was not enough instrumentation available to acquire, simultaneously, electric power and panel temperatures in the same system. Fig. 5.9 shows the different inputs and the output of the fuzzy system during a 300 s interval of heat 16882. In Fig. 5.9 a) the red line represents the electric power setpoint just as reference, while the blue line represents the real electric power. In Fig. 5.9 b) the red line corresponds to the cooling water temperature of panel RT115, while the blue line corresponds to the cooling water temperature of panel RT107. In Fig. 5.9 c) the temperature slopes of the panels are shown, the red line is the slope of panel RT115, while the blue line corresponds to the slope of panel RT107. In Fig. 5.9 d) the raw vibration signal is showed, remember that this variable is conditioned prior entering the fuzzy system. In Fig. 5.9 e) the filtered RMS value of the vibration signal is shown. In Fig. 5.9 f) the output of the Mamdani model is shown, while in Fig. 5.9 g) the output of the TSK is shown.

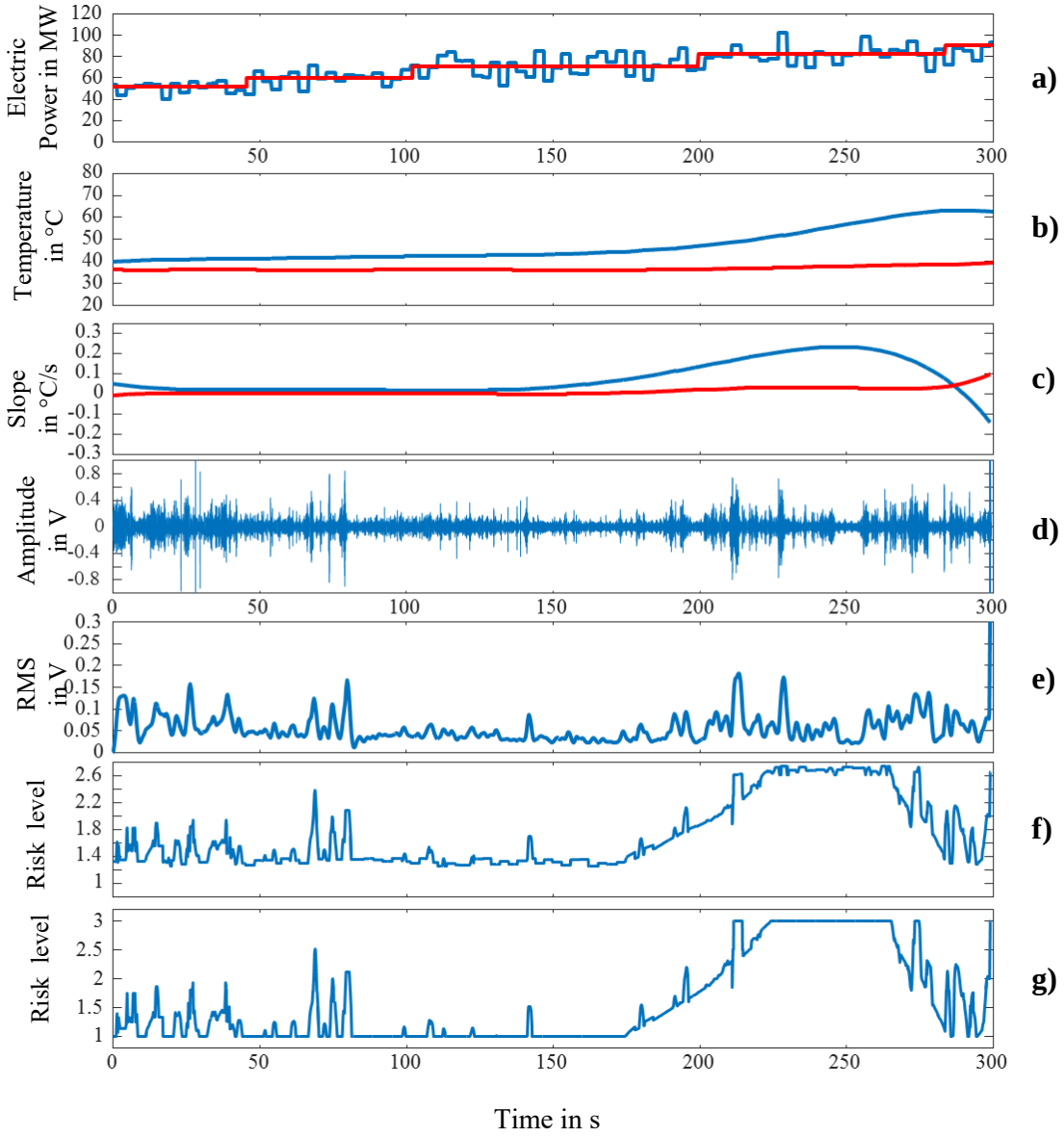

Fig. 5.9 a) electric power, b) panel temperature, c) temperature slope, d) raw vibration, e) RMS vibration, f) Mamdani output and g) TSK output

From second 0 to 100 of the intervals shown in Fig. 5.9 the electric power is between low and medium levels, changing from 50 MW to 60 MW. The vibration is between low and medium levels with sudden peaks that reach high level, while the temperature slope is in low level. Under this scenario the risk indicator maintains its value near level 1 or LOW as expected. The sudden peaks in vibration produces also peaks at the output of the system, however these increments are short in duration, the overall indicator from 0 to 100 seconds show a stable condition inside the furnace. The last can be correlated with the low temperatures of the panels shown Fig. 5.9 b). From second 100 to 175 approximately, the electric power set point was increased to 70 MW, the real power

oscillates between low and medium level. The vibration was lower maintaining its value between low and medium level, also low temperature slope is near zero until 150 s, where an increase in its value begun, reaching medium levels, however this temperature increase was not dangerous. As can be seen in the outputs of the two models from 100 to 150 s the operation was very stable and smooth, correlating very well with panel temperature.

From 175 s the medium level in electric power was maintained, at 200 s the power was increased to 80 MW. Despite this power value is still in the medium level range an increase in vibration occurs reaching even peaks of high level. An increment in the temperature slope also occurs passing from medium to high levels in short time, because of this the risk indicator increased from a value of 1, at 175 s, to a value of 3 at 220 s. It is clear that in this case, the fuzzy system gives a higher ponderation to the temperature slope; this is clearly seen how, the risk indicator behavior is very similar to the behavior of the temperature slope. However, the behavior of the arc risk indicator varies depending on the rules triggered by the inputs. In some scenarios the indicator can behave similar to vibration, in other situation similar to the electric power and in the best cases as a combination of three or two inputs, all of these behaviors were observed and will be showed in the next graphs. Another important observation was how the perturbations of the inputs are transmitted to the output of the system. In the case of the Mamdani model, the oscillations in the electrical power around the setpoint can also be observed at the output, in contrast, the TSK model gives more stable output. In addition, the Mamdani model truncate the output to values between 1.4 to 2.6 while TSK model maintain the behavior of the indicator between 1 and 3. Because of these reasons, the TSK model was chosen over the Mamdani, in subsequent results the analysis is made only considering the TSK model output.

In Fig. 5.10 a new interval of 300 s of heat 16882, which follows the previous interval, is shown. The same signals are shown except for the Mamdani model output, which is discarded. A moving average filter was also implemented at the output of the system, this in order to smooth the peaks that appear due to the violent nature of the melting process. The moving average filter uses 30 samples to perform the calculation, in other words every three seconds an output value is obtained.

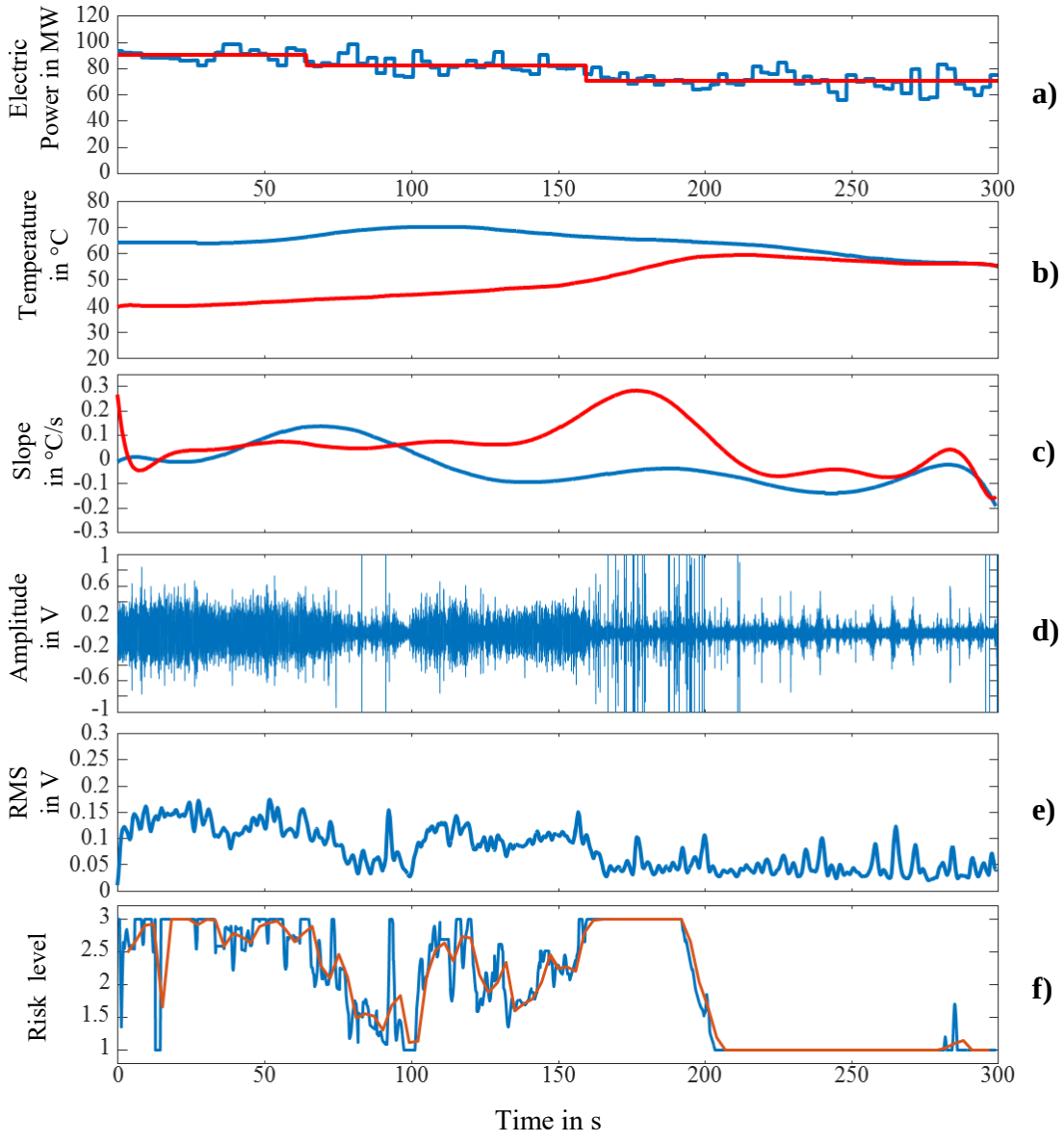

Fig. 5.10 a) electric power, b) panel temperature, c) temperature slope, d) raw vibration, e) RMS vibration and f) TSK output

Note how the temperature of panel RT107 stays above 60 °C at the beginning of the 300 s interval, also note that the electric power was increased to 90 MW. From 0 to 80 s in Fig. 5.10 d) and e) a considerable increase in vibration occurs, in the same period of time the panel temperatures start to increase in a slow fashion, this is shown in the slopes of Fig. 5.10 c). Despite the slow rise of temperature, during the first 80 seconds of the interval the risk indicator rises to danger level (three) due to the combination of high electric power and high vibration, in fact, in this case, the risk indicator is dominated by the RMS value of the vibration. The fuzzy system gives more importance

to this variable rather than the temperature slope as in the previous case. Note how at 60 seconds the electric power was reduced, this caused a decrease in vibration, in consequent, a drop of the risk indicator occurred. Despite the decrease in electric power the vibration rises again and, due to the still high level of power, the risk indicator also rises. In fact, panel temperatures keep raising during this interval. From 150 s it can be seen how the temperature slope of panel RT115 increases, switching the behavior of the risk indicator to follow the behavior of the temperature slope. In Fig. 5.11 an interval of 300 seconds of heat 16883 is shown, in this particular scenario the beginning of the melting (boring period) is discussed, in this stage of the process usually works with a short electric arc to protect the EAF from excessive radiation.

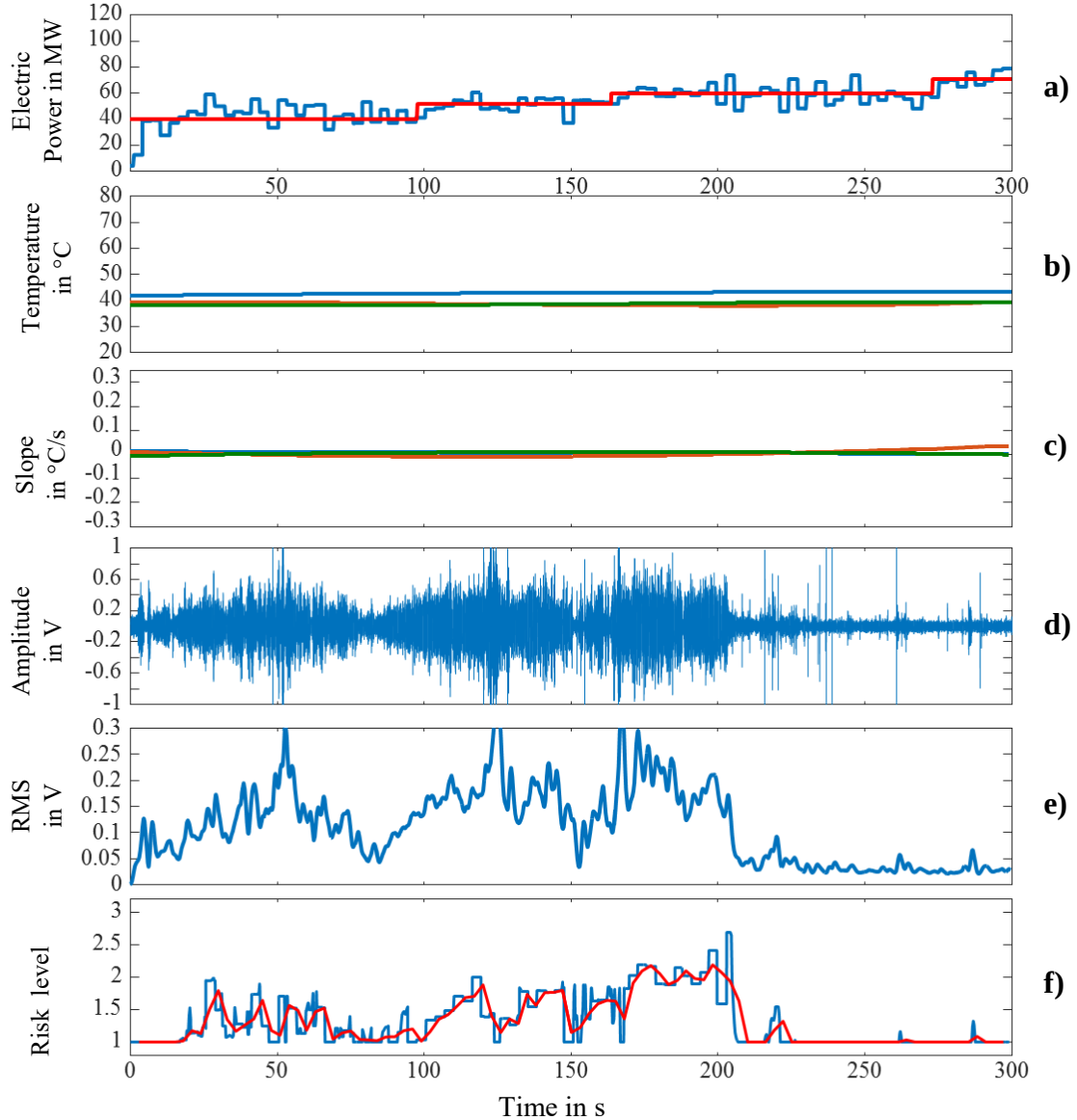

Fig. 5.11 a) electric power, b) panel temperature, c) temperature slope, d) raw vibration, e) RMS vibration and f) TSK output

Note in Fig. 5.11 d) and e) how, at this stage, the vibration is very high, despite low electric power. Here the combination of low electric power and low temperature slope allow the fuzzy system to infer that there is no danger, as it is shown from 0 to 200 s, where the risk indicator was mostly of the time below caution level (two). Note during 100 to 200 s the electric power was increased and the vibration continued to be at a high level, here despite the low temperature slope, the combination of medium power and high vibrations causes the risk indicator to reach level two, this can be seen as a warning indication. Note the reduction of the vibration level from 200 s now, with low vibration, medium power, and low temperature slope, the risk indicator drops to level one. The next interval of heat 16883 (Fig. 5.12), shows another stage of the melting process. Time period 0 to 60 s shows a low risk indication that only increases suddenly due to abrupt vibration, as can be seen in Fig. 5.12 a) the power is at 70 MW, this is a medium value, because of this the vibration impacts directly in the behavior of the risk indicator.

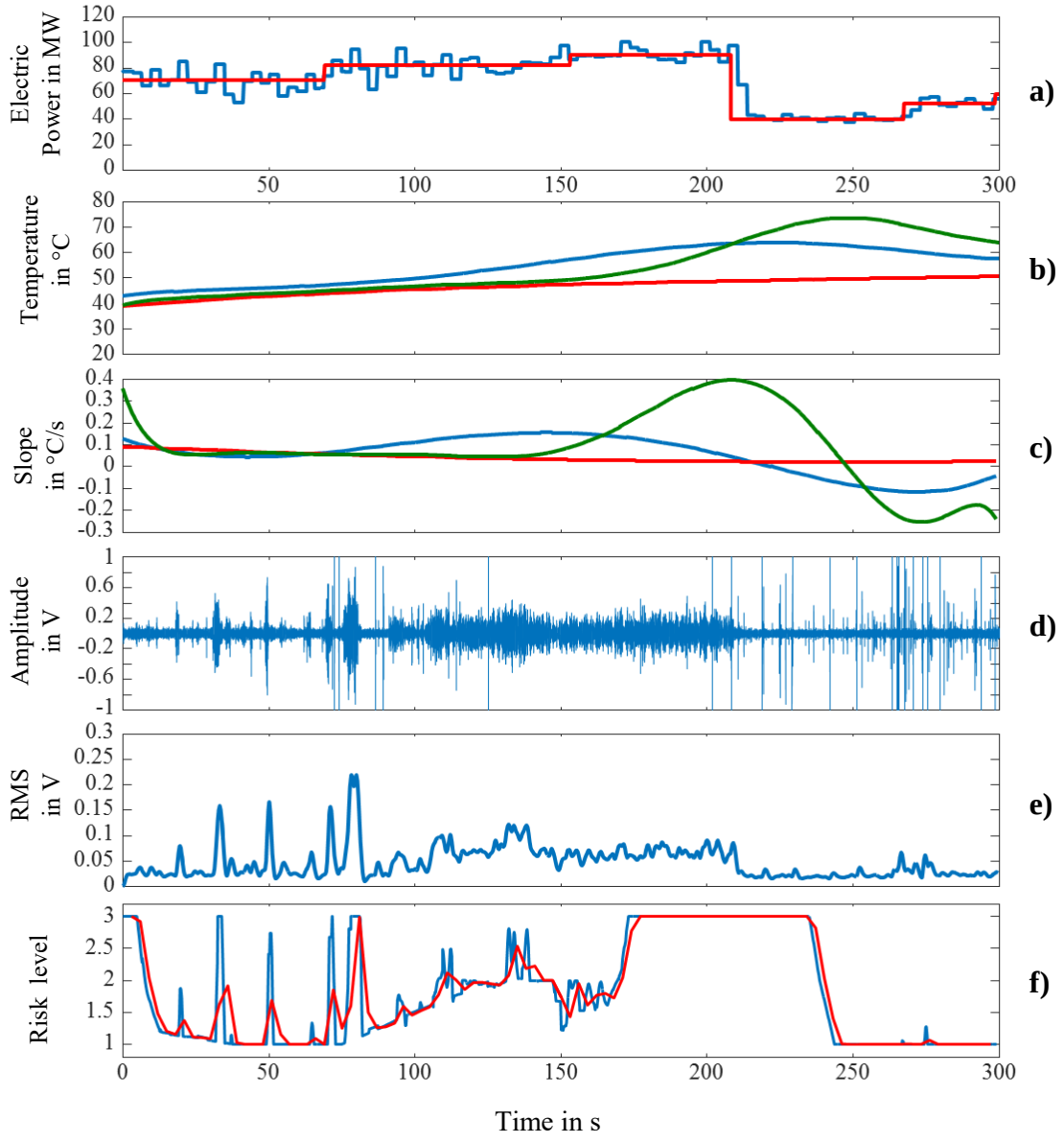

Fig. 5.12 a) electric power, b) panel temperature, c) temperature slope, d) Raw vibration, e) RMS vibration and f) TSK output

During 60 to 150 s the power was increased to 80 MW, in this period vibration increases, producing a rising in the arc risk indicator, however the low and medium values of the temperature slope maintain the risk indicator at level two (caution). During 150 to 210 s the power was increased to 90 MW, in this high-power condition the temperature slope increased to high levels, while the vibration maintains its value oscillating in medium levels. In this case, a dangerous condition is detected, high power, plus considerable vibration, plus rapid heating of panels. As can be seen in Fig. 5.12 f) the risk indicator was saturated at level three (danger level) at 170 s, later at 210 s approximately it can be seen that the electric power was reduced. The difference in time between the risk indicator increases to danger level to power reduction, was 40 seconds approximately.

Another interesting operation condition is shown in Fig. 5.13. It can be seen in Fig. 5.13 a) how from 0 to 300 s the furnace was working at high power (100 MW), also the vibration was low during the same interval, excluding the sudden increases due to the cut of the laser signal by walking operators. However, abnormal panel heating occurred, in this case, due to a failure in the cooling system. This produced a counter intuitive operation condition because a high-power electric arc with low vibration is an indication of a good arc coverage. However, the slope of temperature did not correspond to the coverage of the arc due to external perturbations, however this kind of situations was considered in the construction of the set of rules of the fuzzy model.

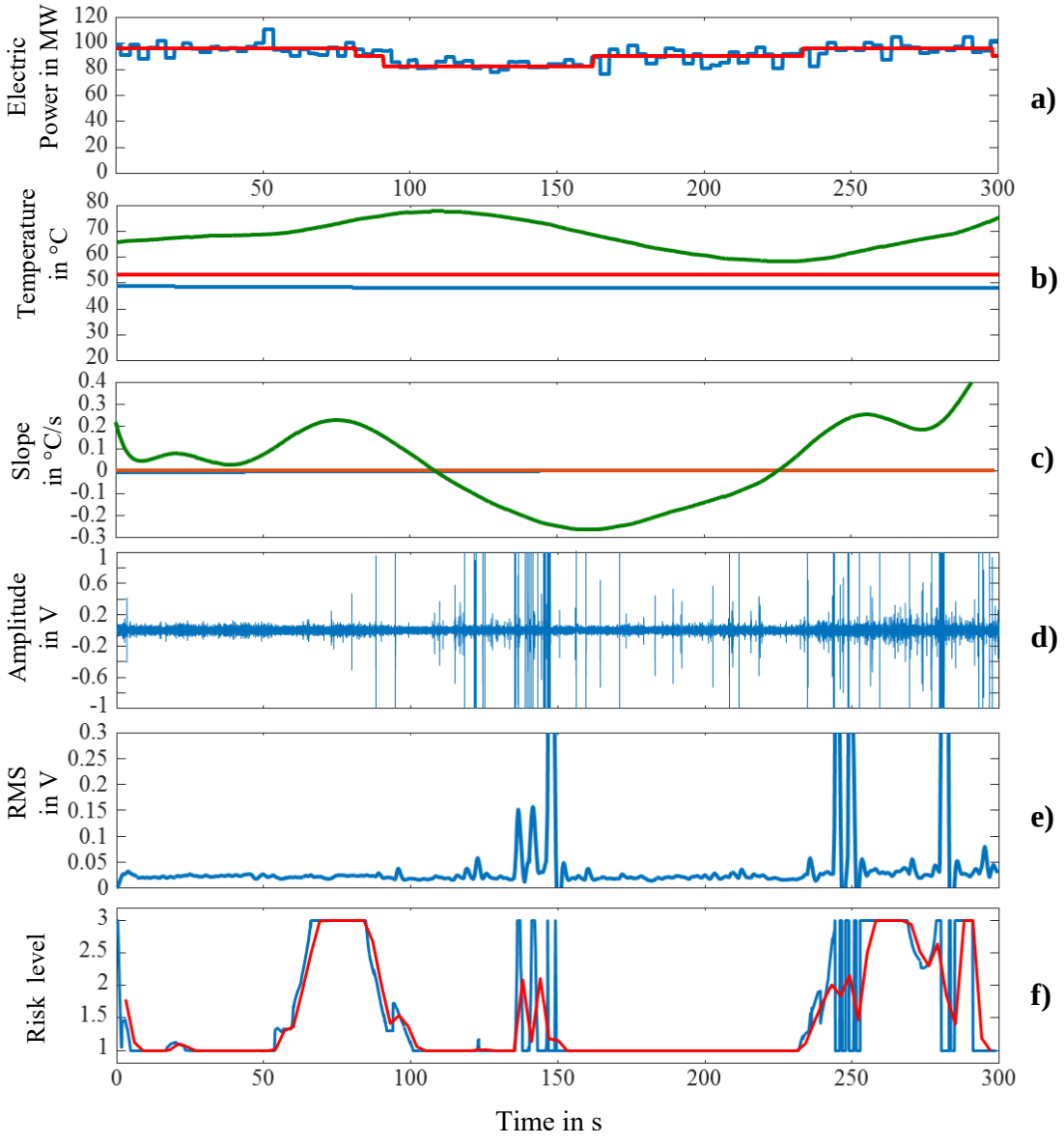

Fig. 5.13 a) electric power, b) panel temperature, c) temperature slope, d) raw vibration, e) RMS vibration and f) TSK output

As can be seen in Fig. 5.13 f) the risk indicator is dominated by the temperature slope. Despite the low vibration, the fuzzy system gives priority to the slope because, independently of the vibration, if the panel is over heated this is a dangerous situation that must be alerted. It is important to mention that this is the worst-case scenario for the fuzzy system, however it can be seen that the response of the model allows to identify an abnormal condition, this thanks to the multivariable processing applied.

5.4 Vibration measurement equipment RSV-150

In this section are discussed more results obtained with the RSV-150 vibrometer. As said before, the main problem of the vibration measurement at the furnace using laser technology, was the necessity of a reflective material mounted on the wall of the EAF. Certainly, no require the reflective material will lead to an easier and more reliable measurement. The last is possible with a more sophisticate laser vibrometer, in this case the RSV-150 from Polytec. This equipment allows to measure in a similar fashion as the CLV, but without the use of reflective material and even at longer distance. This is possible because the equipment emits an infrared beam to perform the measurement. The minimum stand-off distance of the equipment is 5 m and the maximum are 300 m depending on target reflectivity. The velocity output consists in 8 sensitivity ranges: 0.4 mm/s/V to 100 mm/s/V and the analog output can take values from -10 V to 10 V. The Bandwidth goes from 0 Hz to 25 kHz. As can be seen in Fig. 5.14 the emitter of the RSV-150 is bigger in comparison with the CLV emitter, this due to the lens configuration that allow measuring up to 300 meters according to the manufacturer.

Fig. 5.14 RSV-150 laser vibrometer at Tecnológico de Monterrey campus

The RSV-150 was taken to the steel shop and data from several heats were gathered. The equipment is show in Fig. 5.15, it can be seen in the led indicator of the emitter the good reflection level when aiming directly to the EAF wall. In this case due to the flexibility to choose the measurement point, the laser was aimed to a higher position, compared to previous measurements, this because the vibration is more intense above the slag level when there is an uncovered electric arc. The measurement position is shown in Fig. 5.15.

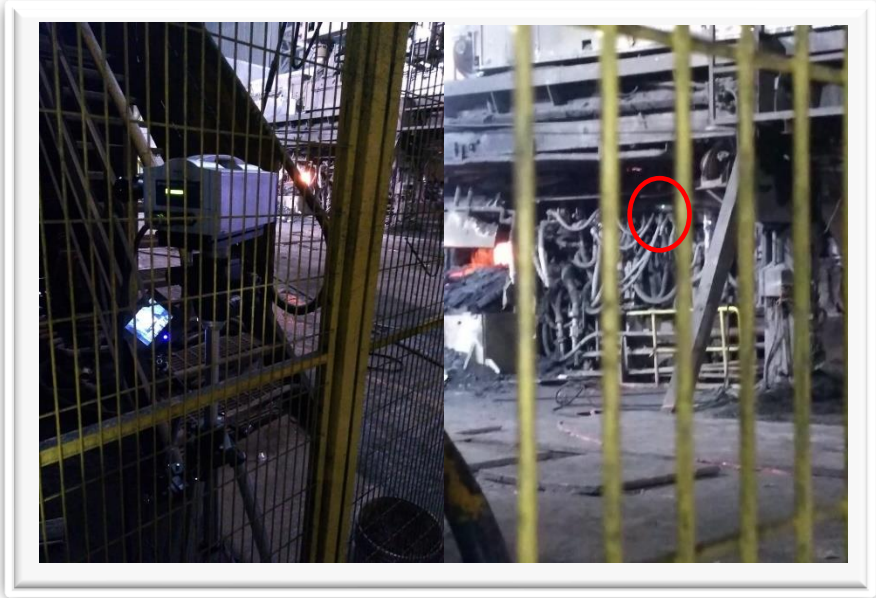

Fig. 5.15 RSV-150 aiming to the new measurement point

The work methodology was the same as with the CLV vibrometer, the vibration signal of several heats was recorded, and then the fuzzy algorithm was tested off-line using as inputs the electric power, the temperature slope of cooling water and the RMS value of the vibration.

5.4.1 Membership functions and rules using the RSV-150

It is important to mention that the use of a new vibrometer and the selection of other measurement point, requires that the MFs for the vibration input of the TSK model have to be reparametrized. In Fig. 5.16 the MFs for the new measure campaign are shown.

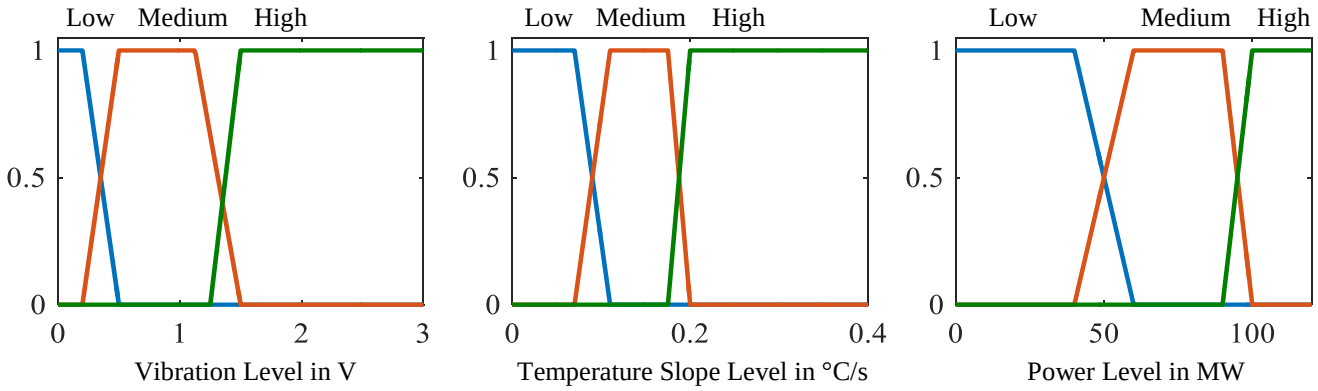

Fig. 5.16 Membership functions for inputs of the RSV-150 measurement campaign

As can be seen not only the range of vibration MFs was modified, in all the inputs the "Medium" triangular MF was replaced with a trapezoidal MF, this change cleans up a little bit the output of the TSK model in values near level two. To show the effect of the trapezoidal medium MF, the output of the TSK model shown in Fig. 5.17 a) was processed again using only trapezoidal MFs.

Fig. 5.17 Comparison between the out of the TSK model using triangular and trapezoidal MFs

As can be seen in the circle in Fig. 5.17 b), some perturbations were not present in the output due to the use of the trapezoidal MF. Another consideration was taken regarding the set of rules. In the case of the new measurement point, rule number eight caused unwanted behavior at the output of the model. This because vibration present sudden increases in a more abrupt fashion, than in the measurement point analyzed in the previous section. This causes that, in some cases, when rule number eight was activated the output of the model oscillated easily between the values one and three. The solve this the consequent part of the rule number eight was modified as show below.

R_8: IF VL is *Medium* AND PL is *High* AND TL is *Low* THEN CL=*3 (original rule)*

R_8: IF VL is *Medium* AND PL is *High* AND TL is *Low* THEN CL=*2 (modified rule)*

The rest of rules of the sets remain the same, only rule number eight was modified. With the set of rules and MFs for all the inputs defined the test of the TSK model was performed.

5.4.2 Results using the RSV-150 vibrometer

As in the previous results, Fig. 5.18 shows the different inputs and the output of the fuzzy system during a 300 s interval of heating 12726, in 5.18 a) the blue line represents the real electric power. In 5.18 b) are shown the cooling water temperatures of panels RT108, RT113, RT115, RT118, RT121 and RT123. Fig. 5.18 c) shows the temperature slopes of the panels shown in the previous chart. In 5.18 d) the raw vibration signal is shown. In 5.18 e) the filtered RMS value of the vibration signal is shown and finally in 5.18 f) the output of the TSK model is presented. It is important to mention that changes were applied to Ternium's database between measurement campaigns, because of this, the electric power data present a more continuous behavior.

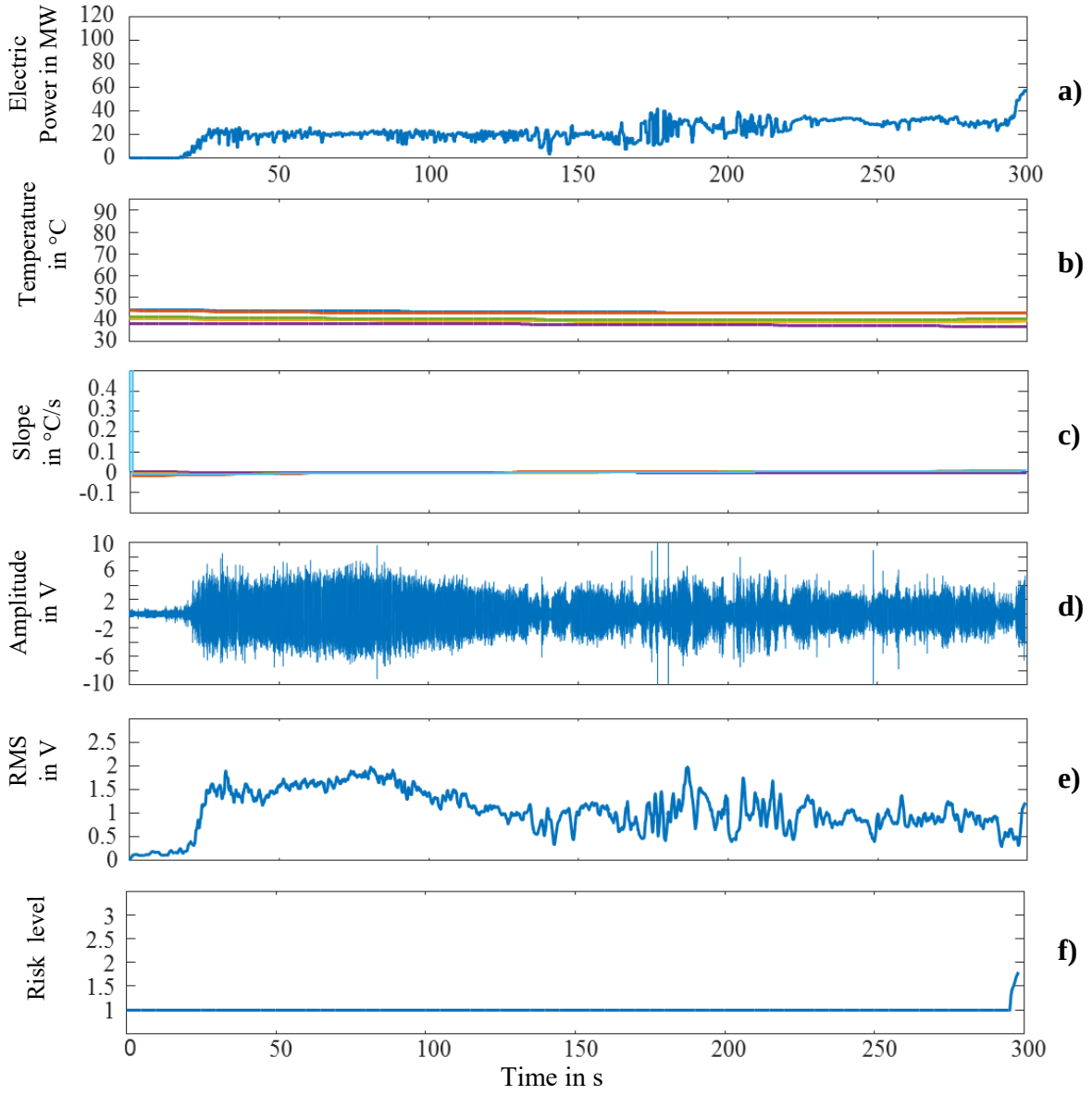

Fig. 5.18 a) electric power, b) panel temperature, c) temperature slope, d) raw vibration, e) RMS vibration and f) TSK output

At the beginning of the melting process, it is expected to observe high levels of vibration even at low electric power and without heating the panels. During 25 to 100 s of the interval it can be seen how in Fig. 5.18 f) the risk indicator remains at level one (safe level) despite high vibration of the EAF. As the melting process progresses, the vibration starts to reduce its intensity. However, at the end of Fig. 5.18 a) can be seen how the electric power starts to increase from values below 40 MW to values near 60 MW, simultaneously the vibration, Fig. 5.18 e), began to increase again. This raise in power and vibration causes that the arc risk indicator also increases as seen at the end of in Fig. 5.18 f). Next Fig. 5.19 shows the continuation of the previous figure.

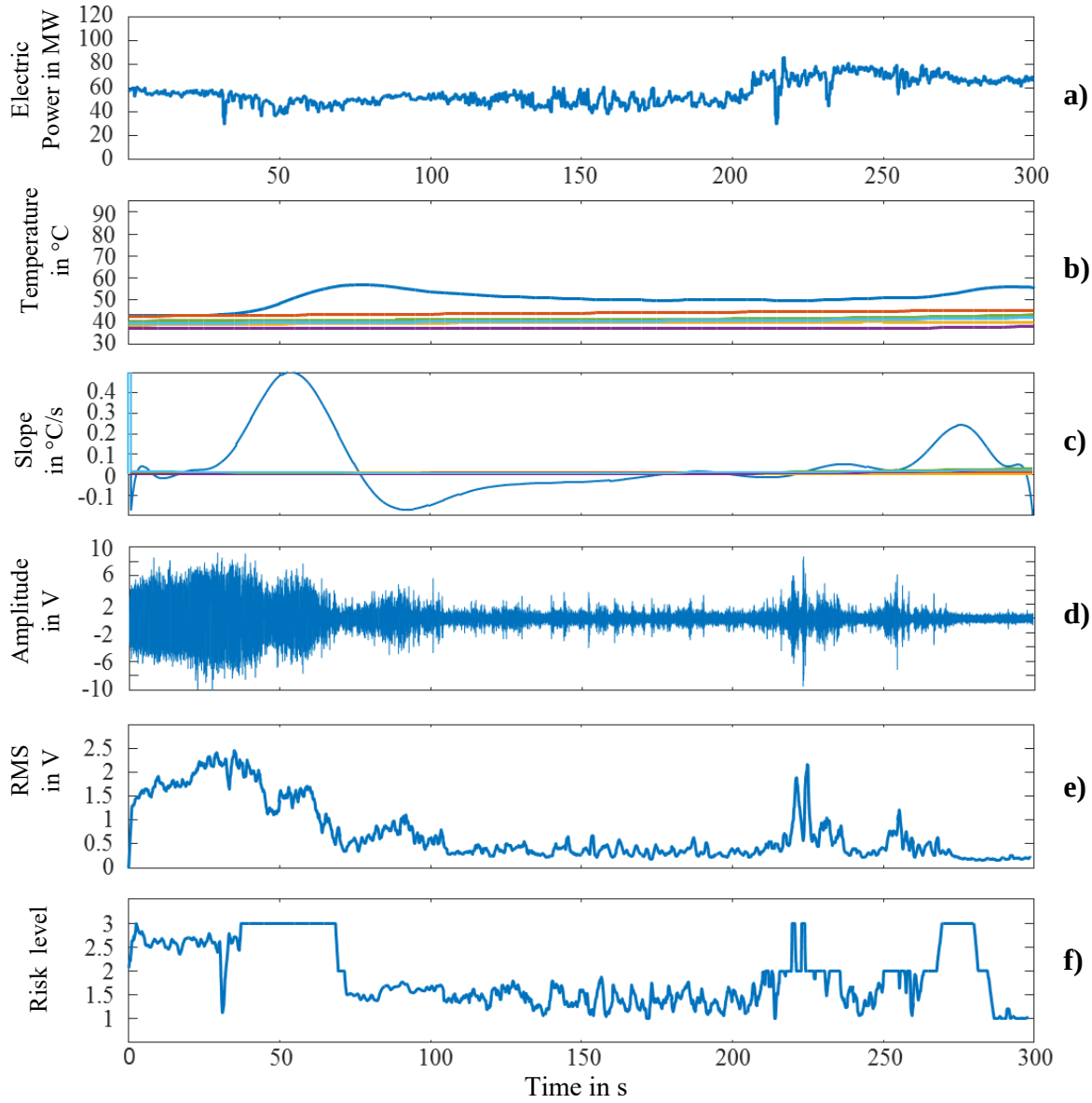

Fig. 5.19 a) electric power, b) panel temperature, c) temperature slope, d) raw vibration, e) RMS vibration and f) TSK output

At the beginning of the interval the electric power amounts approximately 60 MW, with a considerable increase in the vibration. During 0 to 35 s it can be seen how the risk indicator behave in a similar way as the RMS vibration keeping its value near three (danger level), then one of the panels began to heat at a high rate as seen in Fig. 5.18 b) and c). During 35 to 60 s the high temperature slope causes that the risk indicator saturates its value at level three. At 50 seconds a drop in the electric power from 60 MW to 40 MW appeared, consequently a reduction in the vibration of the EAF occurs, the risk indicator drops its value to values near 1.5 and panel temperature also drops. Similar behavior as explained before can be seen in the graphs regarding the less intense temperature increment that occurs between 250 and 300 s. The next figure shows another operative condition during heat 12726. A good arc coverage was present during whole 300 s interval of Fig. 5.20.

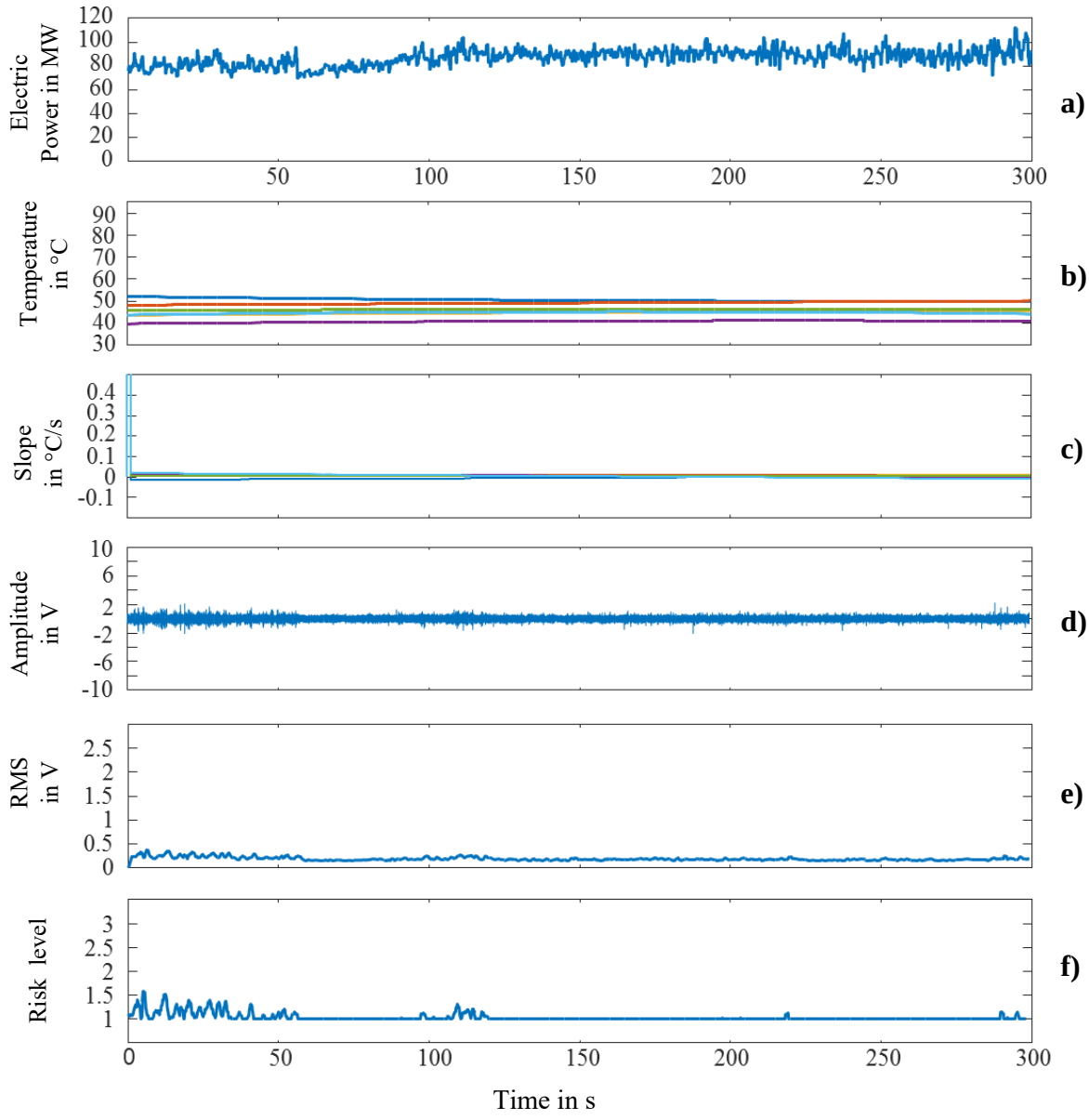

Fig. 5.20 a) electric power, b) panel temperature, c) temperature slope, d) raw vibration, e) RMS vibration and f) TSK output

The electric power began at 80 MW and then increases to values near 100 MW. Vibration and temperature slope are at low levels, all of this is reflected in the low values of the risk indicator in Fig. 5.20 e).

Next in Fig. 5.21 it can be seen how the operative conditions are not as stable as in the previous figure, the electric power was increased near 120 MW and vibration goes to medium levels. The risk indicator rises its value to level two, then the electric power was reduced at 55 s approximately.

Despite the power reduction vibration maintain a medium intensity. Slow and sustained heating of the panels was present from 0 to 225 s and as can be seen the arc risk indicator maintains its value primarily at level two.

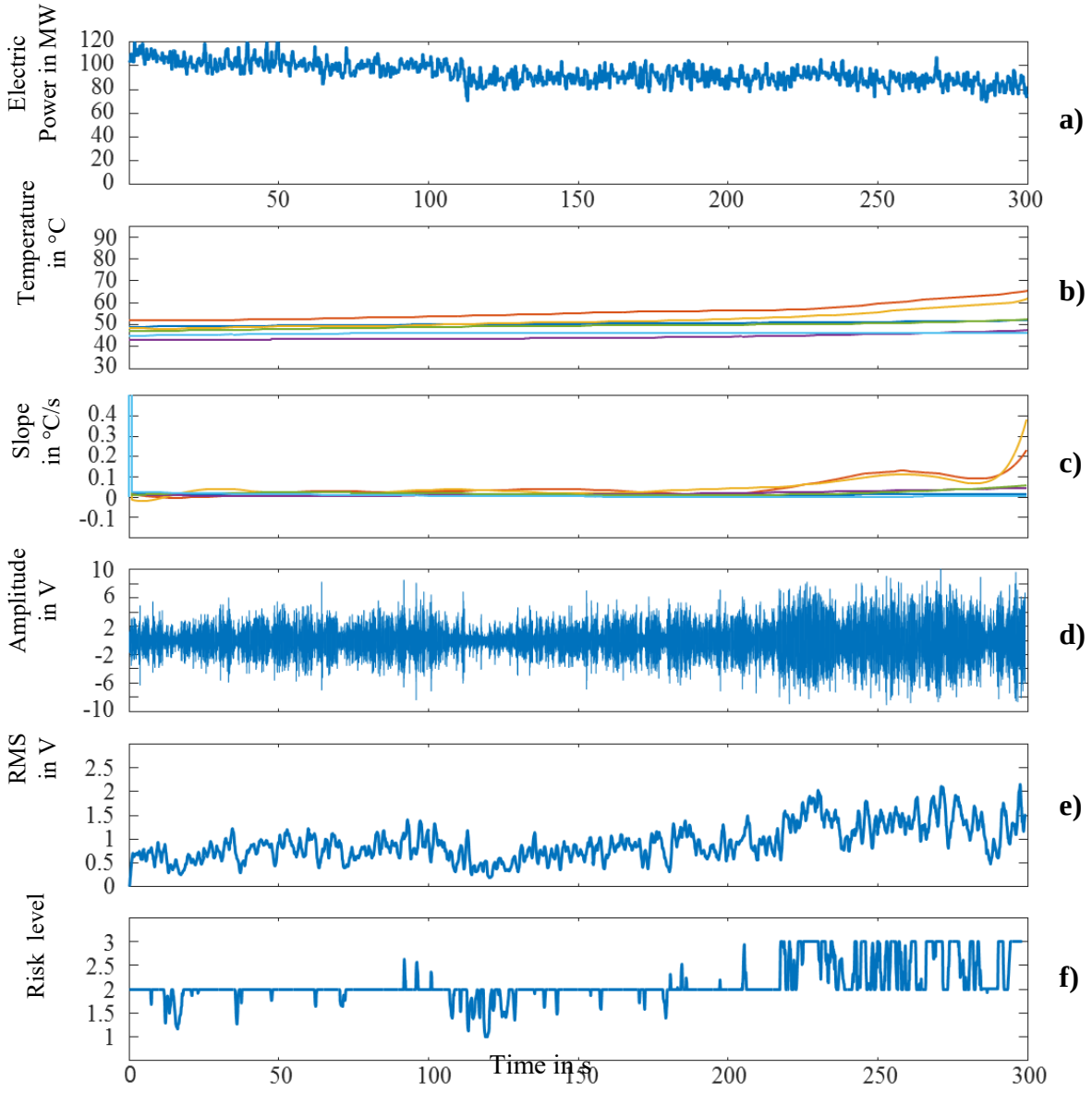

Fig. 5.21 a) electric power, b) panel temperature, c) temperature slope, d) raw vibration, e) RMS vibration and f) TSK output

From the second 225 vibration increases and an increase in temperature slope occurs, the risk indicator reacts according to these changes starting to oscillate between two and three as shown in Fig. 5.21 f), denoting and unstable EAF operation. In Fig. 5.22, at the beginning of the interval

shown, an increment in the temperature slope can be seen also high vibration, this causes the risk indicator maintaining its value primarily at level thee, until approximately 20 s, when the electric power is reduced to near 60 MW.

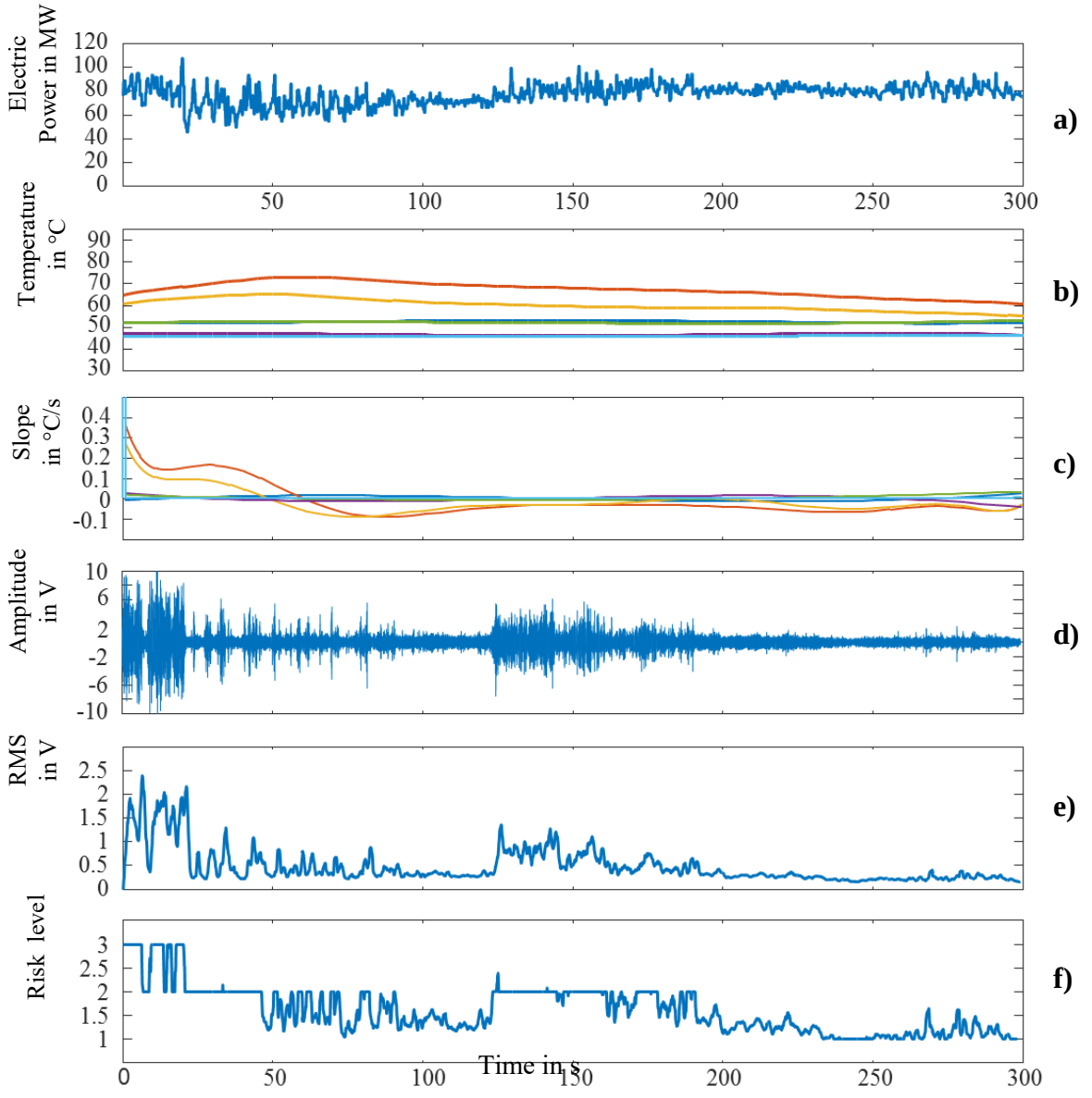

Fig. 5.22 a) electric power, b) panel temperature, c) temperature slope, d) raw vibration, e) RMS vibration and f) TSK output

As can be seen in Fig. 5.22 f) the risk indicator dropped to level two as the vibration reduces its intensity, the panel temperature reaches its peak (70 °C) at 55 s approximately, this due to the thermal inertia, this is shown in 5.22 b). The reduction of vibration and temperature slope causes a reduction in the risk indicator from 50 to 125 s, where its value oscillate between level one and two. From 100 s the electric power starts to be increased and, at 125 s, the vibration increases its

intensity. This power and vibration raise are reflected in the risk indicator, which increases its value to level two again. However, after proximately one minute, the EAF begins to behave in a more stable fashion, as can be seen in the reduction of vibration from the second 180 in Fig. 5.22 e). Despite the electric power level that remains over 80 MW, the low vibration operation is reflected in the reduction of the risk indicator to level one, during the rest of the interval.

Next, in Fig. 5.23 can be seen how from the second 50 of the intervals the electric power was increased to 100 MW approximately, the vibration increases a little bit, reason which the risk indicator started to oscillate between values from one to two as can be seen in Fig. 5.23 f). However, during this section of the interval there is not an increment in temperature.

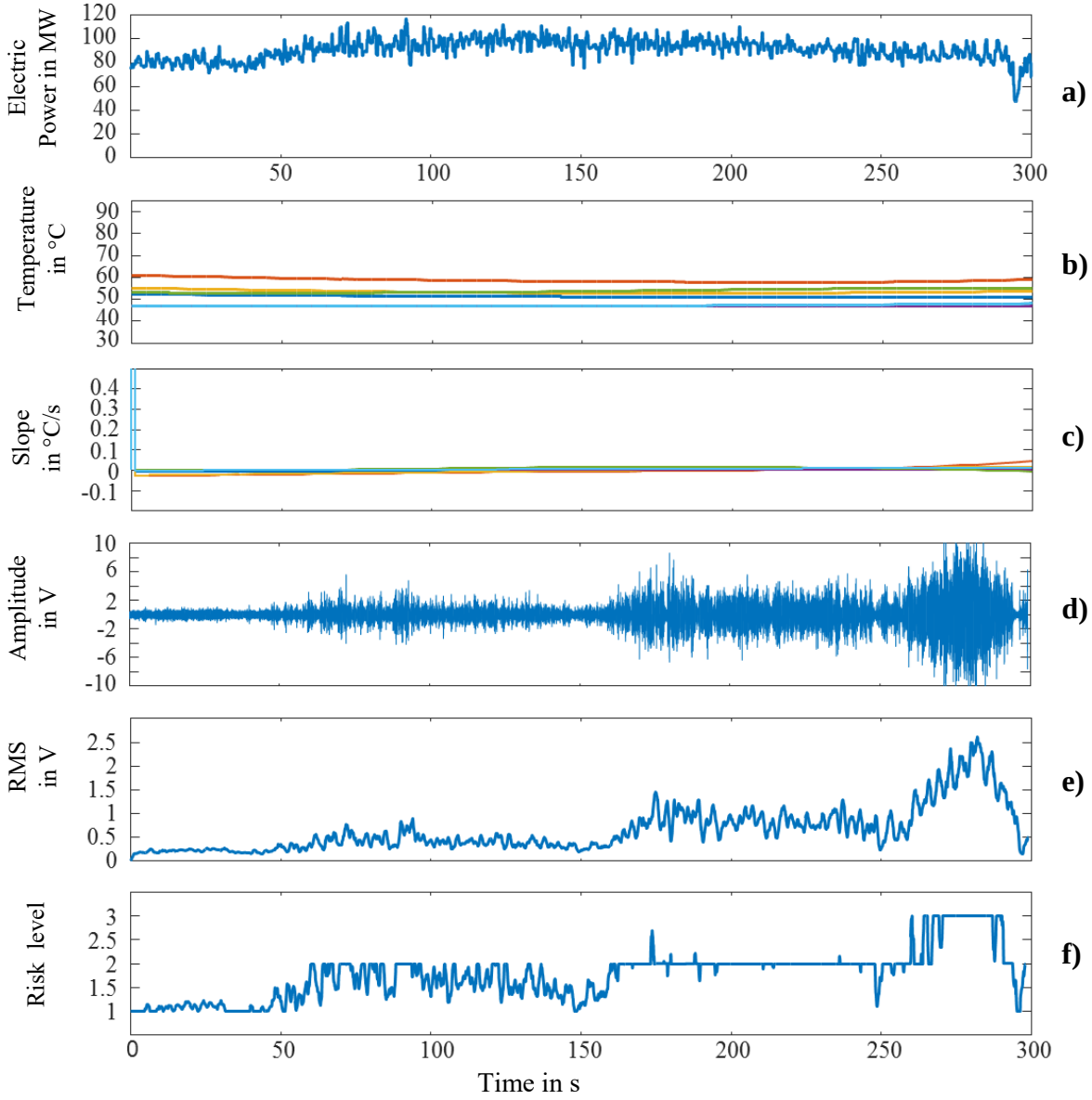

Fig. 5.23 a) electric power, b) panel temperature, c) temperature slope, d) raw vibration, e) RMS vibration and f) TSK output

During 150 to 250 s Fig. 5.23 e) shows and considerable increase in the vibration level at electric power levels over 80 MW, this leads the risk indicator to maintain its value at level two, this is shown in Fig. 5.23 f). From 250 s a severe increment in vibration occurred, the electric power level is above 80 MW, which produces the risk indicator to increase to level three, this until the electric power was considerably reduced as can be seen at the end of Fig. 5.23 a). Despite the reduction in power, heating in the panels occurs, this temperature increment is shown next in Fig. 5.24, which reaches its peak (65°C) at approximately 50 seconds.

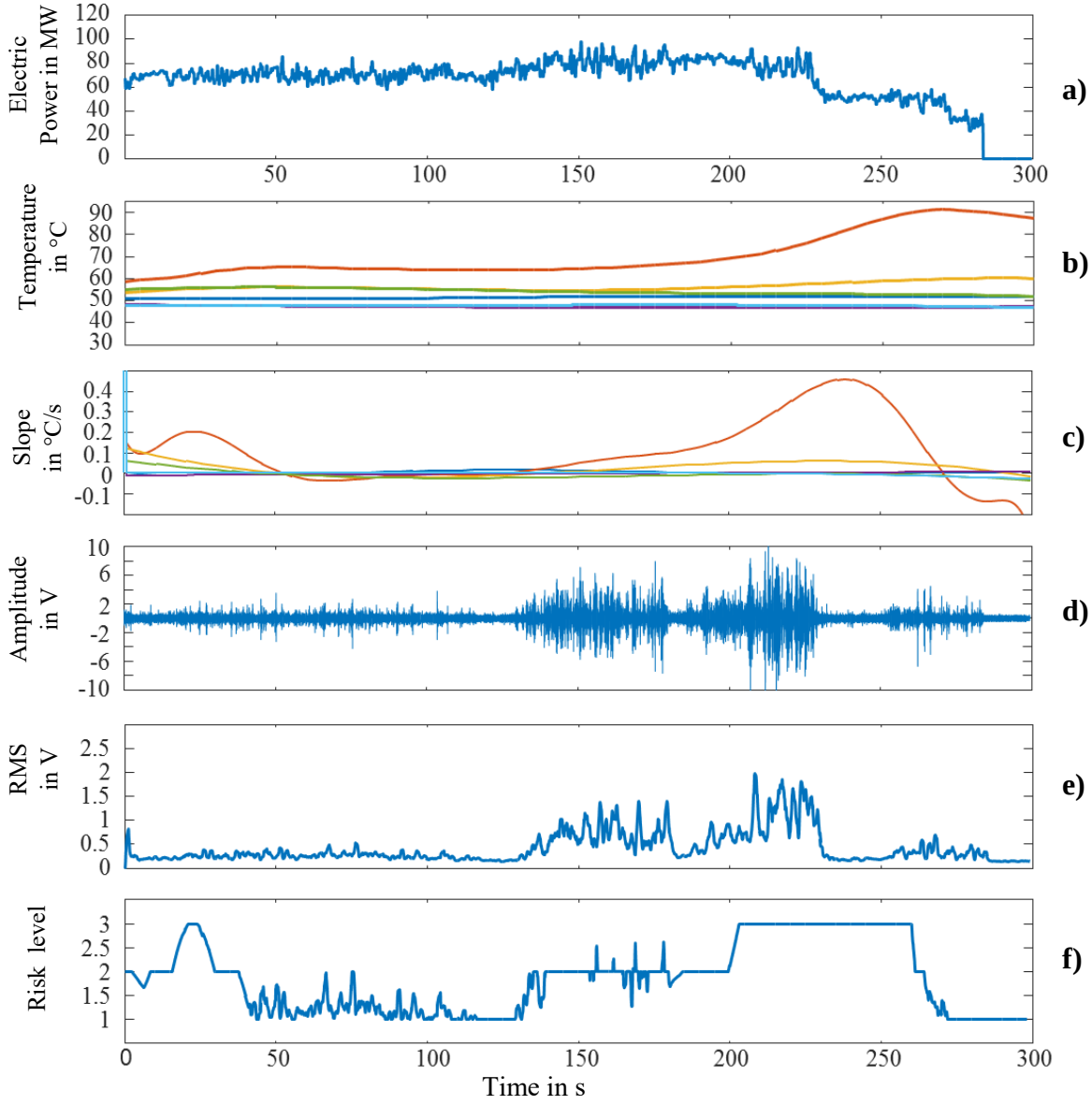

Fig. 5.24 a) electric power, b) panel temperature, c) temperature slope, d) Raw vibration, e) RMS vibration and f) TSK output

As can be seen in Fig. 5.24 c) from 0 to 50 s temperature increase at a considerable rate, however, the temperature peak did not exceed the 70 °C, this is attributed to the reduction of electric power show at the end of Fig. 5.23 a). From the second 50 the electric power was maintained below 80 MW, avoiding that panel temperature keeps increasing, a decrement in vibration intensity was also observed, this until second 125 approximately, when electric power was increased above 80 MW, then vibration and panel temperature began to increase. The last leads the risk indicator to take a value of two from 125 to 200 s. The electric power remains in levels near 80 MW when, at second 200, the vibration and the temperature slope increase in such way that the risk indicator saturate its value at level three. The high temperature increment at the end of the interval surpass the 90 °C. A considerable reduction in the electric power was the applied at the second 225 as shown Fig. 5.24 a). As a final observation, it is important to mention how the risk indicator reaches a danger level approximately at second 200, that it's to say 20 to 25 seconds before the control action (reduction in power level) was taken in order to counter the temperature increase. As can been inferred, the off-line processing only allows to describe many process situations, however, in order to perform an evaluation of the risk indicator a real time processing must be done, this in order to allow the EAF operator to change process parameters depending in the risk level. with this a comparison of the EAF performance can be done, before and after the use of the risk indicator which in intended as a visual help for the operator and not for a closed-loop operation.

Chapter 6. On line Implementation of the multivariable fuzzy system

In order to carry out an on-line arc coverage detection, a LabVIEW application was developed. In this case, a producer-consumer scheme using an enqueuer strategy was applied. The last in order to ensure that no data is missing during the different processing stages. In Fig. 6.1, an operation diagram of the application is shown.

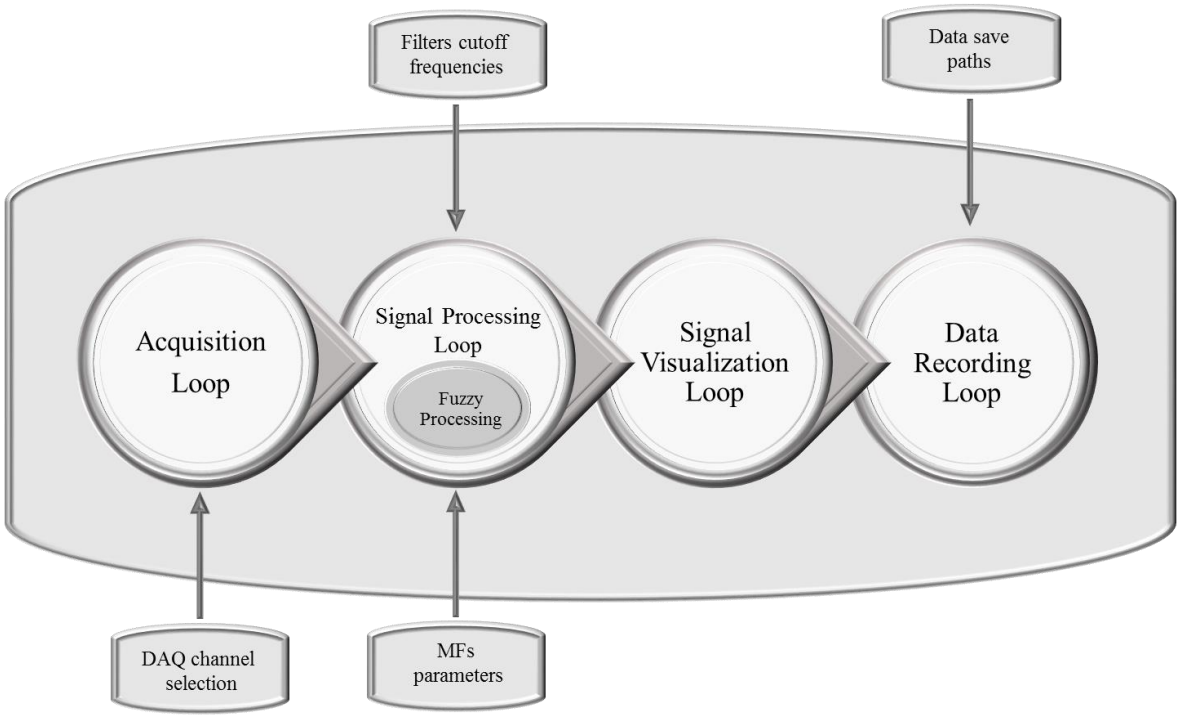

Fig. 6.1 Diagram of the arc coverage application

Multiple loops were implemented; each loop passes data to the next through a data queue, additionally, the user can enter different parameters to each loop in order to configure the application. In contrast to the off-line processing low pass filter were added to the temperature slope and the electric power inputs, the chosen topology was second order Butterworth filters with cut frequencies of 0.35 Hz. To test the application multiple signals were created using generators, this with the objective to emulate the final implementation. In Fig. 6.2 the generators and the data acquisition system are shown.

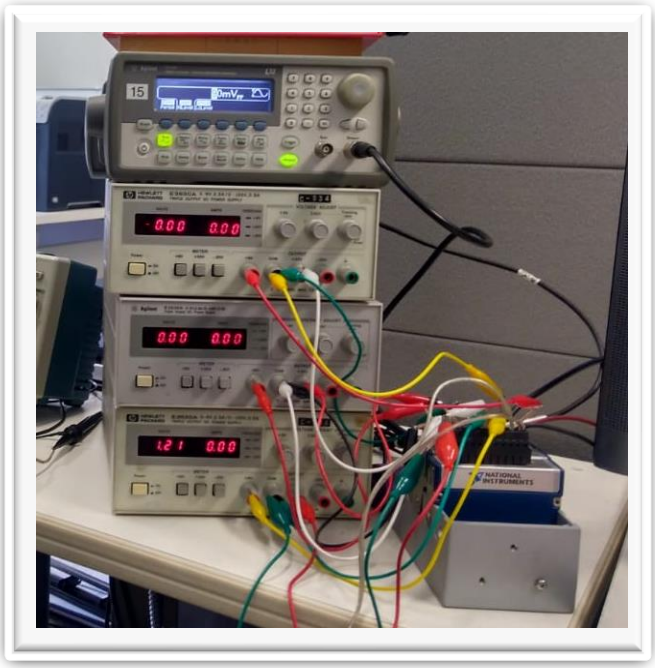

Fig. 6.2 Generators connected to the data acquisition system

The input signals to emulate the real time operation of the application are:

- A sinusoid signal to emulate the raw vibration from the EAF
- A DC signal to emulate the electric power levels
- Five DC signals the emulate the temperature of multiple cooled panels

All the calculations for the conditioning of the inputs, explained in the previous chapter, were implemented in the application to process dynamic data. The RMS value of the raw sinusoid is obtained in real time, as well the maximum slope of the temperature signals. From Fig. 6.3 to 6.5 the application was tested under different scenarios. In Fig. 6.3, scenario A shows how the vibration starts to increase, however due to the low power and low temperature slope the risk indicator remains in level one. In Fig. 6.4, scenario B shows how the vibration is very intense, and how the coverage indicator response in function of the electric power changes, despite the low temperature slope. In fig. 6.5, scenario C shows another example of high-power operation, with low vibration and low temperature slope, these conditions maintain the risk indicator in a safe level. This until high temperature slope is registered, causing the arc coverage indicator to increase.

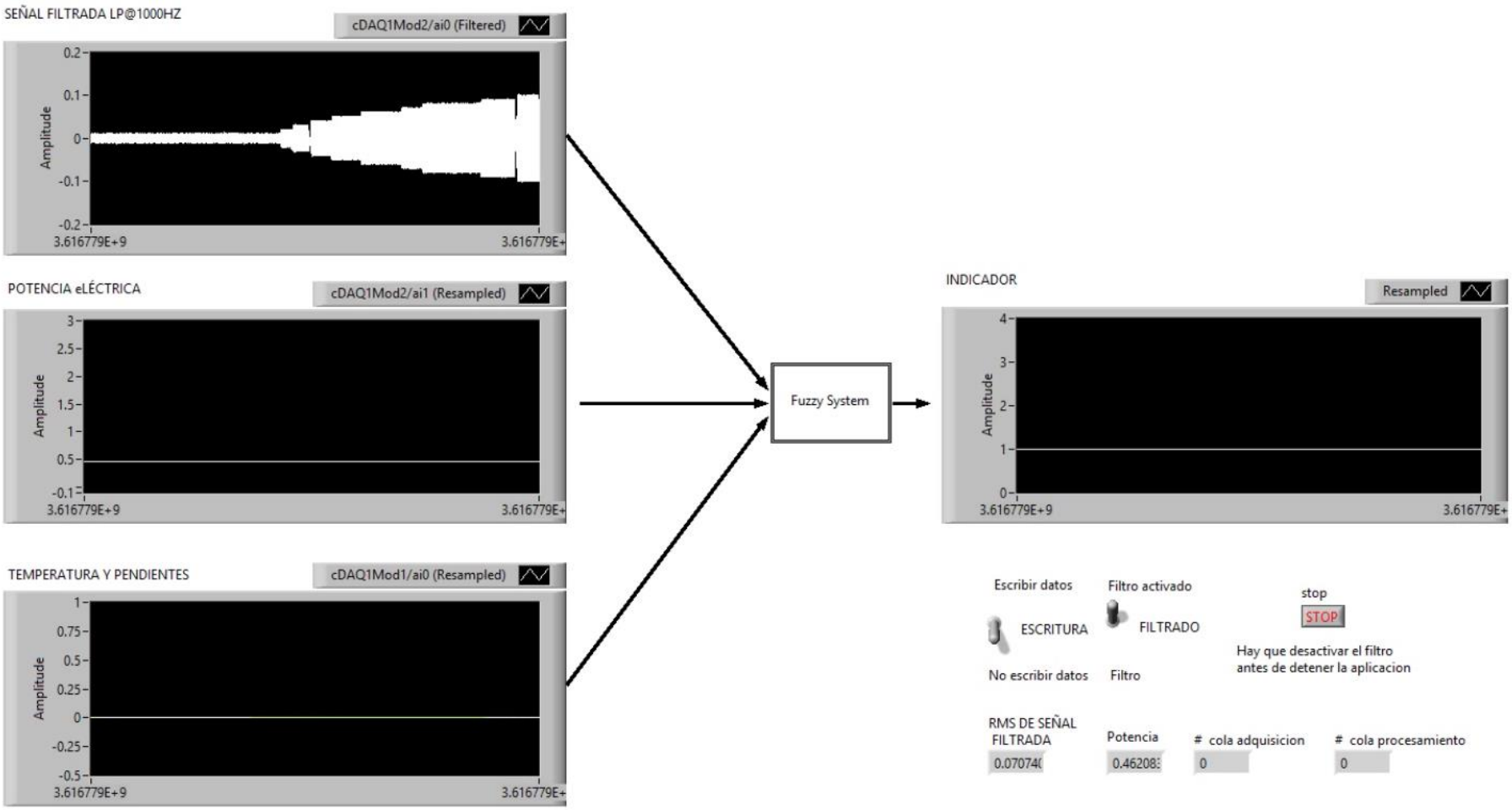

Fig. 6.3 Arc coverage application running in real time, scenario A

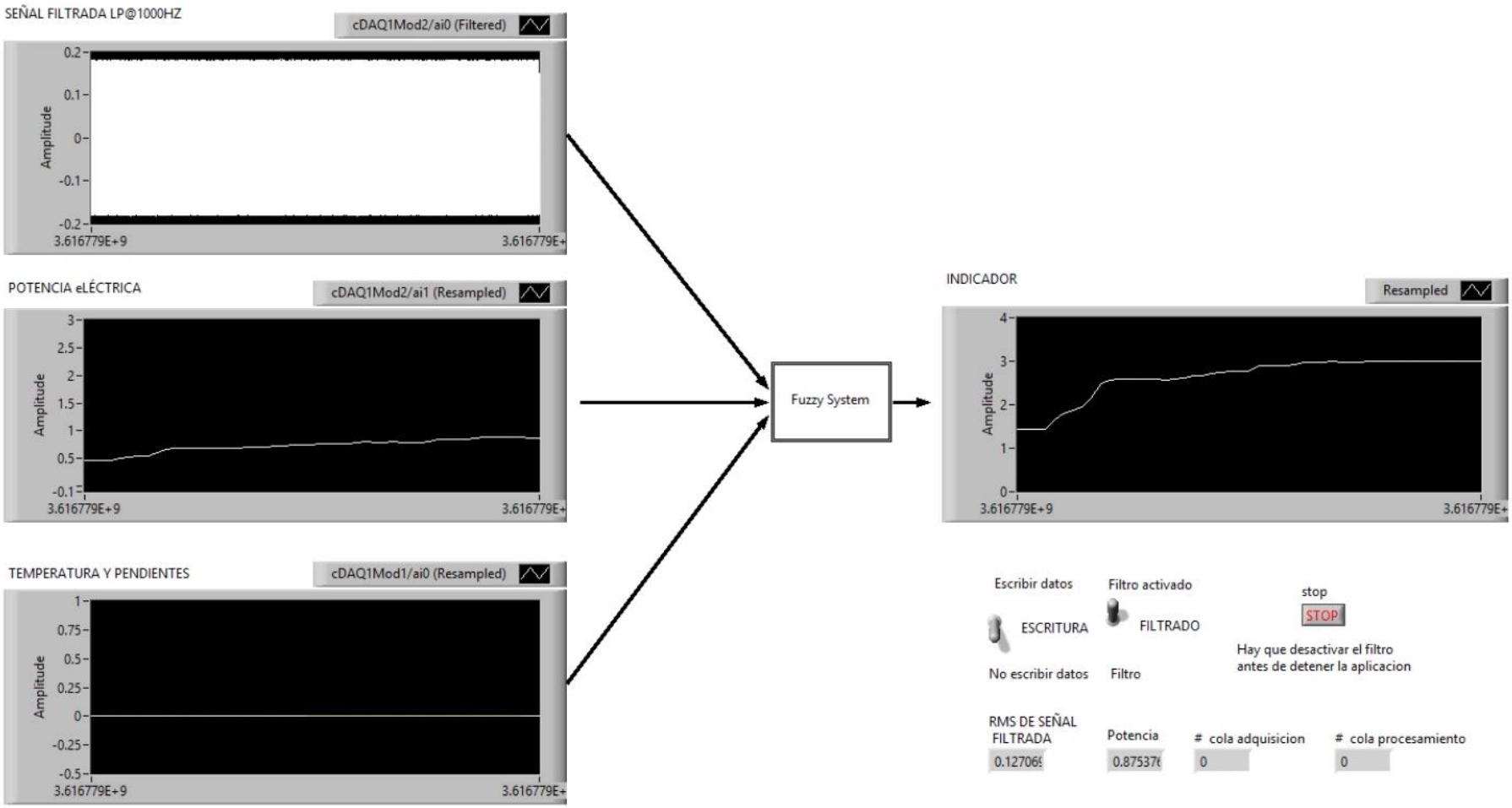

Fig. 6.4 Arc coverage application running in real time, scenario B

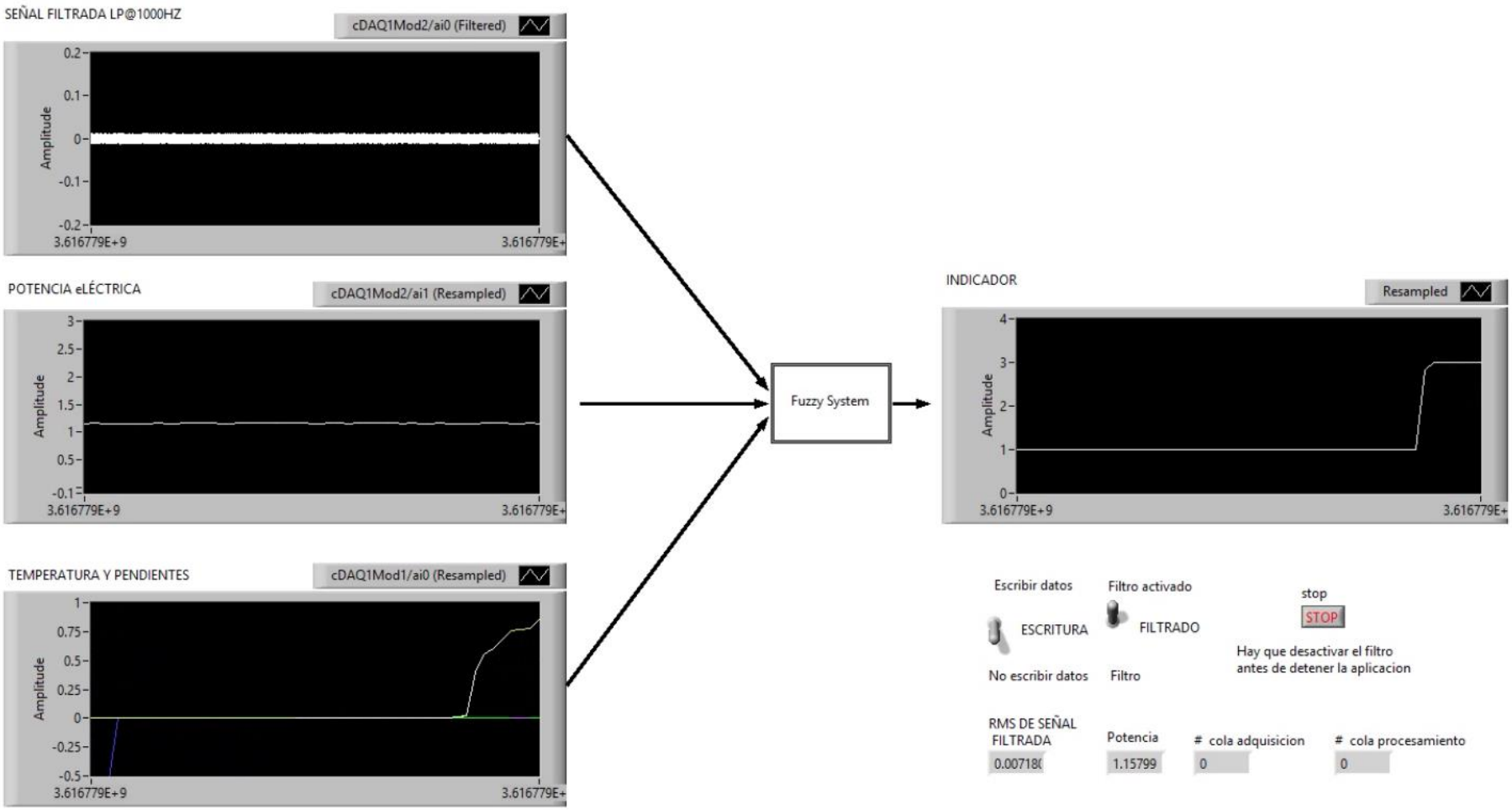

Fig. 6.5 Arc coverage application running in real time, scenario C

Another feature added to the application was the generation of an analog signal proportional to the risk indicator, in other words, a DC signal that can takes values from 1 to 3 V. This signal is intended to be recorded in Ternium's database or be used as a control signal in the future. In Fig. 6.6 is shown the application screen and an oscilloscope where the analog output is displayed.

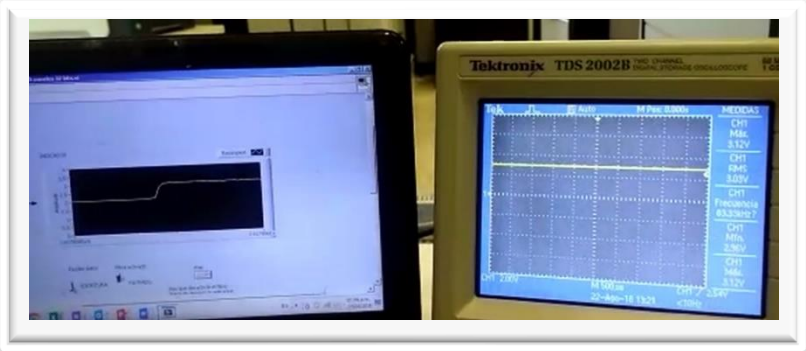

Fig. 6.6 Comparison between arc coverage indicator and its proportional analog signal.

The analog output response was satisfactory, regarding the precision of the voltage level and the velocity when a change in the inputs occurs. For the final validation, the application was tested in the EAF while all the signals are being registered. The results and final considerations are detailed in the next section.

6.1 Real time operation of the risk indicator in the DC EAF

In this section is described the installation of the laser vibrometer, also the installation of the data acquisition equipment and cables in order to measure and process, in real time, panel temperatures an electric power. To protect sensible electronic equipment from hard environment conditions, the processing unit of the laser vibrometer was screwed into a steel box as can be seen in Fig. 6.7, the box is also equipped with a small fan to keep the operating temperature within acceptable ranges.

Fig. 6.7 processing unit of the vibrometer installed inside a steel box

To support the laser emitter head of the vibrometer, Ternium personnel welded a heavy plate in a column of the steel shop, to which the geared head that supports the emitter was screwed, this is shown in Fig. 6.8.

Fig. 6.8 Laser emitter installed in the steel shop

A 60-meter cable was laid from the analog output at the front of the processing unit of the laser vibrometer, to the data acquisition system which was installed in the computer room of the EAF. In the case of temperature and electric power, Ternium personal enabled analog PLC outputs in order to provide electric signals, proportional to the temperature of the five most problematics panels and the electric power. The necessary cable to acquire these signals was installed under the floor of the computer room. The acquisition system with all the wiring is shown in Fig. 6.9.

Fig. 6.9 Data acquisition system installed in the computer room of the EAF

In order to obtain the temperatures and the electric power in its corresponding units, a simple scaling method using the equation of a line, which is described next, was used for each signal.

$$S_s = (V)(C_p) + O$$

where S_s represent the scaled signal, V represent the values that each PLC output provides, C_p is a proportionality coefficient which is obtained as follows.

$$CP = \frac{L_i}{L_o}$$

where L_i represent the input lengths (electric signals from the PLC in V) and L_o represents the output lengths (scaled signals in °C and MW)

$$L_i = V_{max} - V_{min}$$

$$L_o = S_{max} - S_{min}$$

Furthermore, V_{max} and V_{min} represent the minimum and maximum values that the PLC analog outputs can take and S_{max} and S_{min} the maximum and minimum values of the scaled signals. Finally, O represent the offset which is obtained as follows.

$$O = S_{min} - [(V_{min})(CP)]$$

Once the acquisition and scaling of the signals was validated several heats were recorded. To do this the 0 to 3 V signal proportional to the risk level indicator was wired to a Ternium's PLC input, using a 4 – 20 mA converter. The values of the risk indicator were recorded in Ternium's data base for several weeks in order fine tune the fuzzy algorithm proposed. Three fuzzy models were tested, the first one is the explained in section 5.4.1 in which 3 inputs are considered. The second model adds the sound of the EAF as an extra input. Finally, for the third model, the panel temperature (not only the slope) was added to the processing. The three models and some results are shown in the next sections.

6.1.1 Three-Input Fuzzy Model

As said before in this section is discussed the real time performance of the fuzzy model explained in section 5.4.1, which can be seen in Fig. 6.10. This model gave good results and was the starting point to make improvements regarding the fuzzy processing.

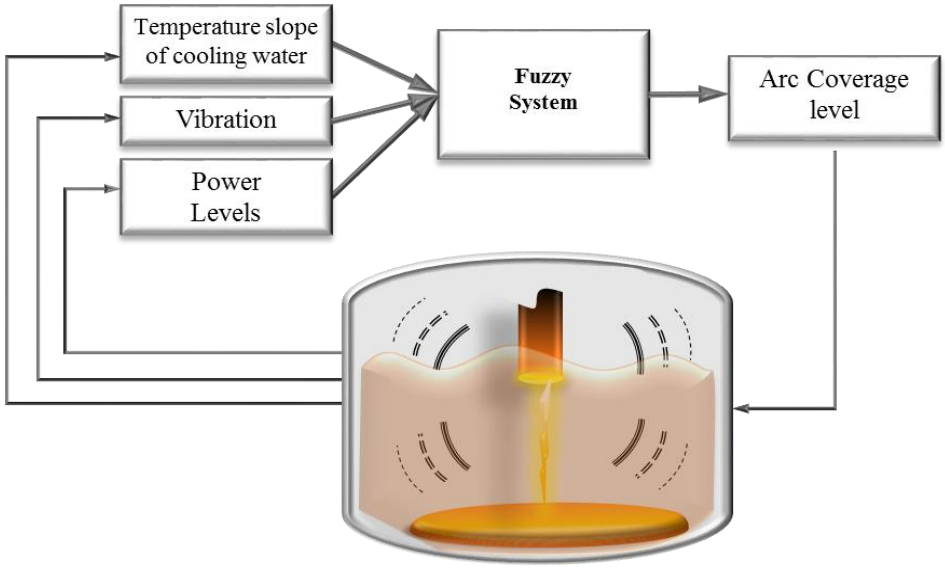

Fig. 6.10 Three-input fuzzy model

In this case the main difference between the off line and the real time application consist in the fine tuning of the MFs for vibration and temperature slope inputs. The new MFs are shown in Fig. 6.11.

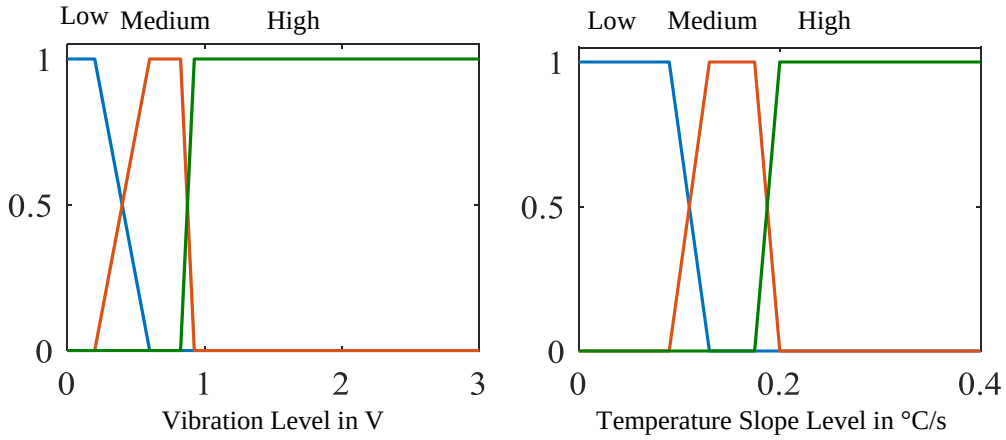

Fig. 6.11 New MFs for the real time application

From figure 6.12 to 6.14 some results obtained with the three-input fuzzy system are shown. In the graphs are displayed the electric power in MW, the temperature of cooling water of the panels in °C and the risk indicator in this order, from top to bottom. In Fig. 6.12 it can be observed that for the panel heating, the risk indicator increased its value to danger levels, anticipating the temperature peaks and anticipating the power reduction. A similar behavior can be observed in Fig. 6.13.

Finally, in Fig. 6.14 a low risk operation of the EAF is shown, this is reflected in the low panel temperatures

.

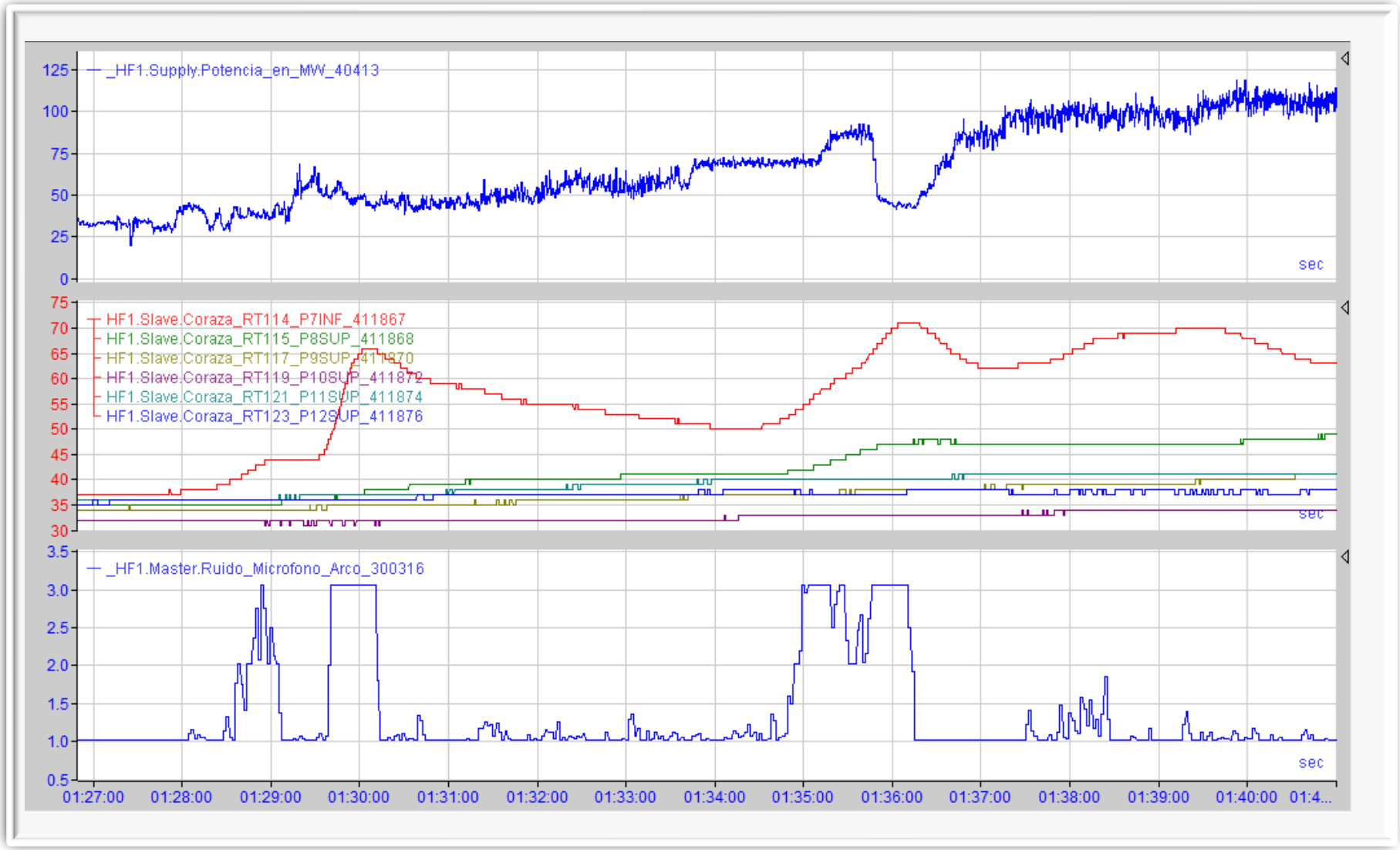

Fig. 6.12 Electric power, panel temperatures and risk indicator for the three-input fuzzy system

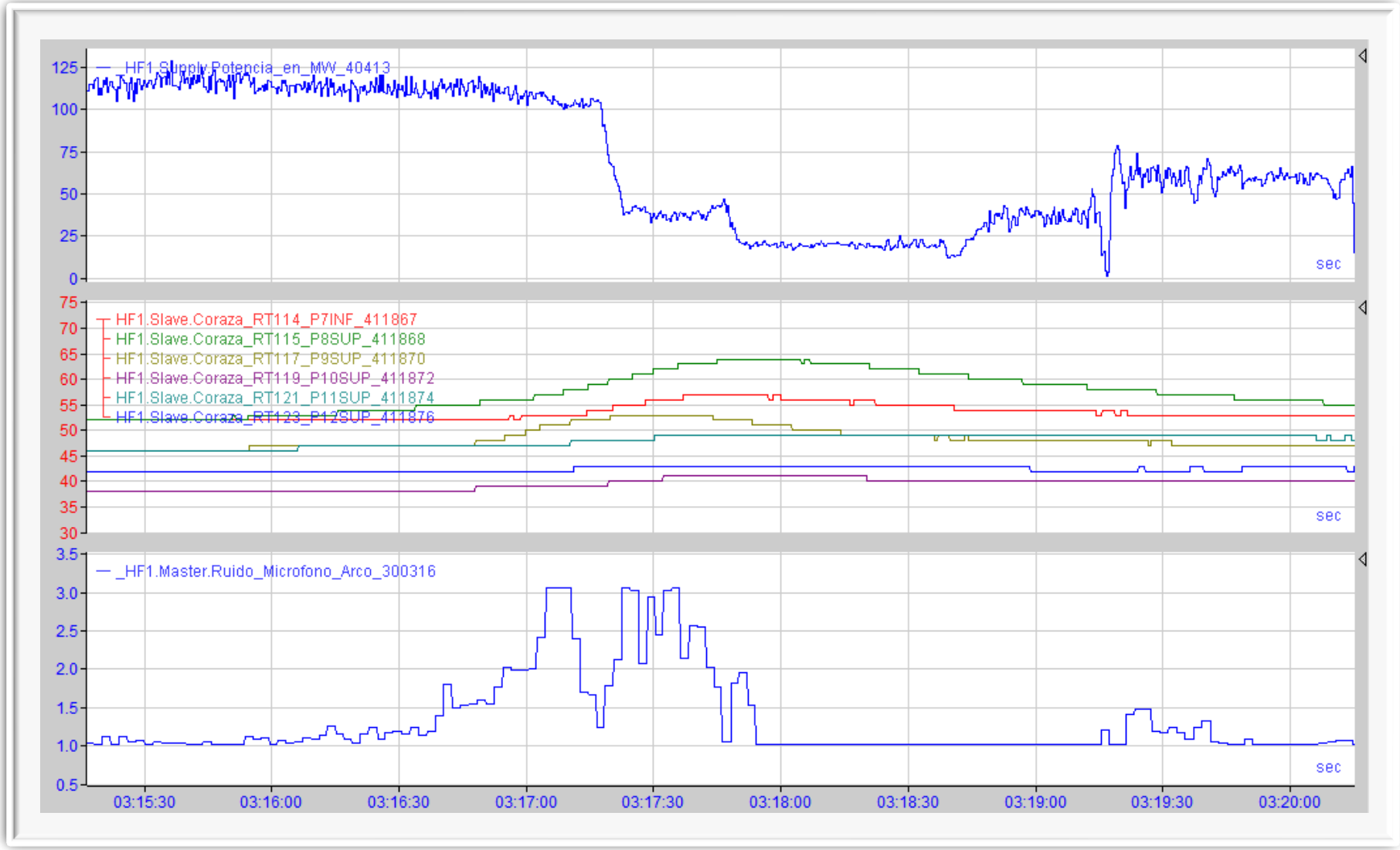

Fig. 6.13 Electric power, panel temperatures and risk indicator for the three-input fuzzy system

Fig. 6.14 Electric power, panel temperatures and risk indicator for the three-input fuzzy system

6.1.2 Four-Input Fuzzy Model

For this model the sound of the EAF was added as an extra input, the measurement and processing of the sound was carried out by M.C. Adrián Torres Rentería in whose doctoral thesis are explained the instruments to capture the noise of the EAF, as well as the necessary circuitry and algorithm for conditioning and generation of the sound signal. With the addition of the sound to the fuzzy processing, some robustness to the system was achieved, for example, if in some stage of the melting process the laser emitter is blocked and the vibration signal is saturated, the sound allows to the system to infer that this increment in the vibration occurs due to an external perturbation. To add one more input to the system, major changes were required regarding the programming of the set of rules, because of this it was decided to generate an auxiliary system as shown Fig. 6.15, thus leaving the original set of rules unchanged.

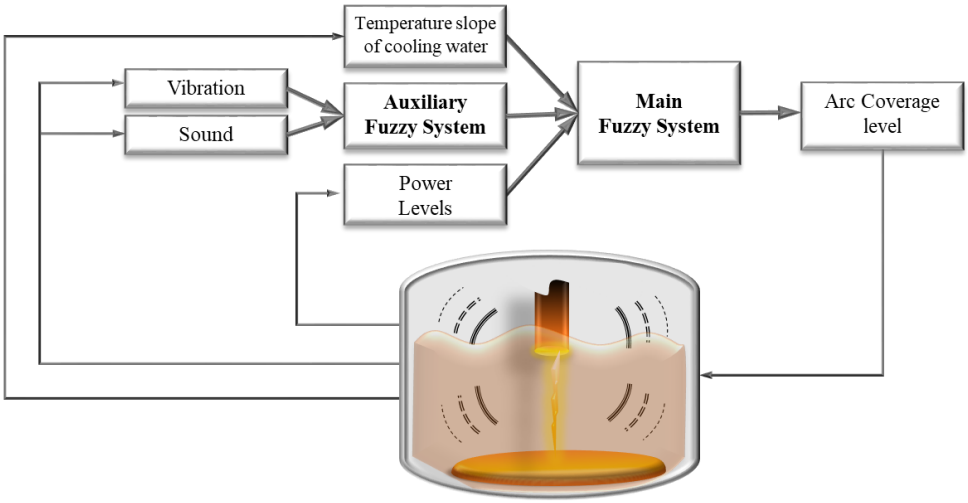

Fig. 6.15 Four-input fuzzy model

The auxiliary system performs a preliminary inference using only the vibration and the sound of the EAF, later the result is combined with the electric power and the temperature slopes to obtain the risk level. The MFs for the sound input are shown in Fig. 6.16.

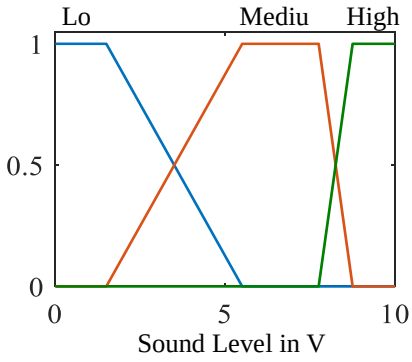

Fig 6.16 Membership functions for the sound input

The set of rules for the auxiliary fuzzy system are shown in the matrix below, where VL represent the vibration level while SL represent the sound level.

VL \ SL	Low	Medium	High
Low	1	1	1
Medium	1	2	2
High	1	2	3

Note that the matrix contains numeric values because the fuzzy model is a TSK. The output of the auxiliary fuzzy system, that can take values from 1 to 3, is now one of the inputs of the main fuzzy system, because of this a new input and its corresponding MFs must be defined for the main fuzzy system. The MFs are shown in Fig. 6.17.

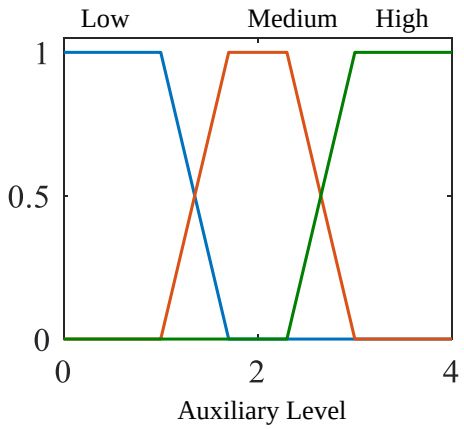

Fig, 6.17 Membership functions for the auxiliary input of the main fuzzy system

From figure 6.18 to 6.20 some results obtained with the four-input fuzzy system are shown. As in the case of the three-input system the graphs show the electric power, the temperature of cooling water of the panels and the risk indicator. In Fig. 6.18 is shown how the risk indicator reaches caution and danger levels before the temperature peak occurs. This behavior is also observed in Fig. 6.19. Finally, in Fig. 6.120 a low risk operation of the EAF is shown, as can be seen in the low panel temperatures.

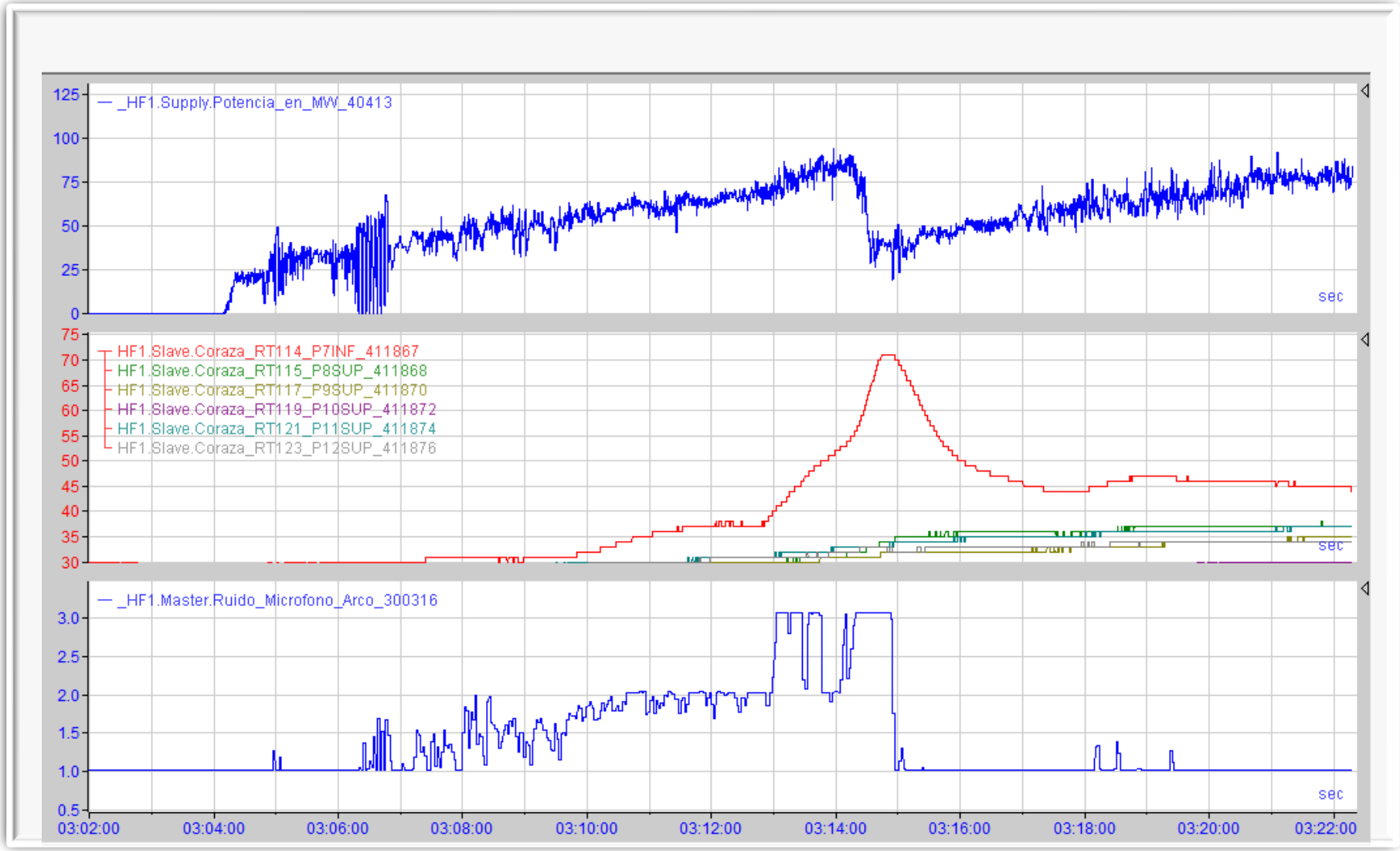

Fig. 6.18 Electric power, panel temperatures and risk indicator for the four-input fuzzy system

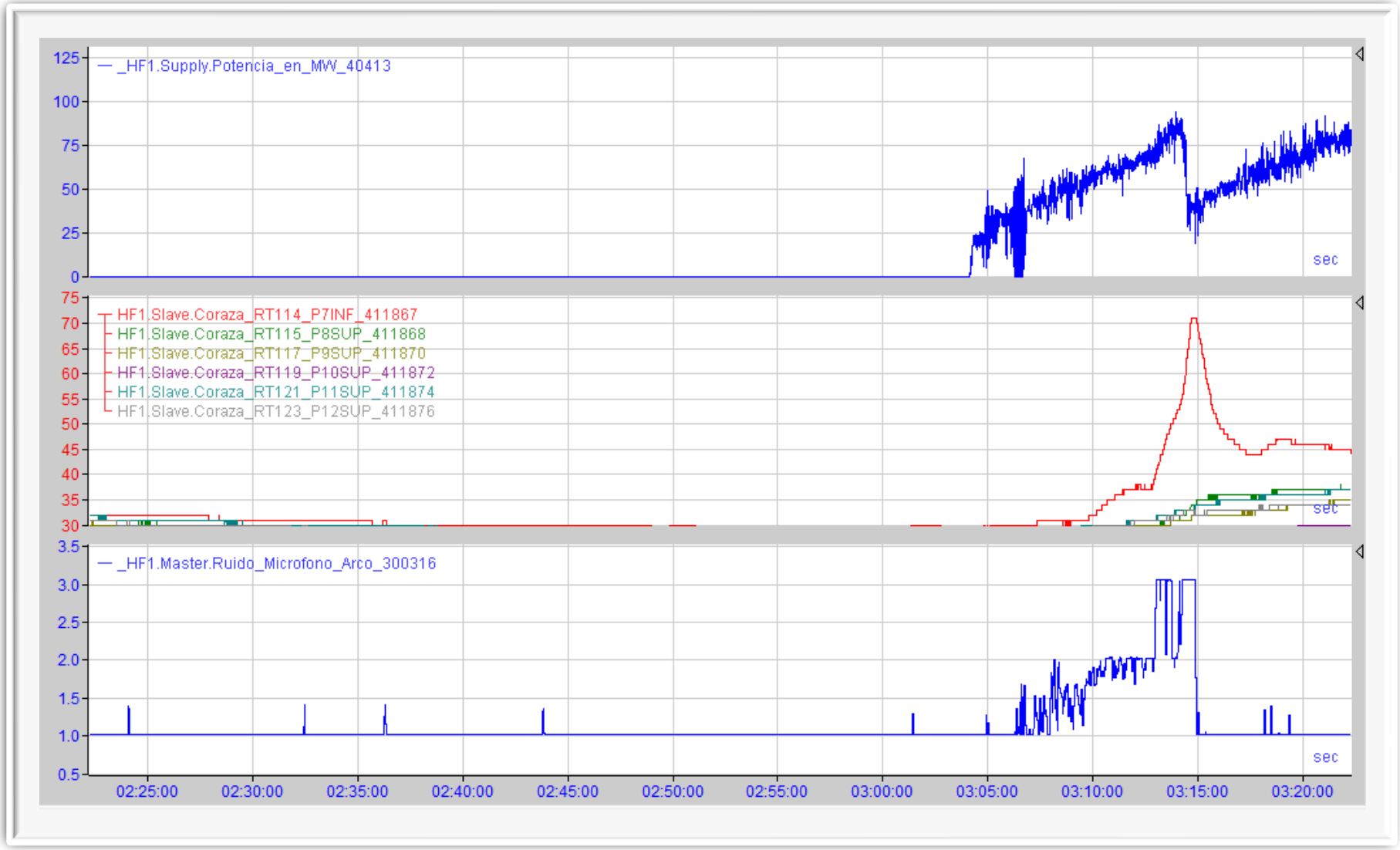

Fig. 6.19 Electric power, panel temperatures and risk indicator for the four-input fuzzy system

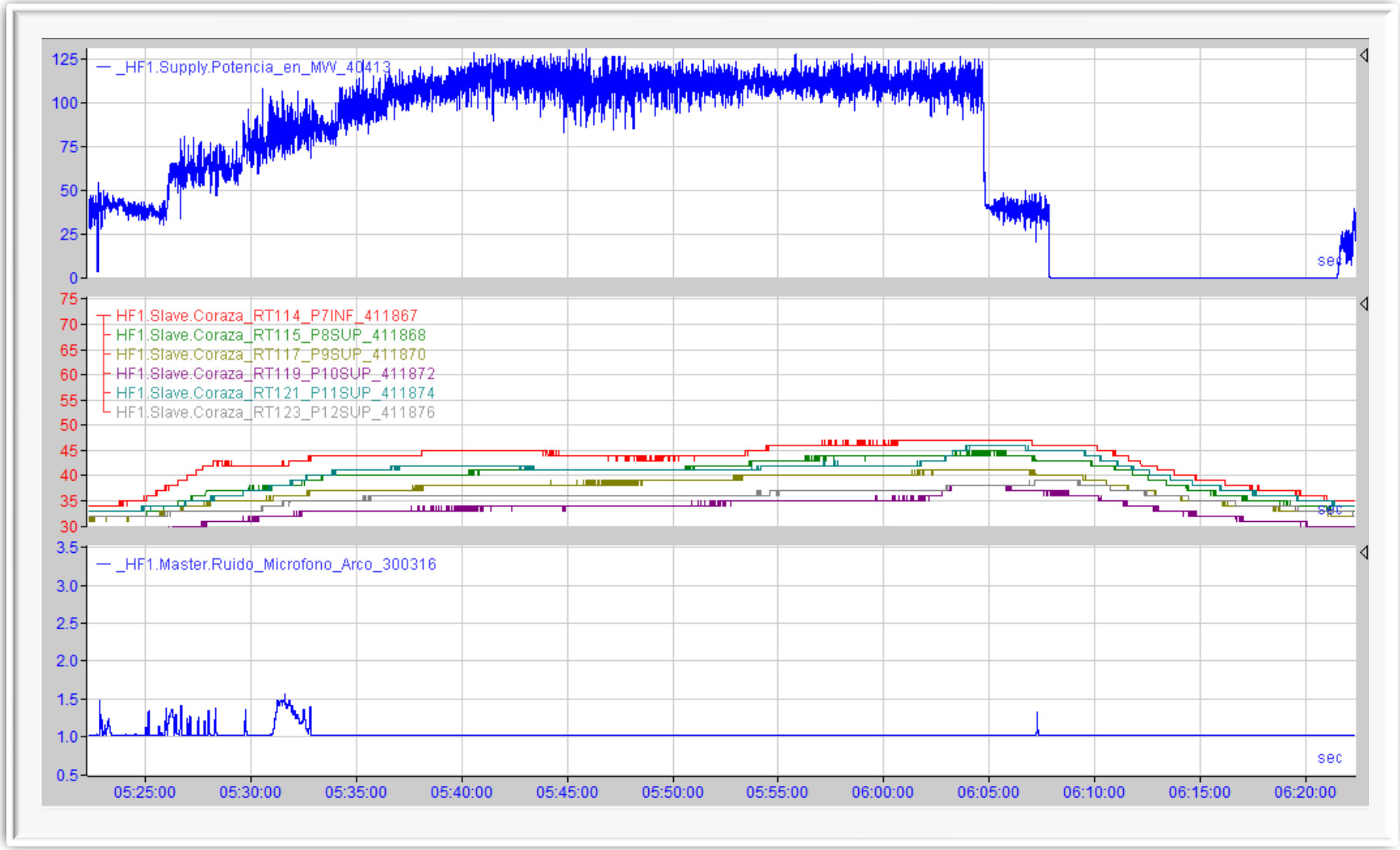

Fig. 6.20 Electric power, panel temperatures and risk indicator for the four-input fuzzy system

6.1.3 Five-Input Fuzzy Model

In this model another auxiliary fuzzy system was implemented in order to obtain a preliminary inference using the temperature and the temperature slope of the cooling water. As said before the objective to include the temperature signal in the processing, consists in avoid critical alarms due to high temperature slope at low temperature values. The model is shown in Fig. 6.21.

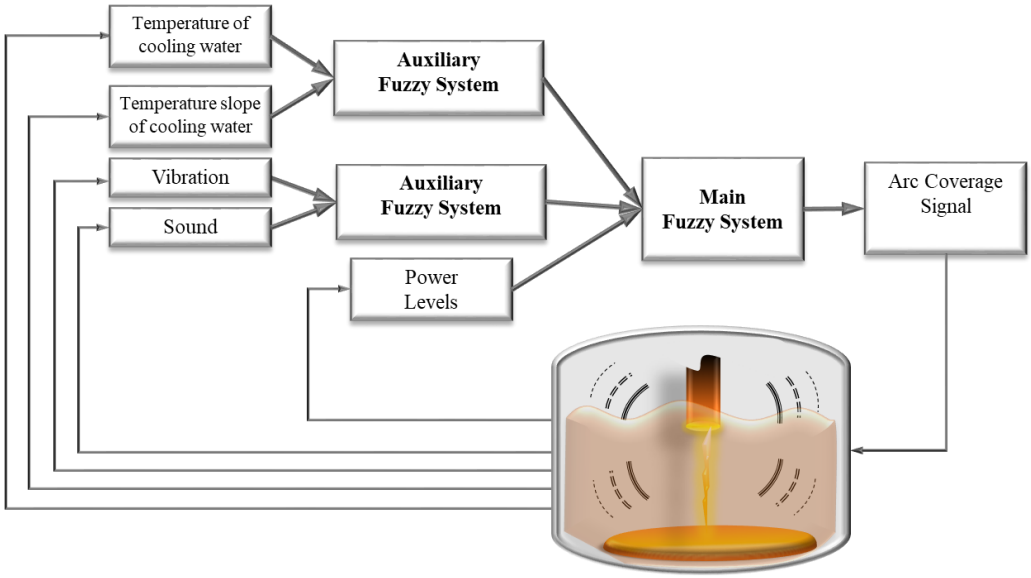

Fig 6.21 Five-input fuzzy system

The membership functions for the temperature input are shown in Fig. 6.22. In this case only two MFs where enough to satisfice the operative criteria.

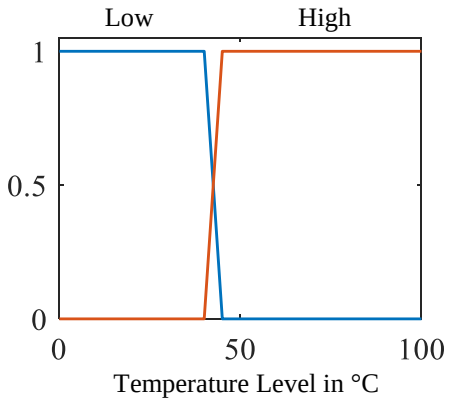

Fig 6.22 Membership functions for the temperature input

The set of rules for the auxiliary fuzzy system are shown in the matrix below, where TL represent the temperature slope level and HL represent the temperature level.

TL \ HL	Low	High
Low	1	1
Medium	1	2
High	2	3

As in the case before, the output of the auxiliary fuzzy system can take values from 1 to 3 and is now one of the inputs of the main fuzzy system. The corresponding MFs for this new input are shown in Fig. 6.23.

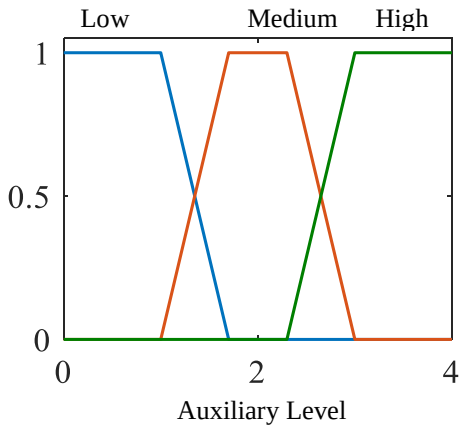

Fig 6.23 Membership functions for the auxiliary input of the main fuzzy system

From figure 6.24 to 6.28 some results obtained with the five-input fuzzy system are shown. At the beginning of Fig. 6.24 is shown how, despite a temperature increment with considerable slope, the risk indicator doesn't reach danger level, this due to the low temperature value (below 45 °C). At the end of the same figure is observed the normal behavior of the risk indicator where caution and danger level are reached before the temperature peak occurs. This normal behavior is also observed in Fig. 6.25, Fig. 6.26 and Fig. 6.27, with the difference that in the last, several temperature increments occurs, all of them alarmed opportunely by the risk indicator, this show the robustness of the algorithm. Finally, in Fig. 6.28 another low risk operation is shown where low temperatures can be seen during the melting process.

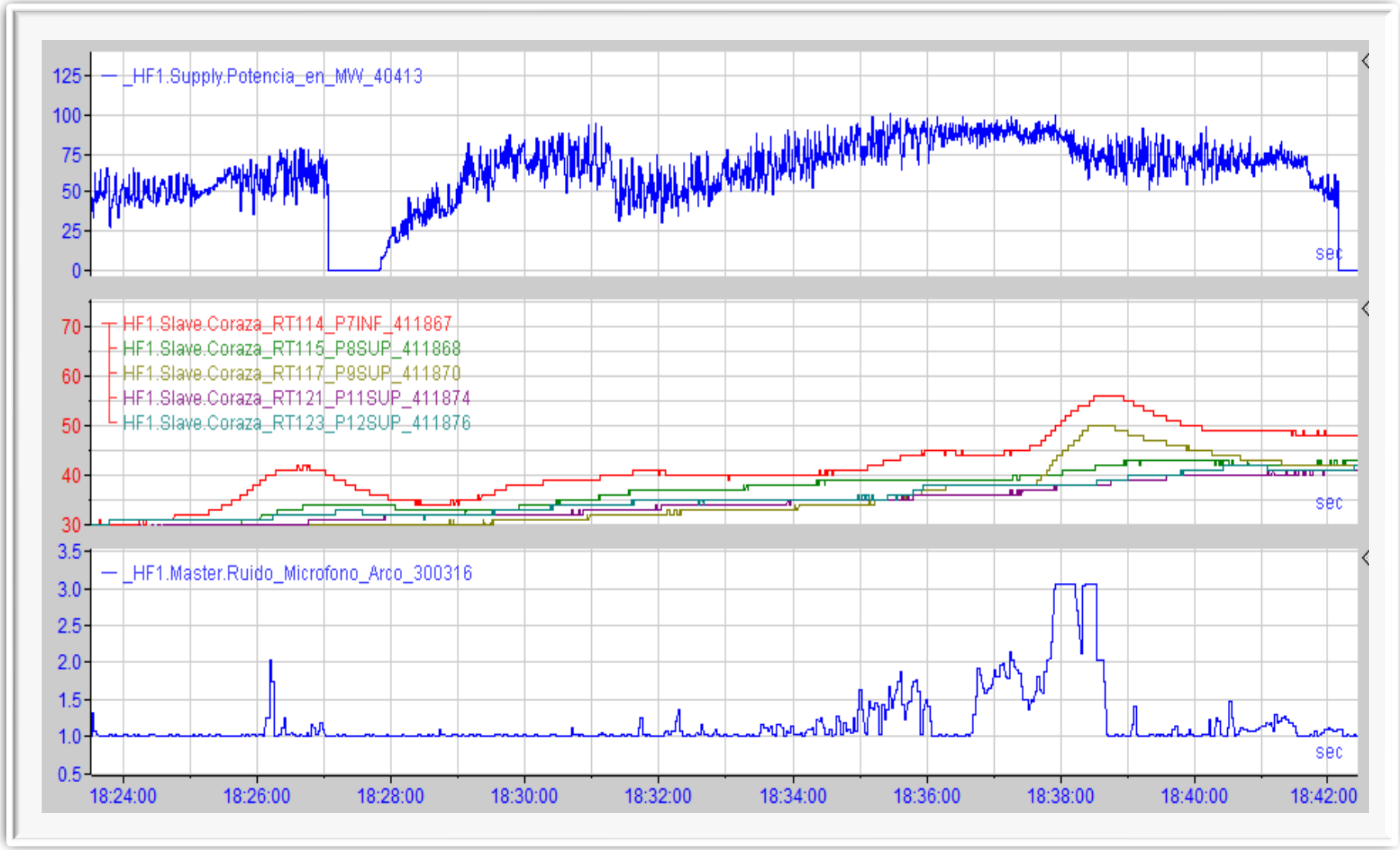

Fig. 6.24 Electric power, panel temperatures and risk indicator for the five-input fuzzy system

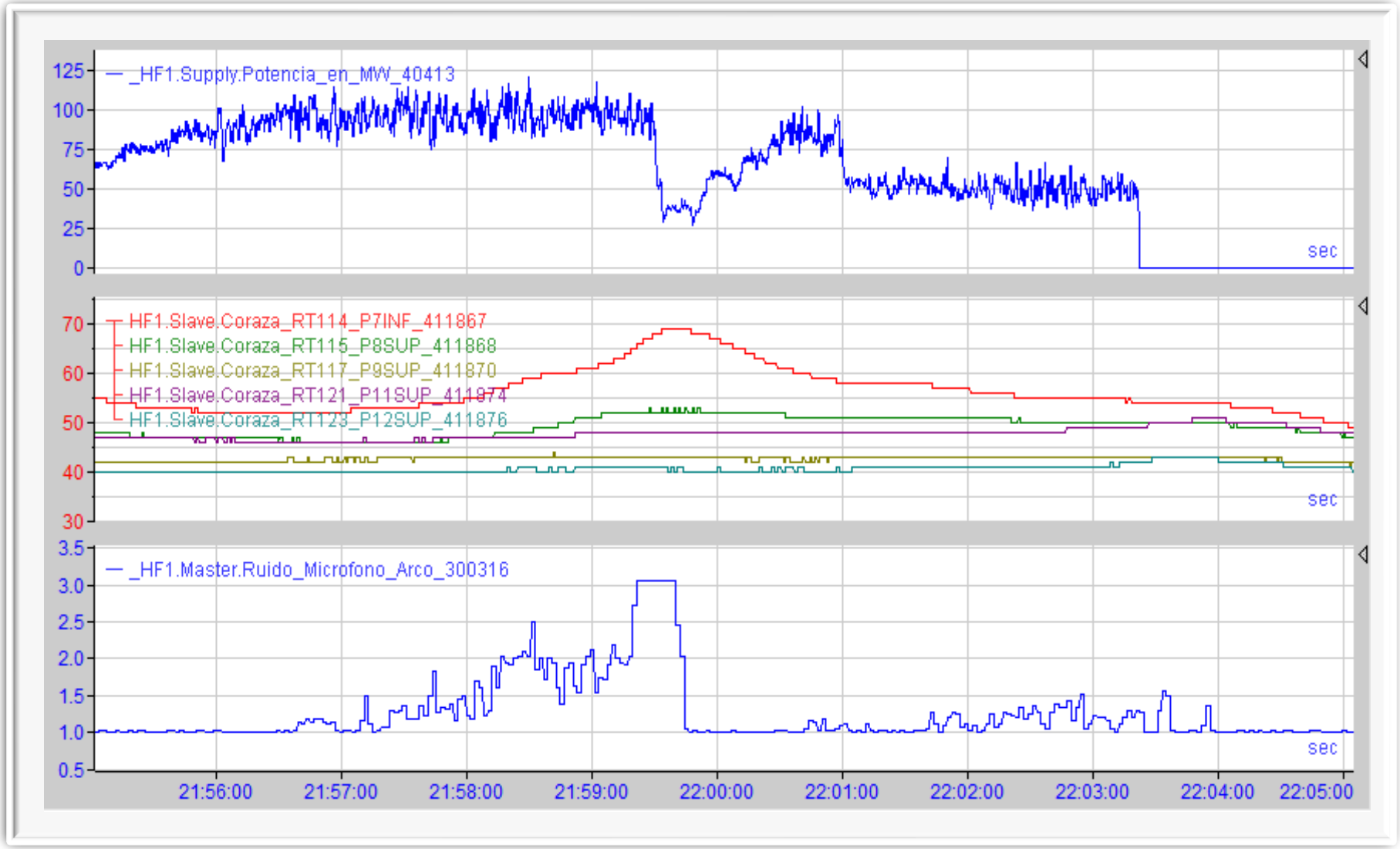

Fig. 6.25 Electric power, panel temperatures and risk indicator for the five-input fuzzy system

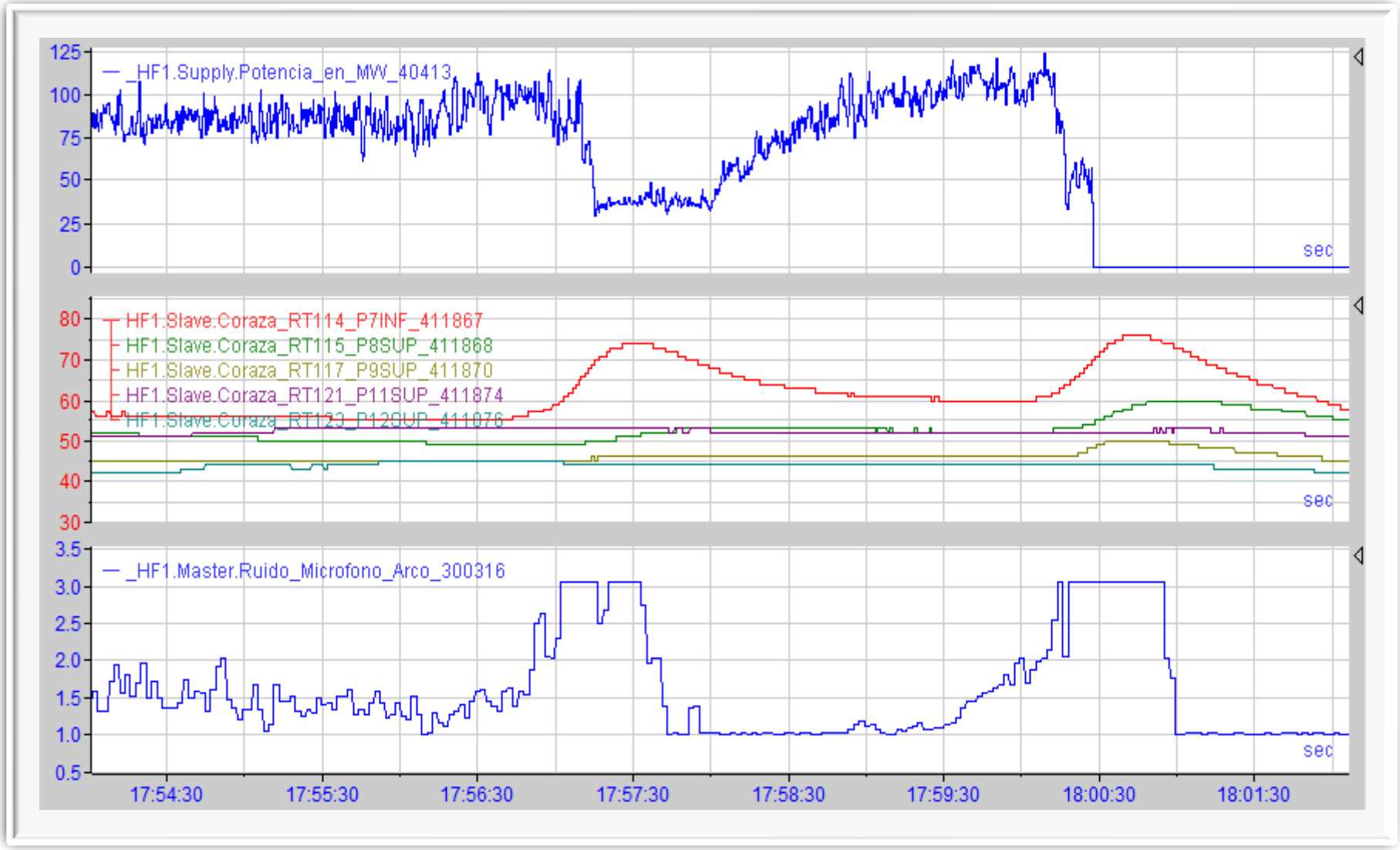

Fig. 6.26 Electric power, panel temperatures and risk indicator for the five-input fuzzy system

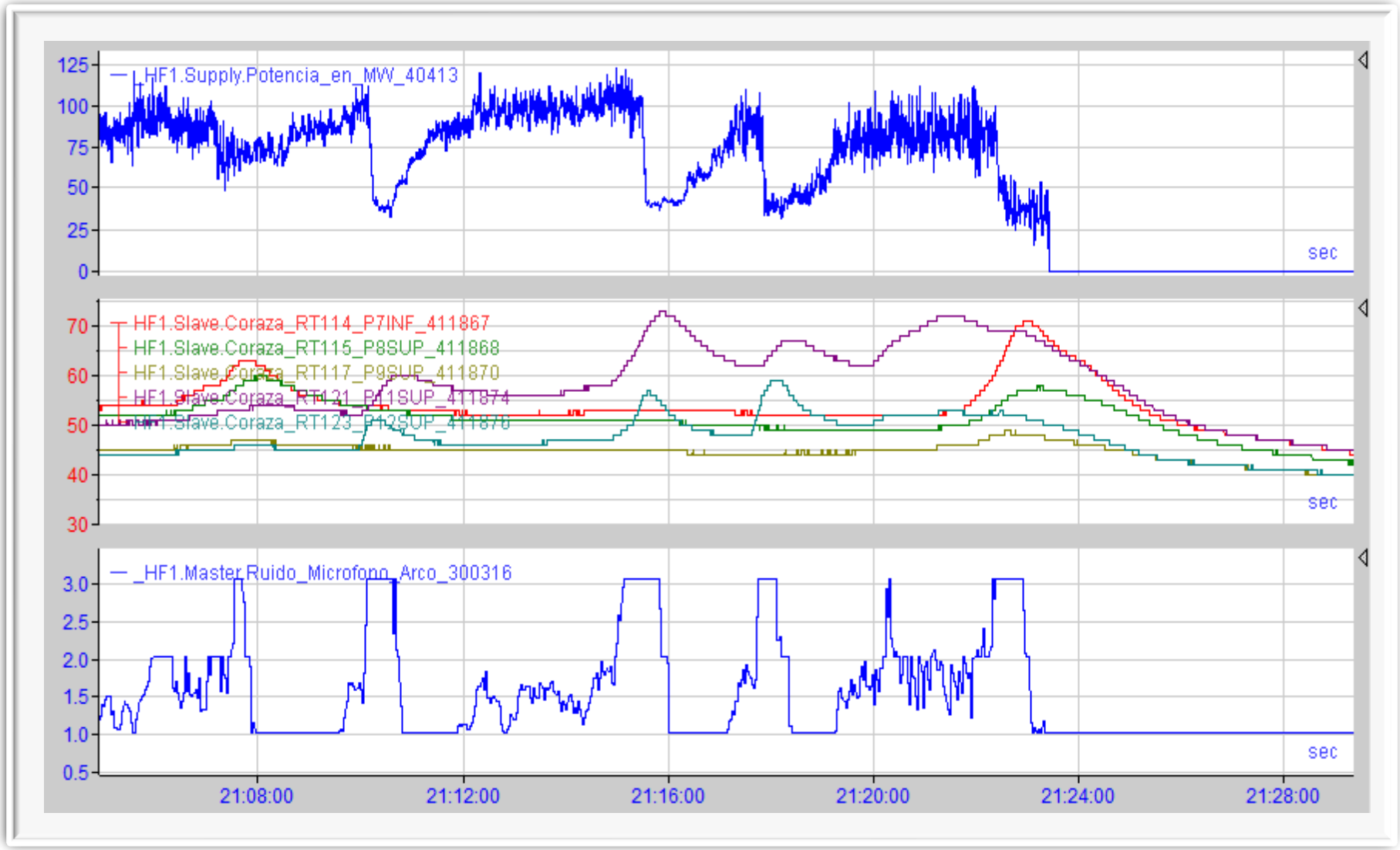

Fig. 6.27 Electric power, panel temperatures and risk indicator for the five-input fuzzy system

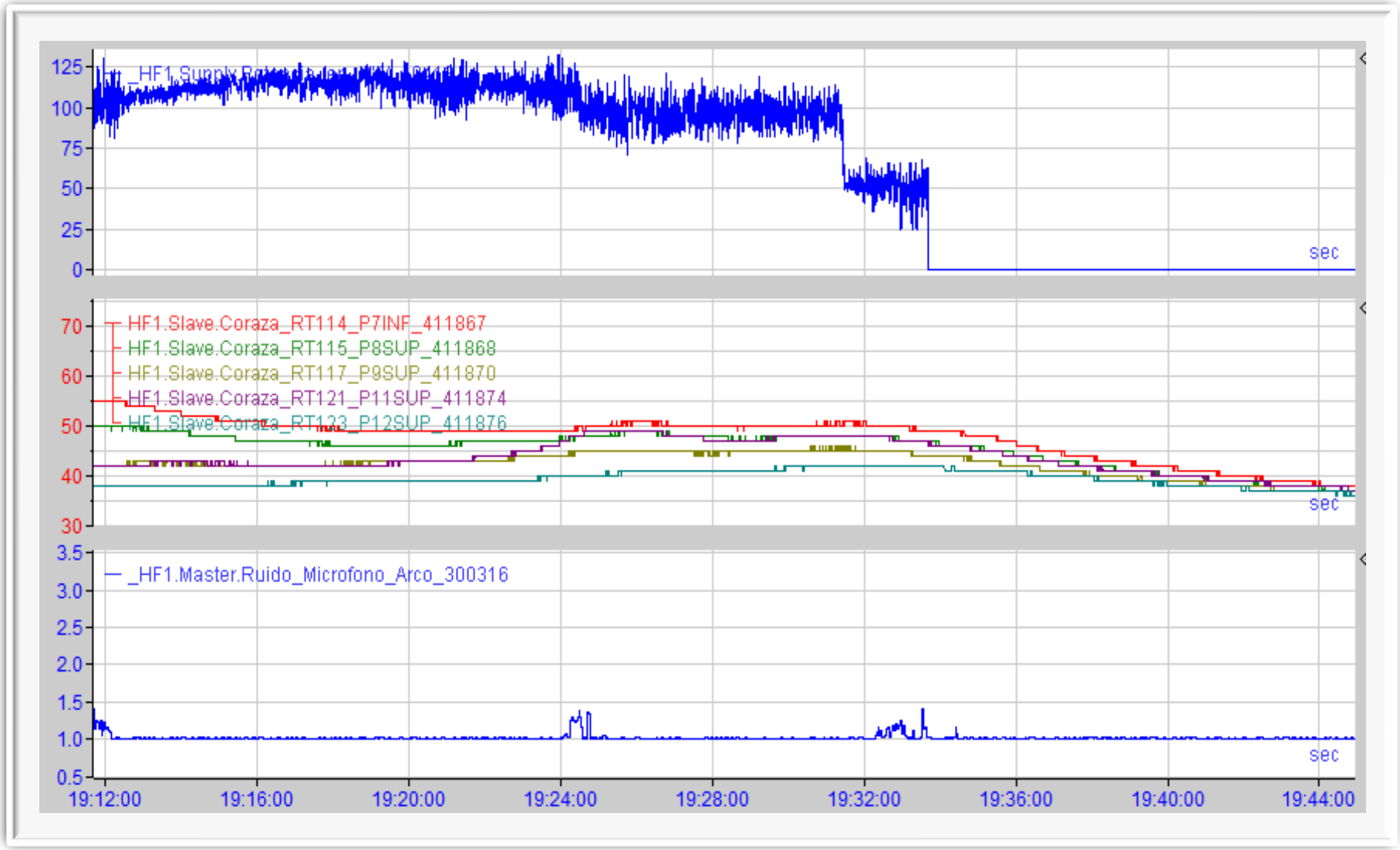

Fig. 6.28 Electric power, panel temperatures and risk indicator for the five-input fuzzy system

In order to provide a good real time representation for the operators of the EAF, a screen that only shows the risk level indicator was placed at the operator ‘s cabin. The indicator can take values between 1 and 3 and the format representation is bar that grow and change its color depending on the value, it is green for values below 2, yellow for values above 2 and red when the indicator reaches 3. In Fig. 6.29 the screen installed at the operator´s cabin is shown.

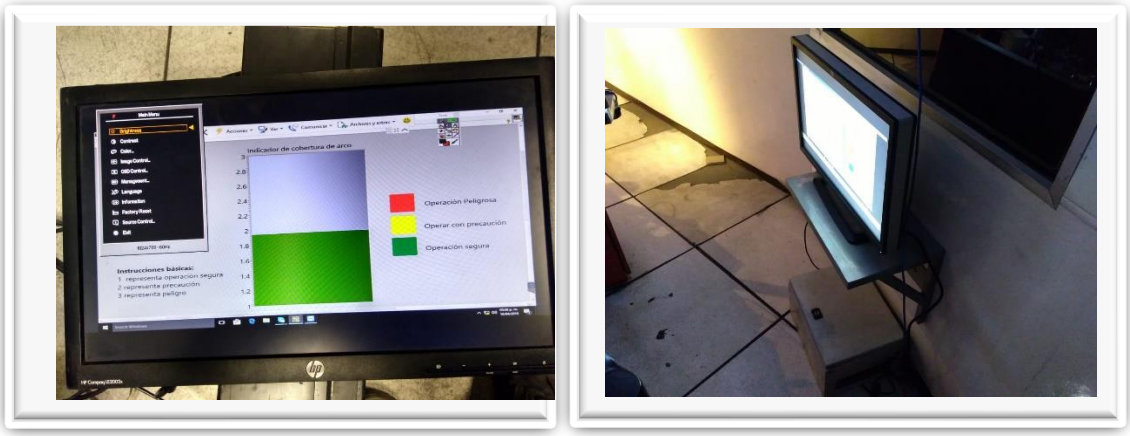

Fig 6.29 Screen that shows the risk indicator to the operator of the EAF

It is important to mention that currently the EAF is not being controlled using the risk indicator. It is only used to assist the EAF´s operator. It is expected that after a prudential period of field testing to validate with 100% accuracy all the panel´s overheating the company will impulse a complementary project to close the control loop and reduce the operator´s responsibility in the EAF manual control.

Chapter 7. Conclusions

The electric arc furnace is a complex system with many areas of opportunity to improve the operative practices and energy consumption. Fuzzy logic has found over the years several applications in the industry due to its capability to solve real world problems with good results and at low cost. Heuristic tools provide a feasible way to implement systems to operate the EAF in a more efficient way. The fuzzy system proposed in this work aims to give a robust tool to homogenize the operative practices in an electric arc furnace, ensuring that a good coverage of the arc (low risk) is achieved during critical stages of the melting process, this without significant differences between experienced and new operators. In other words, it is intended to emulate the best practices of the best operators in an artificial system that works in real time during the melting process. Excellent results were achieved with the real time operation of the algorithm developed, the fuzzy system started with three inputs (electric power, vibration and temperature slope) this allowed us to quantify, with good precision, the risk level during the operation of a DC EAF, however, some opportunity areas were found, and more inputs were added to the system. With the addition of the sound to the fuzzy processing, some redundancy regarding the vibration measurements was achieved, for example, if in some stage of the melting process the laser beam is blocked and the vibration signal is saturated, the sound allows to the system to infer that this increment in the vibration occurs due to an external perturbation, which not represent the conditions inside the EAF. Another improvement in the algorithm consisted in the addition of the panel temperature to the processing, with this, the fuzzy system can differentiate between rapid temperature increments, that put in risk the EAF operation, and rapid temperature increments that don't represent a dangerous condition. The producer-consumer scheme using for the acquisition and processing of the signals provide a robust application that don't present issues during it uninterrupted operation for several weeks, this in addition with the robust and precise detection of risky operations showed in the results of chapter 6, ensures that a solid tool, that assist the EAF´s operator, was provided to the steel company that sponsored this project. Finally, the flexibility of the fuzzy processing gives the opportunity to modify the system in the future, for example adding more inputs or modify the existing ones, this in case that the company require add some functionality that was not contemplate in this dissertation. In light of all the above-mentioned activities and the field experimental results obtained, it is clear that the objectives of the research proposal were fully accomplished and the developed "EAF risk indicator" is a novel contribution to improve safety in the steel industry and at the same time increase productivity and reduce maintenance costs. As a future work the system develop can be the starting point to close a control loop and reduce the operator´s responsibility in the EAF manual control.

Bibliography

[1] F. Martell-Chávez, M. Ramírez-Argáez, A. Llamas-Terres, and O. Micheloud-Vernackt, "Theoretical Estimation of Peak Arc Power to Increase Energy Efficiency in Electric Arc Furnaces." *ISIJ International*, vol. 53, no. 5, pp. 743-750, 2013.

[2] K. Timm, "Principles of AC Arcs." presented at the 5th Electrical Engineering of Arc Furnaces Syposium, Kehl, Germany, 2005.

[3] B. Bowman and K. Krüger, *Arc Furnace Physics* (Stahleisen communications). Verlag Stahleisen, 2009.

[4] T. Emi, "Steelmaking Technology for the Last 100 Years: Toward Highly Efficient Mass Production Systems for High Quality Steels." *ISIJ International*, vol. 55, no. 1, pp. 36-66, 2015.

[5] M. Aula, A. Mäkinen, A. Leppänen, M. Huttula, and T. Fabritius, "Optical Emission Analysis of Slag Surface Conditions and Furnace Atmosphere during Different Process Stages in Electric Arc Furnace (EAF)." *ISIJ International*, vol. 55, no. 8, pp. 1702-1710, 2015.

[6] L. Ghiormez and O. Prostean, "Electric arc current control for an electric arc furnace based on fuzzy logic." in *2015 IEEE 10th Jubilee International Symposium on Applied Computational Intelligence and Informatics*, 2015, pp. 359-364.

[7] A. Sadeghian and J. D. Lavers, "Dynamic reconstruction of nonlinear v–i characteristic in electric arc furnaces using adaptive neuro-fuzzy rule-based networks." *Applied Soft Computing*, vol. 11, no. 1, pp. 1448-1456, 2011.

[8] K. Timm, "Electric Principles of DC-Furnaces." presented at the 5th Electrical Engineering of Arc Furnaces Syposium, Kehl, Germany, 2005.

[9] A. Hübers, "Construction and Operation of DC Electric Arc Furnaces." presented at the 5th Electrical Engineering of Arc Furnaces Syposium, Kehl, Germany, 2005.

[10] Ternium "Practica Eléctrica del Horno de Arco." México, 2013.

[11] F.-h. Wang, Z.-j. Jin, and Z.-s. Zhu, "Fluid Flow Modeling of Arc Plasma and Bath Circulation in DC Electric Arc Furnace." *Journal of Iron and Steel Research, International*, vol. 13, no. 5, pp. 7-13, 2006.

[12] Y. Li, Z.-z. Mao, Y. Wang, P. Yuan, and M.-x. Jia, "Model Predictive Control Synthesis Approach of Electrode Regulator System for Electric Arc Furnace." *Journal of Iron and Steel Research, International*, vol. 18, no. 11, pp. 20-25, 2011.

[13] Ternium, "Descripción de Hornos Eléctricos." México, 2013.

[14] Ternium "ACE-Operación EAF." México, 2013.

[15] G. W. Chang, M. Shih, Y. Chen, and Y. Liang, "A Hybrid Wavelet Transform and Neural-Network-Based Approach for Modelling Dynamic Voltage-Current Characteristics of Electric Arc Furnac." *IEEE Transactions on Power Delivery*, vol. 29, no. 2, pp. 815-824, 2014.

[16] P. N. M. Dorantes and G. M. Mendez, "Type-2 fuzzy logic systems for temperature evaluation in ladle furnace." *IEEE Latin America Transactions*, vol. 14, no. 8, pp. 3914-3920, 2016.

[17] K. Krüger, "Foaming Slag Control." presented at the 5th Electrical Engineering of Arc Furnaces Syposium, Kehl, Germany, 2005.

[18] B. Dehkordi, M. Moallem, and A. Parsapour, "Predicting Foaming Slag Quality in Electric Arc Furnace Using Power Quality Indices and Fuzzy Method." *IEEE Transactions on Instrumentation and Measurement*, vol. 60, no. 12, pp. 3845-3852, 2011.

[19] J. Jae Jin, B. Sung Jun, and K. Sang-Woo, "Estimation of slag foaming height from vibration signals in electric arc furnaces." in *Electrical Engineering/Electronics Computer Telecommunications and Information Technology (ECTI-CON)*, 2010, pp. 866-869.

[20] T. Matschullat, D. Rieger, K. Krüger, and A. Döbbeler, "Foaming Slag and Scrap Melting Behavior in Electric arc Furnace - a New and Very Precise Detection Method with Automatic Carbon Control." *Archive of Metallurgy and Materials*, vol. 53, no. 2, pp. 399-403, 2008.

[21] A. Torres-Rentería, M. Damián-Cuallo, J. Mayo-Maldonado, and O. Micheloud-Vernackt, "Analysis of electric arc furnaces efficiency via frequency spectrum-based arc coverage detection." *Ironmaking & Steelmaking,* vol. 44, no. 4, pp. 255-261,2017.

[22] C. Marique, P. Nyssen, and P. Salamone, "On-line control of the foamy slag in EAF." in *Proc. 6th Electr. Steelmaking Conf.*, 1999, pp. 154-161.

[23] M. D. Cuallo, "Arc Coverage and Stability Measurement Via Vibration Frecuency Spectrum Analysis in Electric Arc Furnaces." Master's Thesis, Tecnológico de Monterrey, Monterrey, N.L, 2014.

[24] H. J. Zimmermann, "Fuzzy set theory." *Wiley Interdisciplinary Reviews: Computational Statistics,* vol. 2, no. 3, pp. 317-332, 2010.

[25] M. Bilgehan, "Comparison of ANFIS and NN models—With a study in critical buckling load estimation." *Applied Soft Computing,* vol. 11, no. 4, pp. 3779-3791, 2011.

[26] C. Min-You and D. A. Linkens, "A systematic neuro-fuzzy modeling framework with application to material property prediction." *IEEE Transactions on Systems, Man, and Cybernetics, Part B (Cybernetics),* vol. 31, no. 5, pp. 781-790, 2001.

[27] J. Yen and R. Langari, *Fuzzy Logic: Intelligence, Control, and Information*. Prentice Hall, 1999.

[28] R. Bellman and M. Giertz, "On the analytic formalism of the theory of fuzzy sets." *Information Sciences,* vol. 5, pp. 149-156,1973.

[29] B. K. Bose, *Modern Power Electronics and AC Drives* (Eastern Economy Edition). Prentice Hall PTR, 2002.

[30] Polytec, "Compact Laser Vibrometer CLV-2534-2 user Manual." https://www. polytec.com/us/

[31] O. Erives-Sánchez and O. Micheloud-Vernackt, " Electric Arc Coverage Indicator for AC Furnaces Using a Laser Vibrometer and Neural Networks." *ISIJ International,* vol. 58, no. 7, pp. 1300-1306, 2018.